Universidad Politécnica de Valencia
Departamento de Máquinas y Motores Térmicos

Combustion studies for high speed direct injection diesel engines under low temperature cold start conditions

Ph.D. Thesis
Presented by:
Mr. José G. Ramírez-Hernández
Directed by:
Dr. José M. García-Oliver

Valencia, June 2012

Ph.D. THESIS

Combustion studies for high speed direct injection diesel engines under low temperature cold start conditions

Presented by: Mr. José G. Ramírez-Hernández
Directed by: Dr. José M.García-Oliver

EVALUATION TRIBUNAL:

President:	Dr. Francisco Payri González
Secretary:	Dr. José Vicente Pastor Soriano
Examiners:	Dr. Francisco Castro Ruiz
	Dr. Octavio Armas Vergel
	Dr. Pedro Acisclo Rodríguez Aumente

Valencia, June 2012

Resumen. El transporte por carretera enfrenta el reto de satisfacer las necesidades crecientes de movilidad disminuyendo cada vez más su impacto sobre el medio ambiente. Para esto se vislumbra en el futuro un panorama en el que se conseguirán niveles de cero emisiones con los vehículos eléctricos (sin tomar en cuenta las emisiones de la producción). Sin embargo, aún quedan cabos por atar para conseguir la venta masiva y uso extendido de este tipo de vehículos. Por una parte la tecnología ha de seguir desarrollándose para aumentar la fiabilidad y reducir los costes de adquisición. Y por otra parte las ciudades, las regulaciones y los mismos usuarios tienen que prepararse para hacer un uso correcto de dichos vehículos. En la actualidad y en el futuro a corto y medio plazo se vivirá la transición que va del motor de combustión interna hacia el vehículo íntegramente eléctrico. En esta transición el motor diesel seguirá teniendo un uso extendido, que incluso se incrementará, por su capacidad de cumplir con los límites de emisiones teniendo un bajo consumo de combustible. Para esto, la tecnología del motor diesel necesita seguir evolucionando para ir a la par con las demandas actuales de mercado y de protección al medio ambiente.

Uno de los campos de mejora para el motor diesel es la fase de arranque y calentamiento. Durante esta fase se producen en el motor una cantidad importante de contaminantes debido a combustiones incompletas por las temperaturas de motor relativamente bajas. A esto se une que los sistemas de pos-tratamiento no funcionan de forma eficiente por no alcanzar sus temperaturas mínimas. Y se le sumaría, si las temperaturas ambiente están por debajo de $0^{\circ}C$, la posibilidad de que no se consiga arrancar el motor. Es esta la fase de la combustión en la que se centra la presente tesis. Distintos autores han realizado esfuerzos con anterioridad para dar directrices de cara a la optimización del arranque. Pero los estudios son escasos y se echa en falta un entendimiento básico de cómo es la combustión diesel en estas condiciones. Al saber esto, se ha planteado como objetivo de la presente tesis contribuir al entendimiento del proceso de combustión en motores diesel de inyección directa para automóviles. Este entendimiento va dirigido a comprender los procesos físicos y químicos que controlan el encendido y la influencia de los distintos parámetros de motor.

En pro de conseguir el objetivo planteado, el primer paso ha sido poner a punto una instalación experimental que permita reproducir de forma fiable, repetitiva y sistemática condiciones críticas de arranque en frío. Dicha instalación aloja un motor óptico de investigación que operando a temperatura ambiente permite reproducir las condiciones de presión y temperatura representativas de esas que alcanzaría, en el primer ciclo de arranque, un motor real a -20$^{\circ}C$. Además, la presión en cilindro y las principales variables de admisión y escape son debidamente monitorizadas y se utilizan como variables de entrada para un modelo termodinámico que calcula la ley de liberación de calor. La medida en el motor se sincroniza con la grabación de imágenes con una alta resolución espacial y temporal que permite "ver" cómo se desarrolla la combustión dentro del cilindro. Esta información experimental se ha complementado con la caracterización experimental del sistema de inyección y herramientas teóricas de cálculo multidimensional.

El planteamiento anterior, la novedosa instalación experimental y los diferentes estudios paramétricos llevados a cabo han permitido profundizar en los conocimientos que se tienen de la combustión en condiciones de arranque en frío. En primer lugar se ha logrado construir una descripción fenomenológica de cómo se desarrolla la combustión diesel en estas condiciones. También se ha puesto en evidencia, con una muestra experimental importante, la influencia de los distintos parámetros de motor tienen sobre el encendido y el desarrollo de la combustión. Y como uno de los aportes principales del trabajo, se ha desarrollado una explicación detallada de cómo interactúan los procesos físicos y químicos que llevan al autoencendido.

Resum. El transport per carretera s'enfronta al repte de complaure les necessitats creixents de mobilitat reduint cada vegada més el seu impacte amb el medi ambient. Per a açò s'albira en el futur un panorama en què s'aconseguiran nivells de zero emissions amb els vehicles elèctrics (sense tindre en compte les emissions de la producció). No obstant això, encara queden caps per lligar per a aconseguir la venda massiva i l'ampli ús d'aquest tipus de vehicle. D'una banda la tecnologia ha de continuar desenvolupant-se per a augmentar la fiabilitat y reduir els costos d'adquisició. I d'altra banda les ciutats, les regulacions i el mateixos usuaris han de preparar-se per a fer un ús correcte dels nomenats vehicles. En l'actualitat i en el futur a curt i mitjà termini es viurà la transició que va del motor de combustió interna cap al vehicle íntegrament elèctric. En aquesta transició el motor dièsel continuarà tenint un ampli ús, que fins i tot s'incrementarà, per la seua capacitat de complir amb els límits d'emissions tenint un baix consum de combustible. Per a açò, la tecnologia del motor dièsel necessita continuar evolucionant per a anar a la par amb les demandes actuals de mercat i de protecció al medi ambient.

Un dels camps de millora per al motor dièsel és la fase d'arrancada. Durant aquesta fase es produeixen en el motor una quantitat important de contaminants a causa de combustions incompletes per les temperatures de motor relativament baixes. A açò s'uneix que els sistemes de post-tractament no funcionen de forma eficient per no aconseguir les seues temperatures mínimes. I se li sumaria, si les temperatures ambient estan per davall de $0^{\circ}C$, la possibilitat de que no s'aconseguisca arrancar el motor. És aquesta la fase de la combustió en què se centra la present tesi. Diferents autors han realitzat esforços amb anterioritat per a donar directrius de cara a l'optimització de l'arrancada. Però els estudis són escassos i se troba a faltar enteniment bàsic de com és la combustió dièsel en aquestes condicions. Per açò, s'ha plantejat com a objectiu de la present tesi contribuir a l'enteniment del procés de combustió en motors dièsel de injecció directa per a automòbils. Aquest enteniment va dirigit a comprendre els processos físics i químics que controlen l'encés i la influència dels diferents paràmetres de motor.

En pro d'aconseguir l'objectiu plantejat, el primer pas ha sigut posar a punt una instal·lació experimental que permet reproduir de forma fiable, repetitiva i sistemàtica condicions crítiques d'arrancada en fred. Aquesta instal·lació allotja un motor òptic d'investigació que operant a temperatura ambient permet reproduir les condicions de pressió y temperatura representatives d'eixes que aconseguiria, en el primer cicle d'arrancada, un motor real a -20°C. A més, la pressió en cilindre i les principals variables d'admissió i fuga són degudament monotoritzades i s'utilitzen com a variables d'entrada per a un model termodinàmic que calcula la llei d'alliberament de calor. La mesura en el motor se sincronitza amb la gravació d'imatges amb una alta resolució espacial i temporal que permet "veure" com es desenvolupa dins del cilindre. Aquesta informació experimental s'ha de completar amb la caracterització experimental del sistema d'injecció y ferramentes teòriques del càlcul multidimensional.

El plantejament anterior, la nova instal·lació experimental i els diferents estudis paramètrics duts a terme han permès profunditzar en els coneixements que se tenen de la combustió en condicions d'arrancada en fred. En primer lloc s'ha aconseguit construir una descripció fenomenològica de com es desenvolupa la combustió dièsel en aquestes condicions. També s'ha posat en evidència, amb una mostra experimental important, la influència que els diferents paràmetres de motor tenen sobre l'encés y el desenvolupament de la combustió. I com una de les aportacions principals del treball, s'ha desenvolupat una explicació detallada de com interactuen els processos físics i químics que porten a l'autoencés.

Abstract. Road transportation sector faces nowadays the challenge of satisfying the growing demands for mobility and at the same time to reduce its negative impact on environment. The panorama for the future is to reduce to zero the tank-to-wheel emissions levels with electric vehicles. Nevertheless, the extended use and massive production of this kind of vehicles is compromised due to different factors. On the one hand, the technology has to keep evolving in order to improve its reliability and to reduce acquisition costs. And on the other hand, cities, legislations and users have to get ready in order to make an appropriate use of these vehicles. What will happen in short and medium term is the transition from current vehicles, powered by internal combustion engines, to 100% electric cars. For this transition, diesel engines will continue having an extended use, or even more, due to their capacity of accomplishing with emissions legislations with low fuel consumption. To be competitive, diesel engine technology has to continue improving in order to satisfying markets requirements being respectful with environment.

Cold start is one of the most problematic combustion phases for diesel engines. During this phase, a large proportion of pollutants are produced within the cylinder due to misfiring and incomplete combustion due to the low engine temperatures. Furthermore, exhaust after-treatment devices work inefficiently since their minimum operation temperatures can not be reached. In addition to this, at temperatures below $0^{\circ}C$ the possibility of continuous misfiring could actually impede the engine start. This is the combustion phase in which this study has been focus on. Different authors have made efforts to give directions in pro of cold start combustion optimization. But these studies are scarce and it is missed a fundamental understanding of how diesel combustion is under this conditions. Knowing this, the planned objective for this thesis is to contribute to the understanding of the cold start combustion process in high speed direct injection diesel engines. This understanding is directed toward the comprehension of the physical and chemical processes that control autoignition and the influence of the different engine parameters.

With the purpose of achieving this objective, the first step has been to set-up an experimental facility which allows to reproduce repeatably and systematically cold start conditions. This facility is equipped with an optical engine which operating at room temperature has been adapted to reproduce in-cylinder thermodynamic conditions as those that can be reached during start in a real engine at -20$^{\circ}C$. During the tests, in-cylinder pressure and the main intake and exhaust variables are carefully measured and are later used as input of a thermodynamic model used to calculate the heat release law. Engine measurements are synchronized with a high speed visualization system with high temporal and spatial resolution which allows to "see" how combustion develops within the combustion chamber. All this experimental information has been complemented with the experimental characterization of the injection system and theoretical modeling tools.

The methodological thesis approach, the novel experimental facility and the different parametric studies performed have allowed to gain more insight about the cold start combustion process. In first place, a complete phenomenological description of how diesel combustion develops under this conditions have been pieced together. In addition, it has been evidenced, with an important experimental sample, the influence that the different engine parameters have on ignition and combustion progress. And, as one of the major contributions of this work, it has been developed a detailed explanation on how interact the physical and chemical processes that lead to autoignition.

A mi familia, mi primera escuela. Todas las cosas que hago y las oportunidades que tengo suceden en alguna forma gracias a lo que de ustedes o con ustedes aprendí. Los quiero!

A Nuria, perquè ara cada pas que done ho done més tranquil, seré i feliç. Et vull!

Acknowledgments As many would know, carrying out a research activity and eventually being able of contributing to a given field is a long, hard and complex work full of uncertainties. For that reason, research institutes need to put together a multidisciplinary machinery of resources (human, facilities, equipment) that eventually makes it possible to make such contributions. This document encloses the outcomes of an extensive research on diesel engines cold-start combustion carried out at the CMT-Motores Térmicos Institute of the Universidad Politécnica de Valencia (UPV). Many efforts have been made by the UPV in order to set a global structure which promotes and supports multidisciplinary and in some cases complementary research activities. Specifically, the CMT-Motores Térmicos Institute has devoted its work for many years to improve knowledge on diesel engines combustion. Part of that work, developed in the past at CMT, has given to the current generation tools and experience to keep evolving which, together with the well-done work of many people during the last years have made it possible to close the research documented in this thesis.

This thesis is just a part of a global research project that have also produced four papers published in indexed journals and two participations in congresses. The beginning of this project was impulsed by Francisco Payri González and José María Desantes as directors of the CMT. The research project have been leaded by José Vicente Pastor Soriano and José María García Oliver. They have had the responsibility along the project of the successful closure of every task. They have been in charge of keeping the focus of the project and taking the decisions that have shown the path to follow.

In this work, the main source of information has been the experimental combustion analysis performed in an optical engine and coupled with high speed visualization. The first tasks of facility set-up and validation, lead by José Vicente Pastor Soriano and performed by Daniel Lérida Sánchez de las Heras, have allowed to count on a reliable facility which allows to reproduce low-speed and low-temperature cold-start conditions systematically. Daniel Lérida was also responsible of all the changes made to the facility, its correct operation and its control during the tests. Another source of experimental information was the hydraulic characterization of the injection system. This task was performed in part by Daniel Lérida but support was also given by José Enrique del Rey. The data obtained during the tests from the engine and the high-speed camera was processed thanks to the software developed by Jorge Buitrago and Daniel Zapata and later improved by Celine Dufeu and Jean-Guillaume Nerva. And finally, important support was also given by many students during their Degree-projects assisting during the tests and processing experimental data. Regarding the theoretical tools employed, a thermodynamic model was used to calculate the heat release law from in-cylinder pressure signal. This model (CALMEC) was developed in the past in the CMT but the adaptations made to the specific requirements of this project were performed by Jaime Martín Díaz. Fluid-dynamic calculations and chemical kinetics were additional sources of information to the experimental tests. In spite of being complementary, these theoretical tools were determinant in order to achieve a well-structured explanation to the experimental results. These calculations were lead by José Manuel Pastor Enguiados and performed by different students during their Degree-projects.

The elaboration of this thesis really started with the preparation of the first methodology paper published in 2009. Then, three more papers were written and finally all the information was enclosed in these pages. During all this process, this thesis has been enriched by the discussions, revisions and ideas of the team of tutors formed by José Vicente Pastor Soriano, José María García Oliver and José Manuel Pastor Enguiados. Regarding this document, its final version was achieved thanks to the exhaustive and detailed revisions made by José María García Oliver.

Contents

List of figures

List of tables

List of symbols

Latins

A	Area
D	Dimension
d	distance
I	Light intensity [a.u.]
N	Nozzle
n	polytropic exponent
NO_x	Nitrogen oxide (NO and NO_2)
m	mass
R	Radiation [$W/sr\ nm\ m^2$]
s	Spray penetration
T	Temperature
U	Speed

Greeks

α	Crank angle
ϵ	Emissivity
λ	Wavelength

Subindexes

AMB	Relative to ambient conditions
$cummul$	Accumulated during a time period
eff	Effective
f	Relative to fuel
i	for a given test point
$IMEP$	Relative to IMEP (Indicated Mean Effective Pressure
$main$	Relative to main injection
max	Maximum
$pilot$	Relative to pilot injection
TDC	Relative to conditions at TDC

Acronyms

ACEA	Association des Constructeurs Europeens d'Automobiles (European automobile manufacturer's association
ASOE	After Start Of Energizing
ASOI	After Start Of Injection
CAD	Crank angle degree
CCD	Charge Coupled Device
CE	Combustion Efficiency
CFD	Computational Fluid Dynamics
CMOS	Complementary Metal Oxide Semiconductor
COV	Coefficient Of Variation
CR	Compression Ratio
DI	Direct Injection
DOC	Diesel Oxidation Catalyst
DPF	Diesel Particulate Filter
ECU	Electronic Control Unit
EGR	Exhaust Gas Recirculation
EOI	End Of Injection
EU	European Union
EVO	Exhaust Valve Opening
FWHM	Full Width at Half Maximum
GP	Glow Plug
GPP	Glow Plug Protrusion
HEV's	Hybrid electric vehicles
HRL	Heat Release Law
HSDI	High Speed Direct Injection
IDI	Indirect Injection
IDRCI	Injection Discharge Rate Curve Indicator
IL	Integrated Luminosity
IMEP	Indicated Mean Effective Pressure
IVC	Intake Valve Closing
LD	Luminosity Delay
LHV	Lower Heating Value
LNT	Lean NO_x Traps
NO_x	Nitrogen oxides (NO and NO_2)
NTP	Nozzle Tip Protrusion
PID	Proportional-Integral-Derivative
PTC	Positive Temperature Coefficient

PM	Particulate Matter
PTC	Positive Temperature Coefficient
ROHR	Rate Of Heat Release
SCR	Selective Catalytic Reduction
SOC	Start Of Combustion
SOE	Start Of Energizing
SOF	Soluble Organic Fraction
SOI	Start Of Injection
TDC	Top Dead Centre
UHC	Unburnt Hydrocarbons
UV	Ultraviolet
VVT	Variable Valve Timing

Chapter 1

Introduction

Contents

1.1 Introduction

This Chapter presents the general framework of this work with the purpose of showing the common and overall scenario from which the particular problematic of this thesis emerges. The chapter shows first a brief summary about the human need for transportation in which the passenger car vehicle is the most used solution. Then, a description of the current passenger cars diesel engine technology is presented. This description ends with the challenges that this technology faces. Finally, the structure of the document is described in order to give a global vision of the document to the reader.

1.2 General framework

Transport represents one of the most important human activities worldwide and it plays an indispensable role in the development of human civilization. The specific purpose of transportation is to fulfill a demand for mobility originated by the variety of socioeconomic activities. The means by which people and freight achieve mobility fall into one of three basic types: land (road, rail and pipelines), water (shipping), and air.

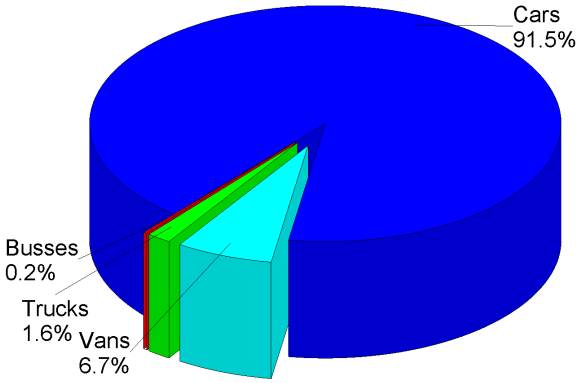

Figure 1.1. *Motor vehicle production by type in 2009. Source: ACEA European Union economic report.*

The growth of the mobility demand in the last years, larger quantities of passengers and freight being moved over longer distances, has led to the multiplication of the number of journeys involving a wide variety of modes that service transport demands. To fulfill these demands, the transportation costs (per unit) have been reduced and infrastructures have been expanded considerably to service new areas adding capacity to existing networks. Transportation studies are therefore a multidisciplinary subject that can involve hard (e.g. engineering) or soft sciences (e.g. economics) depending on the dimension being investigated, such as infrastructure provision, operational management or planning. Important efforts are being made in the European Union in order to make the road transportation system much more efficient in the near future [1, 2].

The vehicles employed in the road transportation sector are normally equipped with internal combustion engines and they can be classified in the following types: cars, vans (reference weight $< 3500kg$), trucks (reference weight $> 3500kg$) and buses. From these types, cars have had the larger percentage of units produced in the last years [3]. As a reference, Figure 1.1 shows the share of the different engine vehicles produced in 2009. In that year, over 90% of this vehicles were passenger cars. Regarding vehicles in use, 230 million passenger cars are currently in use in the European Union, which represent 87% of the total of vehicles on the European roads. Their large number of units and their use, mainly in urban centers, make cars responsible of the biggest share of the pollutant emissions produced by road vehicles. For these reasons, studies dedicated to the reduction of pollutant emissions, fuel consumption and ownership cost for cars are justified.

In the oncoming decades, the challenge for motor vehicles will be the need for a wide range of complementary propulsion systems and fuel/energy types to be developed simultaneously. Electrified mobility is currently given first priority in the United States, Japan, China, Korea and European Union. The announcements of dedicated national programs and the proliferation of qualitative position papers

and reports have contributed to raise the general expectations through announcing the imminent mass production of electric vehicles. Nevertheless, the move from conventional combustion based mobility to more electric or full electric mobility poses many questions with answers depending on a multitude of interdependent parameters [4]. Although the electrification of road transport will be a strong and inevitable trend, the fact is that, the internal combustion engine will remain the dominant propulsion technology in the near future. It will force internal combustion engines to keep evolving to a more advanced technology, in which the distinction between compression and spark ignition may become less clear-cut, and to share their functions with electric engines in hybrid concepts [1, 2]. As a consequence, efforts made in the improvement and development of internal combustion engines technology (for passenger cars) are and will be necessary for the oncoming years.

1.3 Diesel engines for passenger cars

Together with spark-ignition, compression-ignition engines are the most employed propeller to power passenger cars. In fact, according to the European Automobile Manufacturers Association (ACEA), passenger cars powered by diesel engines have reached a share of around 50% of the total number of new car registrations in the last five years in the European Union [3]. As reviewed by Johnson [5], current technology pressure on the HSDI diesel manufacturers is coming from emissions and fuel consumptions regulations, advances in gasoline engines, and increased offerings of gasoline hybrid electric vehicles (HEV's). However, diesel platforms are still very attractive for meeting the emerging CO_2 regulations, in which diesels have a 20% advantage over their gasoline counterparts. Furthermore, given the high cost of batteries for the incremental CO_2 benefits gained from battery electric vehicles [6], it is reasonable that the diesel engine will continue receiving interest before a widespread shift away from the internal combustion engine could occur. This technology pressure is being met with increasingly sophisticated combustion designs and control on diesel engines.

To illustrate the cost-effectiveness of the diesel in meeting CO_2 regulations, Körfer *et al.* [7] compare the costs of bringing a gasoline and a diesel medium-sized Euro 5 car to compliance with the 2020 European CO_2 requirements. In the end, the gasoline car fell 13 gr/km short, despite the 670 EUROS added cost, resulting in a 1270 EUROS penalty. It would need to be hybridized to eliminate the penalty. On the other hand, at an added cost of 380 EUROS, the diesel vehicle had a 5 gr/km CO_2 surplus.

To maintain this advantage, most of the efforts in diesel engine technology are focused on downsizing without sacrificing performance, as offered by improved combustion control. Main improvements are been made in fuel injection, boost, and after-treatment: $>$ 2000 bar piezo-electric injectors, 2-stage turbocharging, variable geometry turbochargers, diesel oxidation catalysts, diesel particulate filters, selective catalytic (SCR) NOx control or lean NOx traps (LNT). In addition, new models are advancing to allow higher peak cylinder pressure (to 200 bar), and to incorporate

a belt drive stop-start system, advanced cooling control, better air handling (2-stage turbocharging and EGR control), improved combustion control strategies, and a variable swirl concept using variable valve train.

In parallel to this solutions, in the last years new combustion modes are being under study. These new combustion modes aim to simultaneously reduce the emissions of NOx and PM. Specifically, it is worth to mention the low temperature diffusion combustion (LTC) [8] and the partially [9, 10] or fully premixed [11] combustion modes. These new combustion concepts have reported very good results at low load but their implementation at high load is not possible nowadays due to the difficulties to control auto-ignition.

In spite of all the progress made in diesel technology to date, certain combustion phases still need to be improved. Among them, engine starting is maybe one of the most critical phases. It is a problem for current HSDI diesel engines at low ambient temperature and it is a limiting factor for new combustion modes. For current technology, during the first minute after start the largest percentage of pollutants are emitted [12–15]. The reason is twofold: on the one hand, the in-cylinder low temperature values achieved for low compression ratio engines favor misfiring with the consequent increase of unburnt hydrocarbons and CO emitted; on the other hand, the catalyst performance is very poor until the light-off temperature is achieved. In future applications, in which compression ratio can be reduced even more [16, 17] so that new combustion modes can be implemented to comply with the near future emissions standards [6, 18], the auto-ignition phase can be even more problematic. The question that raises then is *"how passenger car diesel engine cold start combustion can be improved in order to achieve "clean" and "quick" engine starting?"* Based on this question the available literature has been reviewed and analyzed in Chapter 2. This review has led to the conclusion that the first necessary step before proposing ways of solution is to get a fundamental understanding of the cold start combustion process. The aim of this thesis is to contribute to this understanding.

1.4 Document structure

In this chapter, the framework within which this work is developed has been presented with the purpose of showing the common and overall scenario from which the particular problematic addressed in this thesis emerges. A discussion on the role of the passenger car vehicle to fulfill current and future transportation needs as well as on the technology evolution and the challenges of current passenger car diesel engines, has allowed to establish the main motivation for the development of this thesis.

Chapter 2 contains a literature review devoted to set paths in pro of optimization of the cold start process in HSDI diesel engines. This review starts with a description the characteristic starting sequence at room temperature, identifying its controlling parameters and the problematics associated in such process. Following, the state of the art of the technology employed to improve diesel engines cold starting is reviewed. Then, the review focuses on low temperature cold starting and the main results

obtained in applied studies under such conditions are discussed. After this review, the chapter closes presenting the thesis approach. It contains the literature survey conclusions, the objectives of the thesis and the overall approach of the research.

The methodology presented in Chapter 3 is an answer to the existing needs reviewed and discussed in Chapter 2. The main tool employed is the experimental combustion analysis performed in an optical engine which reproduces low speed and low temperature cold start conditions. This experimental information consists of classical in-cylinder pressure analysis coupled with high speed visualization. In a second place and as support information, nozzle characterization (namely mass flow rate, momentum flux and spray visualization tests) is presented. The third source employed collects two modeling tools for chemical kinetics and CFD calculations. These modeling tools have been employed in order to fill specific blanks which could not be filled with experimental information and add valuable and necessary information to analyze experimental results. The methodology is fully described in Chapter 3 but an important part of it has been previously published in [19].

Chapter 4 presents a full description of the combustion event and its main controlling mechanisms. A qualitative description of the combustion sequence, as a frame of reference showing how combustion occurs under such conditions, is presented first for a nominal engine configuration. Taking that frame as starting point, ignition and combustion development are characterized using high speed visualization and in-cylinder pressure analysis. After that, first parametric variations are presented with the purpose of understanding the mechanisms that control ignition and combustion progress. This Chapter allows to plan the next parametric studies having a certain reference of how combustion is under such conditions. Most of the findings presented in this chapter have been published in [20].

The parametric studies performed have been planned in order to investigate the hardware and injector nozzle configuration influence on cold start combustion. The influence of the hardware configuration is presented in Chapter 5. And the influence of the injector nozzle is presented in Chapter 6. The main contents of both chapters can also be found in [21, 22].

Chapter 7 is devoted to piece together an explanation of the mechanisms, processes and sub-processes that lead to ignition under glow-plug assisted cold start conditions. The main experimental results, regarding pilot ignition, presented along this thesis are grouped with specific modeling results with the purpose of showing a single and coherent explanation. Finally, Chapter 8 presents the main outcomes derived of this work and a proposal for future research.

Bibliography

[1] ERTRAC Strategic Research Agenda 2010. *Towards a 50 percent more efficient road transport system by 2030 - Technical document.* European Road Transport Research Advisory Council (ERTRAC), October 2010.

[2] ERTRAC Working Group on Energy and Environment. *Future light-duty powertrain technologies and fuels.* European Road Transport Research Advisory Council (ERTRAC), August 2011.

[3] Huynh Quynh-Nhu. *European Union economic report.* European Automobile Manufacturers Association (ACEA), March 2010.

[4] ERTRAC European Roadmap. *Electrification of road transport.* European Road Transport Research Advisory Council (ERTRAC), European Technology Platform on Smart Systems Integration (EPoSS) and European Technology Platform for the Electricity Networks of the Future (Smart Grids), November 2010.

[5] Johnson Timothy V. "Diesel Emission Control in Review". *SAE Paper 2011-01-0304*, December 2011.

[6] Johnson Timothy V. "Review of CO_2 emissions and technologies in the road transportation sector". *SAE paper 2010-01-1276*, 2010.

[7] Körfer T, Schnorbus T, Kalenborn M, Kolbeck A, Bourgoin G, Cecur M and Raimondi E. "Integrated diesel engine concept for lowest CO2 emissions requirements". In *Aachen Colloquium*, October 2010.

[8] Pickett Lyle M. and Siebers Dennis L. "Non-Sooting, low flame temperature mixing-controlled DI diesel combustion". *SAE Paper 2004-01-1399*, 2004.

[9] Iwabuchi Y., Kawai K., Shoji T. and Yoshinaka T. "Trial of new concept diesel combustion system - premixed compression-ignited combustion". *SAE Paper 1999-01-0185*, 1999.

[10] Kimura S., Ogawa H., Matsui Y. and Enomoto Y. "An experimental analysis of low-temperature and premixed combustion for simultaneous reduction of NOx and particulate emissions in direct injection diesel engines". *International Journal of Engine Research*, Vol. 3 n^o 249-259, 2002.

[11] Ryan T. and Gray A. "Homogeneous charge compression ignition (HCCI) of diesel fuel". *SAE Paper 971676*, 1997.

[12] Yassine M. K., Tagomori M. K., Henein N. A. and Bryzik W. "White smoke emissions under cold starting of diesel engines". *SAE paper 960249*, February 1996.

[13] Peng Haiyong, Cui Yi, Shi Lei and Deng Kangyao. "Effects of exhaust gas recirculation (EGR) on combustion and emissions during cold start of direct injection (DI) diesel engine". *Energy*, Vol. 33 n^o 3, pp. 471 – 479, 2008.

[14] Peng H.-Y., Cui Y., Deng H.-Y., Shi L and Li L.-G. "Combustion and emissions of a direct-injection diesel engine during cold start under different exhaust valve closing timing conditions". *Proceedings of the Institution of Mechanical Engineers, Part D: Journal of Automobile Engineering*, Vol. 222 n^o 1, pp. 119–129, 2008.

[15] Weilenmann Martin, Favez Jean-Yves and Alvarez Robert. "Cold-start emissions of modern passenger cars at different low ambient temperatures and their evolution over vehicle legislation categories". *Atmospheric Environment*, Vol. 43 n^o 15, pp. 2419–2429, February 2009.

[16] Pacaud P., Perrin H. and Laget O. "Cold Start on Diesel Engine: Is Low Compression Ratio Compatible with Cold Start Requirements?". *SAE Paper 2008-01-1310*, April 2008.

[17] MacMillan D., La Rocca A., Shayler P. J., Murphy M. and Pegg I. G. "The Effect of Reducing Compression Ratio on the Work Output and Heat Release Characteristics of a DI Diesel under Cold Start Conditions". *SAE Paper 2008-01-1306*, April 2008.

[18] Johnson Timothy V. "Review of diesel emissions and control". *SAE paper*, Vol. 2010-01-0301, 2010.

[19] Pastor J. V., García-Oliver J. M., Pastor J. M. and Ramírez-Hernández J. G. "Experimental facility and methodology for systematic studies of cold startability in direct injection Diesel engines". *Measurement Science and Technology*, Vol. 20, pp. 09519, August 2009.

[20] Pastor J V, García-Oliver J M, Pastor J M and Ramírez-Hernández J G. "Ignition and combustion development for high speed direct injection diesel engines under low temperature cold start conditions". *Fuel*, Vol. 90 n^o 4, pp. 1556 – 1566, 2011.

[21] Pastor J. V., Bermúdez V., García-Oliver J. M. and Ramírez-Hernández J. G. "Influence of spray-glow plug configuration on cold start combustion for high-speed direct injection diesel engines". *Energy*, Vol. 36 n^o 9, pp. 5486–5496, 2011.

[22] Desantes J. M., García-Oliver J. M., Pastor J. M. and Ramírez-Hernández J. G. "Influence of nozzle geometry on ignition and combustion for high-speed direct injection diesel engines under cold start conditions". *Fuel*, Vol. 90 n^o 11, pp. 3359–3368, 2011.

Chapter 2

Cold starting in HSDI diesel engines and approach of the research

Contents

2.1 Introduction

This Chapter contains two main pieces of information, a review of the literature devoted to set paths in pro of optimization of the cold start process in HSDI diesel engines and the overall thesis approach. *"Cold start"* means here any engine start when the temperature of oil, coolant and engine block is equal to the ambient temperature. The review commences describing the characteristic cold starting sequence at room temperature, identifying its controlling parameters and the problematics associated to such process. Following, the state of the art of the

technology employed to improve diesel engines cold starting is reviewed. Then, the review focuses on low temperature cold starting, and the results obtained in applied studies under such conditions are discussed. It is worth noting that such studies are scarce because of difficulties to control critical engine parameters. After the literature review, the chapter closes presenting the thesis approach. It contains the literature review conclusions, the detailed objectives of the thesis and the overall approach of the research.

2.2 Room temperature cold start

The cold starting process under conventional conditions is described in this subsection. Diesel engine cold start refers here to the starting sequence of a diesel engine at room temperature. Even under such conditions, cold starting is a problematic operation mode due to its highly transient nature and due to the lack of control on the autoignition process [1].

The starting sequence of a diesel engine is a highly transient process, which can be divided into four distinct phases as shown in Figure 2.1: (1) cranking, (2) start, (3) after-start and (4) idle. This sequence begins with cranking (1) of the engine by means of the starter motor. It is cranked at a speed which is within the range of 200 to 300 *rpm* and depends on room temperature, engine characteristics, electrical motor characteristics and oil properties. Once a minimum speed has been reached, the start phase (2) begins with the first injections. The engine speeds up, thanks to combustion, until the assistance of the electrical motor is not longer necessary. During this phase, load must be in the range of 8-11 *bar* IMEP in order to overcome mechanical losses and speed up the engine. Then, the after-start phase (3) begins. In this phase, engine speed is relatively high (around 900 *rpm*) but still unstable due to large load and combustion phasing variations. Finally, the last phase commences when engine speed stabilizes at the nominal idle speed (4). Then, the engine warms-up until the coolant temperature is stabilized around 80°C. During this whole sequence, the main concern are the high emissions levels, since engine start can normally be achieved. Specifically, emission control is concerned with UHC, CO and PM. These pollutants are emitted mostly at the beginning of the starting sequence, as shown by Bielaczyc *et al.* [2]. In that paper, the authors show that CO and UHC emissions during the first 60*s* is more than 40% of the total emission in the 3 *min* cold start, and PM even more than 50%.

A very important characteristic of cold start combustion is the very long ignition delay of the sprays, compared to conventional (warm) diesel engine combustion. The autoignition process in a diesel engine is a complex phenomena in which physical and chemical processes coexist in a time and space dependent fashion, as described by Edwards [3] previously in a quite original way. *"A multi-component liquid fuel at a relatively low temperature is atomized by pressure and shearing forces and injected with high velocity into a relatively quiescent, but high temperature, gaseous environment. Mass is transferred from the liquid to the gas phase, while energy is drawn from the gas to support the transfer. The high momentum of the liquid phase ensures that*

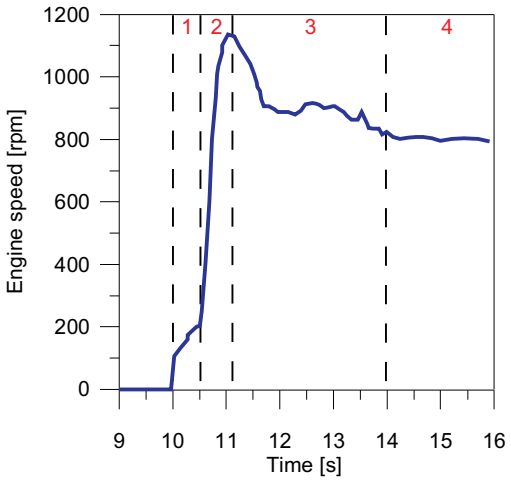

Figure 2.1. *Engine speed as a function of time during a typical cold start sequence: (1) Cranking, (2) Start, (3) After-start and (4) stable idle.*

the air and fuel begin to mix intimately. Concurrent with these processes, the air and fuel begin to undergo chemical reaction. The large hydrocarbon molecules break into smaller fragments, driven by energy from the gas phase and attacked by oxygen or radical species. A chemical soup is formed: fuel molecules, stable intermediates, radical species, oxygenates. This chemical soup is, in turn, mixed with other parcels of fluid with similar or very different compositions and histories. These include parcels of pure air, pure fuel, and liquid fuel, as well as those with similar constitutions. The new parcels continue to cook, mix and convect as time passes. A race is now afoot between the parcels to see which, if any, can mature to the point where its preferred chemical pathways are no longer strongly endothermic or leading to non-participative intermediate species, but lead to the release of chemical energy. The race is won when a parcel produces sufficient exothermicity that it can survive subsequent material and energy exchanges from the mixing process and still remain exothermic". Summarizing, the processes involved during autoignition can be divided in three main physical sub-processes: atomization, vaporization and mixing and the complex chemical reactions.

Regarding atomization, complete atomization conditions [1] are reached at a short distance from nozzle hole for DI diesel sprays. Such distance is called *break-up length* and according to Arrègle [4], under conventional HSDI diesel engines conditions, it is independent of speed at nozzle exit and it is of the same order of magnitude as the orifice diameter. As already pointed out by Correas [5], it is generally accepted that density ratio between air and fuel is the controlling parameter on break-up length. In this regard, Hatori [6] measured the break-up length by means of visualization for the same fuel at two ambient density conditions (30 and 11 kg/m^3). A similar evolution is observed at both density values, the break-up length grows at the beginning of

[1] Liquid fuel is distributed in form of drops surrounded by air

injection until approximately 70 μs. Then, the break-up length decreases until its value is practically zero. The effect introduced by the change in density ratio is a short time lag between both penetration signals. For these reasons, it is widely accepted to consider the diesel spray as a two-phase flow in which the liquid phase is completely distributed in form of small drops, assuming complete atomization. Recently, Bracho [7] presents a detailed study about the injection process at low temperature. The author states that internal processes within the nozzle hole can be affected at low temperature: viscosity increases and the flow regime goes to the laminar or transitional regime zone, producing higher pressure losses during injection, which translates into a lower effective speed. However, the effects on atomization have not been specifically studied. For this reason, there is not evidence to think that the complete atomization conditions could considerably change under cold start conditions.

Regarding fuel vaporization, it is influenced by two different processes: turbulent mixing and local interphase transport. Siebers [8] concludes that vaporization under warm engine conditions is controlled by air entrainment into the spray (*i.e.*, by turbulent mixing). When this occurs the local interphase transport rates of mass, momentum, and energy that control liquid breakup and droplet evaporation must be fast relative to turbulent mixing rates. Nevertheless, Siebers [8] also suggest that conditions may exist where local interphase transport processes become limiting factors. This may occur with be very low volatility or high viscosity fuels, with very low injection pressures or during cold start and warm-up. In fact, in a posterior paper Siebers [9] shows significant disagreements, even in the trends, between experimental data and a scaling law based on the mixing-controlled hypothesis when air temperature and density are low ($T < 850\ K\ and\ \rho < 14.8\ kg/m^3$). In that paper, the author states that one of the reasons for such disagreement may be a shift in the processes controlling fuel vaporization. As the ambient temperature is decreased, the overall surface transport rates should ultimately become slow relative to the mixing process. During cold start, such low density and low temperature in-cylinder conditions can be reached, depending on ambient temperature and engine compression ratio, and fuel vaporization may be affected by both processes, turbulent mixing and local interphase transport. In this situation, the vaporization process can be delayed due to lower in-cylinder densities, larger nozzle hole diameter, higher fuel density and higher fuel velocity. As a consequence, severe wall impingement is expected during cold start and warm-up for HSDI diesel engines, which lowers mixing rates and increases emissions of unburned and partially burned species [10].

Chemical processes are affected by in-cylinder temperature, which controls the reaction rate, as well as by reactants composition (fuel and air-charge). High air-charge temperatures are desirable in order to speed up chemical kinetics but also to improve vaporization. This temperature is specially affected during the start phase of the whole starting sequence. The maximum temperature reachable by the air charge during the compression stroke, without combustion, is a function of intake temperature (ambient temperature T_{AMB}) and compression ratio (CR). This peak temperature is commonly expressed in the polytropic model presented in [11] and discussed in [10]:

$$T_{TDC} = T_{AMB} \cdot CR^{\,n-1} \tag{2.1}$$

where n is the polytropic exponent that depends on engine characteristics (it is around 1.3). Compression ratio is around 16:1, for current technology, and future trends actually pretend to reduce this value. As compression ratio is a design parameter, intake temperature determines the resulting peak compression temperature to a large extent. Cranking speed also has certain influence on peak in-cylinder temperature, since it determines the time available for heat losses and blow-by, which are critical during start. In this regard, increasing cranking speed reduces these heat and mass losses producing an increase in peak in-cylinder temperature (through a change of the value of the exponent n in Equation 2.1). However, according to Phatak and Nakamura [12], above a certain speed the loss of time for autoignition reactions overweights any marginal gain in peak in-cylinder temperature and the effect is no longer positive.

Regarding fuel properties, the cetane number influence depends on its value. Increasing cetane number, for instance from 50 to 60, has negligible influence on ignition [11]. Whereas a drop in cetane number from 50 leads to a significant increase of ignition delay [11]. Hara *et al.* [13] studied the effect of cetane number improver additives on engine cold startability using iso-octyl nitrate. Their results show that the improvement in startability by adding the cetane improver is more significant with fuels of lower cetane number at ambient temperature above $5°C$. But, at $-5°C$ the additive was no longer effective.

Regarding air-charge composition, Liu and Karim [14] investigated the effects of residual gas on combustion. Their results showed that residual gas has both positive and negative effects on ignition depending on its composition. Residual gas produced by partial oxidation reaction has mainly kinetic effects, which promote ignition, while products of more complete combustion also have significant thermal, diluting effects. Kwon *et al.* [15] investigated the effects of residual gas on ignition delay through experiments conducted in a constant volume combustion bomb. They found that the addition of C_2H_6 and C_3H_8 shortened the ignition delay, while the addition of CO and CO_2 had a reverse effect. These results were later confirmed by Peng *et al.* [16]. They found that introducing a certain amount of EGR during the first cycles of the start, promotes ignition. However, when combustion became stable, EGR could lead to longer ignition delays and even misfiring.

2.3 Ignition aids

The term *"Ignition aid"* is used to refer to a sort of devices employed in diesel engines to reduce the ignition delay when in-cylinder temperature is not high enough. At room temperature, they are used with the purpose of reducing pollutant emissions during start and warm-up. At very low temperatures, ignition aids are necessary to promote ignition. Two pre-heating concepts (and their corresponding devices) have

been commonly employed in HSDI diesel engines: heating all the gas entering in the cylinder with electrical intake heaters or generating a hot spot in the combustion chamber by means of an electrical glow plug. Both procedures are described in this sub-section.

2.3.1 Intake air heating

In one of the ignition aid concepts, a heater is installed in the intake system to warm up all the air aspirated by the cylinder[2]. This solution is the one employed in medium and large diesel engines, since engines with large combustion chambers (displaced volume bigger than 800 cm^3) present more favorable surface to volume ratio and relatively low blow-by rate. Intake heaters such as intake manifold burners or electrical heaters provide the engine with sufficiently high air temperature to achieve nearly warm start conditions.

In spite of the fact that intake heaters are used exclusively in medium and large size diesel engines, some research has dealt with the viability of its use in passenger car diesel engines. The design and development of this system as well as the first validation tests have been presented in two doctoral theses (Giménez [17] and García [18]) and direct applications of the system have been presented in [19, 20]. The heater developed in these works is an electrical supplied intake heater with 6 parallel plates made of $KANTHAL$ alloy. It has the capacity of warming up intake air of a conventional passenger car engine at start speed, from $-20°C$ to $20°C$ consuming an electrical power of 135 kW. This device allows to reach peak temperatures as high as $410°C$ in an 1.4 liter DI diesel engine equipped with standard EURO IV hardware. With this solution, the authors [18] have reported that start delay time is very similar to that obtained by using glow plugs but with lower power consumption (compared with glow plug technology in 2003). At the same time, an overall reduction of pollutant emissions (soot, HC and CO) was obtained. The only exception was the NO emissions which were increased, most probably due to the increased temperature. However, this solution still remains as an alternative, since the totality of the commercial diesel passenger car engines are equipped with glow plugs.

2.3.2 Hot spot ignition aid

In the other solution, a glow plug is assembled in the cylinder head so that its tip protrudes into the combustion chamber a few millimeters generating a hot spot. A glow plug is a pencil-shaped piece of metal with a heating element at the tip. The heating element, when electrified, heats due to electrical resistance and begins to emit radiation in the visible portion of the electromagnetic spectrum, hence the term "glow". During engine start, a voltage is supplied to the glow plug and within

[2]Note that the turbogroup of current HSDI engines is not in use during start due to the low engine speed, so that it behaves as a naturally aspirated reciprocating engine. Only engines equipped with mechanical compressor could behave differently

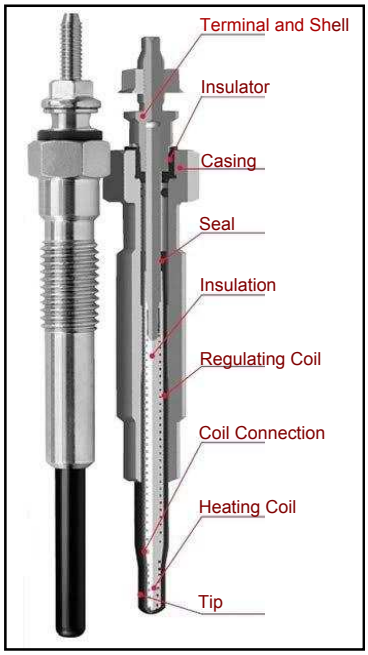

Figure 2.2. *Sketch of the parts that form metal glow plugs.*

a few seconds the tip reaches a maximum temperature above 1273 K. Short heating-up time, high operating temperature, low current input and long life service are the main demands that modern glow plugs must fulfill. Glow plugs have also been studied as ignition aids for alternative fuels like methanol [21, 22], ethanol [23] or natural gas [24] in diesel engines.

The glow plug solution has been imported from IDI diesel engines, in which mixture was formed in a relatively small pre-chamber where the injector and the glow plug were located [25]. Within this pre-chamber, fuel was injected at relatively low injection pressure, and ignition occurred after spray impact against the walls and fuel contact with the glow plug. Due to the small pre-chamber volume, a fuel and air mixture atmosphere around the glow plug was formed in a short period of time and remained there until combustion occurred. When using glow plugs in HSDI diesel engines the situation changes. Fuel is injected within a bigger volume (combustion chamber) where it is spread and, thanks to improvements on injection systems, at higher velocity. Nevertheless, the role of the glow plug is still to serve as a hot spot. For this reason, manufacturers [26] warn that it is important that the heater rod surface of the glow plug contacts the rim zone of the fuel spray in order to achieve satisfactory cold start.

Different technologies and materials are employed nowadays by glow plug manufacturers. Metal glow plugs [26], as sketched in Fig. 2.2, consist of a body

with an external thread and a hexagon in which the sheathed heater rod is forced in. Inside the heater rod a combination of a heating coil with virtually no temperature dependent resistance and a regulating coil is embedded in a MgO-filling. The MgO-filling provides electrical insulation and stabilization of the coils while being a good thermal conductor. This type of glow plug can reach temperatures as high as 1250 K in less than 4 seconds and it also has the ability of post-heating at 1330 K in order to reduce noise, pollutant emissions and the roughness of run up. Secondly, the ceramic glow plugs [27] have a similar configuration as the metal glow plugs but with a silicon nitrite-filling (Si_3N_4) housing the resistance coils. In comparison to metal glow plugs, the heating coil of the ceramic glow plugs has higher melting point which combined with the ceramic filling allows them to reach higher temperatures. According to the manufacturer, ceramic glow plugs can reach temperatures as high as 1250 K in less than two seconds and can after-glow[3] for more than ten minutes at temperatures up to 1620 K. The other type are the composite-ceramic sheathed-element glow plug [28], which is a new approach in which the heater element is integrated in the glow plug tip. In these glow plugs the heater element is a new material composite whose electrical characteristics can be adjusted as required within a wide range. These glow plugs can reach temperatures as high as 1273 K in less than 2 seconds and can after-glow at temperatures as high as 1473 K. Furthermore, the composite-ceramic sheathed-element glow plug operates, on an 11 V design, with half of the current of that used by an 11 V metal glow plug.

2.4 In-cylinder conditions for low temperature cold start

Differently to conventional (room temperature) cold star, low temperature cold start is defined in the present thesis as any engine start when the temperature of oil, coolant and engine block is such that mixture ignition needs to be assisted. In-cylinder conditions reached by a HSDI diesel engine under that situation have been carefully estimated by Broatch *et al.* [29]. For such estimations, the authors combined $3D$ and $0D$ calculations with experimental data obtained from passenger car engines in a cold chamber. This methodology was applied for estimating in-cylinder conditions below which ignition must be assisted. The total displacement of the engine was 1.9 L and two compression ratios were considered for the study: $18:1$ and $14:1$, which are representative of the Euro IV and Euro VI engine configurations, respectively.

The methodology developed by Broatch *et al.* is sketched in Fig. 2.3 and can be summarized as follows. First, startability tests were carried out in a climatic chamber set at the desired ambient temperature and different engine parameters were measured (*i.e.* cranking speed, fluid temperatures, in-cylinder pressure, etc). These experimental data were used as boundary conditions and validation data for the models (CFD and 0D). Then, a CFD calculation of the intake stroke during the

[3]The afterglow phase lasts several minutes after the engine has started in order to minimize pollutant emissions and noise

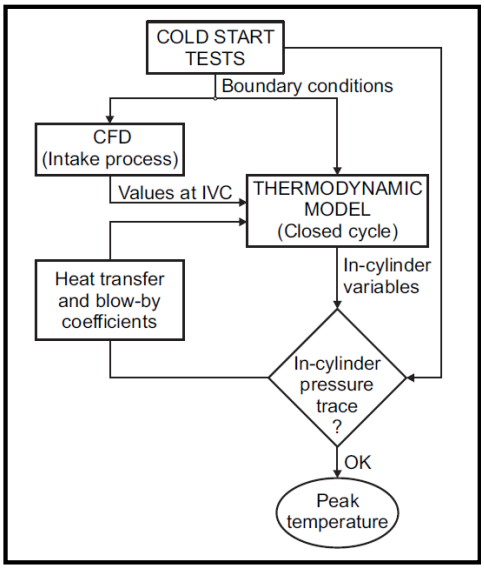

Figure 2.3. *Sketch of the methodology employed in [29] to estimate cold start in-cylinder conditions.*

cranking phase of the engine was performed [30]. This made it possible to obtain an accurate estimation of the variables that define the thermodynamic conditions of the gas at Intake Valve Closing (IVC), which cannot be directly measured in such conditions. CFD calculation results were used as input data for a 0D model described in [31], allowing a fast simulation of the thermodynamic evolution of in-cylinder air during the closed loop in the cycle. In this model, relevant phenomena which take place during engine starting at low temperatures, such as heat transfer and blow-by, were considered. As a result, in-cylinder thermodynamic conditions can be determined as a function of the crank angle position.

In that way, the ambient temperature at which the engine starts without any aid was determined experimentally by performing tests with the glow plug switched off. The climatic chamber set point temperature was swept from -20 $°C$ with increasing steps of 5 $°C$ and it was further refined with an uncertainty of 1 $°C$. The criterion used by the authors to qualify the engine startability was defined by the conditions in which combustion started just after the first injection cycle and progressed adequately. The $18:1$ CR engine started without aid at -11 $°C$ and the $14:1$ CR engine started without aid at 10 $°C$. Then, in-cylinder thermodynamical conditions were estimated using the models, and the results are summarized in Table 2.1. This table shows engine results (ambient temperature and cranking speed), conditions at IVC calculated by the 3D model and peak in-cylinder conditions estimated by the 0D model. According to these results, a minimum peak in-cylinder temperature as high as 688 K is required to ensure fuel self-ignition at any ambient temperature.

Table 2.1. *In-cylinder parameters during cranking conditions calculated at the ambient temperatures for which the two engine configurations start without aid and at the critical temperature of -23 °C [29].*

Variable/engine configuration	18:1	14:1	18:1	14:1
Ambient temperature [°C]	-11	10	-23	-23
Cranking speed [rpm]	190	250	150	160
Mass at IVC [mg]	584	547	602	614
Temperature at IVC [K]	272.6	298.8	263.9	265.9
Pressure at IVC [bar]	1.07	1.08	1.06	1.07
Peak pressure [bar]	37	28	36	27
Peak temperature [K]	683	687	660	620
Blow-by level [%]	17	10	25	22

As a reference to more severe ambient conditions, Broatch *et al.* applied their methodology to estimate in-cylinder conditions at an ambient temperature of -23 °C. Results are also shown in Table 2.1 for both CR configurations. According to these results, peak in-cylinder temperatures reached are below the threshold temperature shown previously: 660 K and 620 K for the high and low CR engines, respectively. It evidences how necessary ignition aids are for current and future diesel engines.

2.5 Review of relevant results under low temperature cold start conditions

Available studies on low temperature cold start combustion process start from the 1970's, but only recently they have become more systematic aiming at engine cold start optimization. Some of this information stems from experimental studies focused upon trial-and-error procedures [19, 32–34], where the first minute of the starting sequence is reproduced in cold rooms set at the desired temperature. In this type of studies the information obtained is limited to measured in-cylinder pressure, cycle performance and the observation of the overall engine behavior. Some information has been gained from these studies, for example, the benefits obtained by using split injections has been reported by Osuka *et al* [34]. And, Zahdeh *et al* [33] detected the possible presence of cool flames before the sharp pressure rise in combustion cycles. Nevertheless, several measurement uncertainties and the incapability of using extra diagnostic tools have prevented from making a detailed explanation of the results obtained in this kind of facilities. More systematic approaches to the problem

have been presented only recently. These studies coupled in-cylinder analysis with spray and combustion visualization under better monitored and controlled engine conditions.

The parameters with some influence on this problem are, on the one hand, the common engine parameters (injection pressure and air conditions) and, on the other hand, the particular parameters of this problem (glow plug-nozzle arrangement and engine temperature). During the starting sequence, air conditions are not modified since the turbo-compressor do not boost, they are fixed conditions of the problem and will not be studied. For this reason, this section summarizes the main reported results according to the specific parameters of interest: hardware configuration, injection strategy and engine temperature.

Hardware configuration

Hardware configuration studies comprise: variations in the glow plug arrangement relative to one fixed spray, variations of the nozzle tip protrusion, nozzles with different included angle and glow plug temperature (sketched in Fig. 2.4). Any of the first three parametric variations provoke a variation of the distance between the glow plug tip and one of the sprays, which, has been believed to have an effect on ignition. In fact, the impact of the glow plug-spray distance has been previously reported in different works. Walter *et al.* [35] tested four different distance values by rotating the injector around its axis in the up-swirl direction with respect to the glow plug. Larger values of engine speed standard deviation and opacity were obtained when the spray was positioned farther from the glow plug. With a rotation angle below 10°, drastic reductions in both engine speed standard deviation and opacity were obtained. In the same work [35], two different glow plug protrusion configurations were tested for the same orientation angle. Lower opacity values and better stability were obtained when the spray to glow plug distance was shorter. These reductions came as a result of better ignition conditions that promote an earlier start of combustion in which more fuel can be burnt, as shown with images in that paper. The results corresponding nozzle arrangement variations, *i.e.* nozzle tip protrusion and included angle, shown in [36], follow the logical trend. Start delay is reduced if the distance between the tip of the glow plug and the spray axis is reduced. Similar trend is observed for the included angle. When the included angle is larger, the distance between the spray and the glow plug is shorter, which induces a decrease of the start delay.

Special attention was paid by Pacaud *et al.* [36] when they study the glow plug orientation angle effect. They found that, besides the spray-glow plug distance, the actual orientation direction (up-swirl or down-swirl) had an effect. This paper shows that, for two different orientation angles with the same glow plug to spray distance, the lower start delays were obtained when the spray is positioned in the up-swirl direction. This result evidences that air motion also plays a role on ignition.

In the same way, Walter *et al.* [35] present a study of the glow plug temperature influence on start delay, opacity, engine speed stability and ignition. Regarding the engine start delay, according to Walter *et al.* the glow plug temperature (between

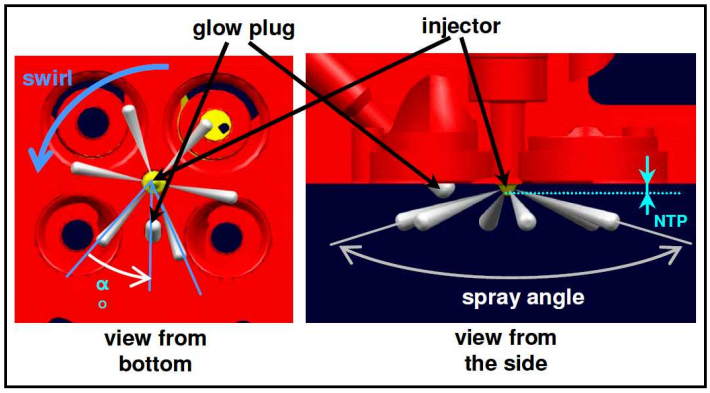

Figure 2.4. *Sketch of some of the hardware configuration parameters with influence on cold start combustion.*

1273 K *and* 1673 K) seems to have quite no effect, which remains around 1s. Nevertheless, a clear effect can be seen on opacity and engine stability, specially for the cold idle. The opacity is very high for low glow plug temperature (1273 K), during start phase (where it reaches maximum values) as well as during cold idle. Even if there is a logical decrease due to engine warm up, the opacity is still around 50% after 120s. A higher glow plug temperature (1473 K) allows immediately to reduce the opacity peak to 60% during start phase and then decreasing to less than 20% after 100s. Nevertheless, this trend is not linear: 1673 K glow plug temperature allows to reach a lower opacity in idle (about 10%) but does not really improve the results before 40s. Regarding combustion progress, with the highest glow plug temperature target (1673 K), combustion appears with both pilot and main injections. When the temperature is reduced to 1473 K combustion occurs on the two injections but with lower intensity. With 1273 K glow plug temperature the pilot combustion disappears and main combustion takes a longer time to initiate. This work shows that glow plug temperature certainly has influence on cold start combustion but within a certain range. Apparently, above a certain temperature value the benefits of increasing glow plug temperature start being negligible.

Injection strategy

Old cold start injection strategies were based on delivering a large amount of fuel, usually more than full load fuel delivery [37, 38]. This was based on the assumption that the more the fuel delivered, the more opportunity was given for fuel evaporation and combustion. This approach was widely applied in diesel engines with mechanically controlled fuel pumps, since the possibilities for parameters adjustment was limited. Injection strategies have evolved thanks to the appearing of common rail fuel injection systems. Features given by this systems (high injection pressure and high degree of flexibility in the injection timing and quantity control of multiple injections)

have allowed to reduce and control NOx, soot, combustion noise and specific fuel consumption in warmed up states [39–42]. But also, multiple injection strategies have been used to improve cold startability to reduce white smoke emissions and combustion noise during cold starting at low temperatures [34, 43, 44].

Evidence has been found in the literature about the difficulties of starting at low temperature by using single injection strategies. Recently, Zhong *et al.* [45] tested a single injection strategy (25 mg) in a passenger car diesel engine in a cold chamber for different ambient temperatures. The authors found that the cranking period increased up from 1.5 cycles at $20°C$ to more than 60 cycles at $10°C$, 60 cycles was the limit assumed by the authors to consider starting fail. When using a split injection strategy the 60 cycles limit was reached at -10$°C$. These results show the benefit on startability given by multiple injection strategies and how sensitive engine starting is to these kind of configuration parameters. The authors explain that the poor startability achieved with a single injection strategy could be due to the high drop in the mass average temperature due to fuel injection and evaporation(about 45 $K°C$ with a 25 mg injection) which reduces the reaction rates. Regarding the unburned HC emissions, the paper shows the logical trend: for longer cranking periods (single injection) the amount of unburned HC emissions is larger. In a different work, Chartier *et al.* [46] also test a single injection strategy under cold start conditions but during the after-start phase. Results show large cycle-to-cycle variations in pressure trace, intermittent combustion and increasing peak pressure and pressure rise rate with time when using the single injection strategy. The authors attribute this result to the large amount of fuel being injected at once, impeding evaporation. They state that the poor ignition conditions produce a fuel accumulation within the cylinder, and when combustion occurs part of the accumulated fuel is also burnt together with the injected fuel. It produces higher and uncontrolled peak pressure values.

Walter *et al.* [35] present the role of pilot injection when using a split injection strategy during cold start. Although the conditions shown by the authors do not exactly correspond to low temperature cold start, they are able of showing at some extent the start of pilot flame and the subsequent interaction with main injection. Thermodynamic conditions tested in this paper cannot being directly correlated with others, they use a $13:1$ compression ratio engine within a cold chamber at $5°C$. Peak in-cylinder temperature can be estimated to be around $648K$, by using a polytropic model [10] and assuming a polytropic exponent of 1.33. Ignition aids are necessary at this temperature (as shown in Section 2.4). All results presented in this paper show an instantaneous (few seconds) start, which is due to the fact that engine settings were previously optimized, and probably because in-cylinder conditions are not too critical. As startability is not an issue under this conditions, the main effect detected by the authors when using pilot injection is a reduction on opacity. The authors also show, with images and heat release traces, that pilot injection reduces main combustion delay in the first firing cycle of the start phase. It happens because pilot injection generates a hot flame, after ignite close to the glow plug, which promotes main combustion start. As a consequence, combustion is more intense (higher peak heat release values) and it is also shorter in duration. A limited experimental sample

and the particular optimized settings of a particular engine are the main concerns to consider these results as valid in different conditions for different engines.

Pacaud *et al.* [36] present an optimization study of the injection settings for a pilot + main strategy during cold start. This study was performed in a 13.7 : 1 compression ratio engine in a climatic chamber at -20°C. The criteria used in this paper to evaluate cold operation is the start delay, which is defined as the time period between the moment when the starter is switched on and the moment when idle phase is reached. This paper shows separated variation of different injection settings: start of pilot injection, start of main injection, rail pressure, pilot fuel quantity and total fuel quantity. Results show that start delay is degraded with an increase of rail pressure and early timings for the main injection are necessary. Some enhancement was detected as well if the pilot injection was closer to the main pulse. According to the amount of fuel injected in the main injection, no clear trend is observed. Long start delays were detected when the amount of fuel was too small or too large, with a minimum value between them. Finally, it is shown that increasing the total fuel quantity is positive until certain value, from which no significant benefit is obtained. These results certainly contribute as some kind of guidelines when optimizing injection strategies, but more efforts are necessary in order to extent these trends to other engines in different conditions.

Chartier *et al.* [46] tested multiple injection during the after-start phase. In that paper, strategies with 1, 2 and 3 pilots are presented within a total of 6 strategies. In general, the authors observe that increasing the number of pilot injections improves stability of combustion phasing and maximum values. The authors attribute this result to a less important global in-cylinder temperature drop when using multiple injections. They also state that several injection events create pulsations that remove the fuel film from the piston and provide time for the fuel to evaporate during dwell periods. However, these assumptions are not supported since it is not easy to access to this kind of information. In addition, explaining cold start ignition in terms of the global temperature drop should be better supported, since ignition under this conditions is a highly local phenomenon (close to the glow plug).

Having clear that multiple injections improve combustion during start and after-start phase at low temperature, Payri *et al.* [42] present a study for better understanding of the interaction between injections. This work was carried out in a 15 : 1 compression ratio engine within a climatic chamber at -10°C, the idle period after cold start was the combustion phase under study. In this paper, two different multiple injection strategies were tested: (1) pilot + main and (2) two pilots + main. For these strategies, the amount of injected mass and the dwell time between injections were variated. Regarding single pilot strategy, the authors found out that both the amount of injected mass and the dwell time have effect on combustion. Two tests with different amount of pilot injected mass were compared. If the amount of injected mass was high enough ($5mg$) an increase in heat release was detected before the start of the main injection, as a consequence the main combustion delay was shortened and the IMEP of the cycles was high (around $7bar$). On the contrary, if the amount of injected mass is too small ($1mg$) no heat release was detected before main injection causing large combustion delays and low IMEP values (around $4bar$). On the other

hand, several dwell times were tested and it was found that no effect is obtained when the injections are too separated (more than 18 CAD) or too close (2-4 CAD). In between, an optimum value (maximum IMEP) was found at 6 CAD. When using a second pilot (1^{st} pilot $2mg$ and 2^{nd} pilot $3mg$), a slight improvement was detected (with respect to the case of $5mg$ single injection) on IMEP and combustion efficiency. These results evidence the positive impact of multiple injection to improve combustion stability and how important choosing appropriately the injection settings when using these strategies is.

Engine temperature

The particular approach presented by Chartier *et al.* [46] allowed, by cooling down specific circuits of an optical HSDI diesel engine, to know the impact of different fluids temperature on the after-start phase. Block temperature, intake air temperature and fuel temperature were cooled down independently. Engine block temperature and intake air temperature were found to have a considerable effect on combustion stability during the after-start phase. On the contrary, no fuel temperature effect was detected. These results show how important the contribution of the engine temperature is, by warming up intake air and controlling fuel temperature.

2.6 Thesis approach

2.6.1 Literature review conclusions

The whole starting sequence is a critical transient operation mode for diesel or gasoline engines. In diesel engines, long cranking periods and unstable combustion translates into a large amount of UHC, CO and PM due to ignition problems. During the whole sequence, start and after-start are the most critical phases due to their transient nature and the lack of control on in-cylinder conditions and hence on combustion. These phases are strongly affected by in-cylinder temperature which, at the same time, is determined by ambient temperature and engine compression ratio. For this reason, at low ambient temperature, increasing in-cylinder temperature is compulsory in order to improve and control startability, combustion stability and, consequently, pollutant emissions.

Low temperature cold start conditions are defined in this work as those in-cylinder conditions at which ignition assistance is required. They are usually reached for current diesel engine technology, at ambient temperatures below $-10°C$. For future trends with reduced compression ratio, such limiting conditions can be found below $10°C$. These ambient temperatures result in peak in-cylinder temperatures as high as 688 K. At very low ambient temperature ($-23°C$), the peak in-cylinder temperature can be reduced to 660 K and 620 K for current and future diesel technology, respectively. All these facts evidence that cold start problems are not only present for below zero ambient temperature conditions, it will become an issue

in the near future at above zero ambient temperature values. To assist ignition under such conditions, glow plugs are the most employed device in HSDI diesel engines. The glow plug tip work as a hot spot within the combustion chamber which is able of reaching temperatures above 1273 K.

Regarding hardware configuration, three general conclusions can be drawn from different studies available in the literature. In first place, glow plug to spray distance plays a major role on ignition since the glow plug works as a hot spot within the combustion chamber. This has been shown in studies devoted to improve a specific engine configuration for which this information serves only for calibration or optimization purposes. More information is necessary in order to understand the interaction between the spray and the glow plug, and then to propose improvements in arrangement of the glow plug in the cylinder head. Secondly, swirl motion also has an effect on ignition under cold start conditions. This is a surprising result due to the low air speed, relative to fuel, at such low engine speeds. Anyway, further research is necessary to understand such effect. In third place, glow plug temperature certainly has influence on cold start combustion but within a certain range. As shown in the literature, higher glow plug temperatures help to ensure pilot injection ignition, reduce opacity and improve engine stability. Nevertheless, it has been evidenced that effect starts being negligible above a certain temperature value.

With regard to injection strategy, important improvements have been achieved in cold start ignition thanks to the introduction of common rail fuel injection systems. It has been demonstrated in different studies that single-pulse injection strategies result in poor ignition, low combustion efficiency and unstable combustion. However, there is not a well supported explanation of this poor behavior of single injections. As an alternative, pilot plus main injection strategies are commonly used in order to improve startability, to reduce white smoke emissions and combustion noise during cold starting. The challenge with these kind of strategies is to be able of setting up all the parameters (number of injections, rail pressure, mass of fuel and dwell time) according to engine characteristics and in-cylinder conditions. For this reason, information that allow to explain the influence of this parameters and the interaction between injections is necessary to have some guidelines when designing a pilot + main injection strategy.

In general, fundamental knowledge that allows to explain ignition and combustion mechanisms during cold starting is necessary. In that way, the effect of different design and calibration parameters can be better understood and a path can be set toward the improvement of diesel engine technology during this critical operation mode. The main limitation faced by researchers when studying cold start combustion is to reproduce in a systematic and repeatable manner this event. Most of the results presented in the literature have been obtained in cold rooms in which only one or two tests can be performed per day and considerable efforts have to be made to reduce the uncertainties in important variables like intake pressure. These conditions do not allow to record enough experimental samples of a phenomenon which is supposed to be disperse or monitor reliably the changing in-cylinder conditions. In addition, the impossibility of using extra diagnostic tools have not allowed to look beyond the pressure traces. Only recently, cold start studies have become more systematic and

other techniques, namely calculus and experimental, techniques have been employed with the aim of understanding fundamental processes.

2.6.2 Objectives of the thesis

Taking into account the information available in the literature, the general objective of this work is to contribute to the understanding of the cold start combustion process in direct injection passenger diesel engines, in terms of:

- Physical and chemical processes that govern ignition and combustion progress under such conditions.
- Influence and importance of different geometry and operation parameters.

This should be regarded as an early, but necessary, step before proposing more specific optimization guidelines.

In order to achieve this general objective, the following specific objectives are established:

- Given the necessity of generating reliable, repeatable and systematic experimental information, evidenced in the literature review, the first step would be to develop, set up and validate an experimental facility which allows:
  - To reproduce thermodynamical conditions representative of a real engine cold start.
  - To perform parametric variations of the geometry and functioning parameters with influence on ignition and combustion progress.
  - To reproduce the geometry and dynamics of the real engine as close as possible.
  - To control and reproduce in a repetitive way the test conditions.
  - To employ advanced diagnostic tools, including optical techniques.
- To apply experimental techniques, data acquisition procedures and post-processing and analysis methodologies for systematic studies given the particular conditions under which the engine is operating.
- To obtain a clear description of the events that occur during the low temperature cold start combustion.
- To determine the influence of the most relevant parameters (injection strategy, in-cylinder thermodynamic conditions, geometric arrangement between the glow plug and the sprays) from systematic studies.

2.6.3 General methodology and research development

In general, the methodology used in this work is based in the use of three different information sources: experimental combustion analysis performed in an optical engine, nozzle characterization (namely mass flow rate, momentum flux and spray visualization tests) and modeling tools (chemical kinetics and CFD calculations). The main tool is the experimental combustion analysis and the other two are used for filling specific gaps. How these tools have been used in this thesis is fully described in Chapter 3.

Regarding the research development, the first step is to carry out the facility set-up. An optical engine was adapted to reproduce thermodynamical in-cylinder conditions reached by a passenger car during low temperature cold start. Efforts were done in order to achieve conditions repeatably and systematically. Control and measurement of the main engine signals is also necessary.

After the facility set-up a large amount of tests were carried out in order to explain trends and investigate possible hypothesis about how cold start combustion is controlled. Nevertheless, only a representative sample has been selected to be presented in this dissertation with the purpose of showing a well structured and coherent explanation.

In Chapter 4, a phenomenological description has been built on the analysis of a specific injection strategy which is very common under low temperature cold start conditions. Anyway, the findings presented in Chapter 4 can be generalized for different situations since they are focused on understanding fundamental mechanisms and not on optimizing a specific strategy.

After defining the phenomenological description, the effect of different engine or injection parameters is presented. These studies give a reasonable explanation of how cold start diesel combustion is controlled. The characteristic systematic approach have allowed to obtain a large statistical sample in order to ensure each parameter effect. When necessary, other experimental or modeling tools have been used as support information to the experimental combustion analysis.

At the end, all the experimental results are organized and a single explanation is given supported by the modeling tools.

Bibliography

[1] Rakopoulos C. D. and Giakoumis Evangelos G. *Diesel engine transient operation : principles of operation and simulation analysis*. Springer, 2009.

[2] Bielaczyc Piotr, Merkisz Jerzy and Pielecha Jacek. "Investigation of exhaust emissions from di diesel engine during cold and warm start". *SAE paper 2001-01-1260*, 2001.

[3] Edwards C. F., Siebers D. L. and Hoskin D. H. "A study of the autoignition process of a diesel spray via high speed visualization". *SAE Paper 920108*, 1992.

[4] Arrègle Jean. *Análisis de la estructura y dinámica interna de chorros diesel*. Tesis Doctoral, Departamento de Máquinas y Motores térmicos. Universidad Politécnica de Valencia, 1997.

[5] Correas David. *Estudio teórico experimental del chorro libre diesel isotermo*. Tesis Doctoral, Departamento de Máquinas y Motores térmicos. Universidad Politécnica de Valencia, 1998.

[6] Hatori H., Narumiya K., Tsue M. and Kadota T. "Photographical analysis of initial breakup process of diesel spray". In *Proceedings of the Thiesel 2002 Conference on Thermo-and fluid dynamic processes in diesel engines*, pp. 33 – 43, Valencia, Spain, September 2002. CMT - Motores térmicos. Universidad Politécnica de Valencia.

[7] Bracho León Gabriela. *Experimental and theoretical study of the direct diesel injection process at low temperatures*. Tesis Doctoral, Departamento de Máquinas y Motores térmicos. Universidad Politécnica de Valencia, July 2011.

[8] Siebers Dennis L. "Liquid-phase fuel penetration in diesel sprays". *SAE Paper 980809*, 1998.

[9] Siebers D. "Scaling liquid-phase fuel penetration in diesel sprays based on mixing-limited vaporization". *SAE paper 1999-01-0528*, 1999.

[10] Heywood John B. *Internal Combustion Engine Fundamentals*. McGraw-Hill, Inc., 1988.

[11] Hardenberg H. O. and Hase F. W. "An empirical formula for computing the pressure rise delay of a fuel from its cetane number and from relevant parameters of direct-injection diesel engines". *SAE paper 790493*, 1979.

[12] Phatak R. and Nakamura T. "Cold startability of open-chamber direct-injection diesel engines - part I Measurement technique and effects of compression ratio". *SAE paper 831335*, 1983.

[13] Hara H., Itoh Y., Henein N. and Bryzik W. "Effect of cetane number with and without additive on cold startability and white smoke emissions in a diesel engine". *SAE paper 1999-01-1476*, 1999.

[14] Liu Z. and Karim G. A. "An examination of the role of residual gases in the combustion processes of motored engines fuelled with gaseous fuels". *SAE paper 961081*, 1996.

[15] Kwon S. I., Arai M. and Hiroyasu H. "Ignition delay of a diesel spray injected into a residual gas mixture". *SAE paper 911841*, 1991.

[16] Peng Haiyong, Cui Yi, Shi Lei and Deng Kangyao. "Effects of exhaust gas recirculation (EGR) on combustion and emissions during cold start of direct injection (DI) diesel engine". *Energy*, Vol. 33 n^o 3, pp. 471 – 479, 2008.

[17] Giménez Plá Juan Fernando. *Diseño de un sistema de arranque en frío para motores diesel de inyección directa de pequeña cilindrada*. Tesis Doctoral, Departamento de Máquinas y Motores térmicos. Universidad Politécnica de Valencia, Valencia, 2000.

[18] García Ibáñez Javier Ángel. *Nuevo concepto de arranque en frío para motores diesel de inyección directa de alta presión*. Tesis Doctoral, Departamento de Máquinas y Motores térmicos. Universidad Politécnica de Valencia, Valencia, 2003.

[19] Payri F., Broatch A., Serrano J. R., Rodríguez L. F. and Esmorís A. "Study of the Potential of Intake Air Heating in Automotive DI Diesel Engines". *SAE Paper 2006-01-1233*, April 2006.

[20] Broatch Alberto, Luján José M., Serrano José R. and Plá Benjamín. "A procedure to reduce pollutant gases from Diesel combustion during European MVEG-A cycle by using electrical intake air-heaters". *Fuel*, Vol. 87 n^o 12, pp. 2760–2778, 2008.

[21] Goetz Wendel A., Barringer Chris G. and Bozzelli Marco A. "Utilizing neat methanol and glow plug ignition in DI diesels: Laboratory testing of a single and multi-cylinder engine". *SAE Paper 941044*, 1994.

[22] Mueller Charles J. and Musculus Mark P. "Glow plug assisted ignition and combustion of methanol in an optical DI diesel engine". *SAE Paper 2001-01-2004*, 2001.

[23] Karthikeyan B. and Srithar K. "Performance characteristics of a glowplug assisted low heat rejection diesel engine using ethanol". *Applied Energy*, Vol. 88 n^o 1, pp. 323–329, 2011.

[24] Aesoy Vilmar and Valland Harald. "Hot surface assisted compression ignition of natural gas in a direct injection diesel engine". *SAE Paper 960767*, 1996.

[25] Kowalewicz A. *Combustion systems of high-speed piston internal combustion engines*. Elsevier science publishers, New York, 1984.

[26] Lindl Bruno and Schmitz Heinz-Georg. "Cold-start equipment for diesel direct-injection engines". *SAE Paper 1999-01-1244*, 1999.

[27] NGK-GlowPlugs. *Ceramic glow plugs*. Technical information available in http://www.ngk-dpower.com/en/technik/keramik-gluehkerzen/.

[28] Kern Christoph, Dressler Wolfgang, Lindemann Gert and Rothacker Volker. "An innovative glow system for modern diesel engines". *SAE paper 1999-01-1240*, March 1999.

[29] Broatch A., Ruiz S., Margot X. and Gil A. "Methodology to estimate the threshold in-cylinder temperature for self-ignition of fuel during cold start of Diesel engines". *Energy*, Vol. 35, pp. 2251–2260, March 2010.

[30] Payri F., Benajes J., Margot X. and Gil A. "CFD modeling of the in-cylinder flow in direct-injection Diesel engines". *Computers and Fluids*, Vol. 33 n^o 8, pp. 995 – 1021, 2004.

[31] Lapuerta M., Armas O. and Bermúdez V. "Sensitivity of diesel engine thermodynamic cycle calculation to measurement errors and estimated parameters". *Applied Thermal Engineering*, Vol. 20 n^o 9, pp. 843 – 861, 2000.

[32] Henein Naeim A., Zahdeh Akram R., Yassine Mahmoud K. and Bryzik Walter. "Diesel engine cold starting: combustion instability". *SAE Paper 920005*, February 1992.

[33] Zahdeh Akram R., Henein Naeim A. and Bryzik Walter. "Diesel cold starting Actual cycle analysis under border-line conditions". *SAE Paper 900441*, February 1990.

[34] Osuka Isao, Nishimura Masataka, Tanaka Yasushi and Miyaki Masahiko. "Benefits of new fuel injection system technology on cold startability of diesel engines Improvements on cold startability and white smoke reduction by means of multi injection with common rail fuel system (ECD-U2)". *SAE Paper 940586*, February 1994.

[35] Walter B., Perrin H., Dumas J. and Laget O. "Cold operation with optical and numerical investigations on a low compression ratio diesel engine". *SAE paper 2009-01-2714*, November 2009.

[36] Pacaud P., Perrin H. and Laget O. "Cold Start on Diesel Engine: Is Low Compression Ratio Compatible with Cold Start Requirements?". *SAE Paper 2008-01-1310*, April 2008.

[37] Bosch R. *Automotive handbook*. 4th edition, 1996.

[38] Bosch R. *Diesel engine management*. 2nd edition, 1999.

[39] Badami M., Nuccio P. and Trucco G. "Influence of injection pressure on the performance of a DI diesel engine with a common rail fuel injection system". *SAE paper 1999-01-0193*, March 1999.

[40] Badami M., Mallamo F., Millo F. and Rossi E. "Influence of multiple injection strategies on emissions, combustion noise and BSFC of a DI common rail diesel engine". *SAE paper 2002-01-0503*, March 2002.

[41] Corcione F. E., Vaglieco B. M., Corcione G. E. and Lavorgna M. "Potential of multiple injection strategy for low emission diesel engines". *SAE paper 2002-01-1150*, March 2002.

[42] Payri F., Broatch A., Salavert J. M. and Martín J. "Investigation of diesel combustion using multiple injection strategies for idling after cold start of passenger-car engines". *Experimental Thermal and Fluid Science*, Vol. 34 n^o 7, pp. 857–865, 2010.

[43] Ueda T., Zhang L. and Gabe M. "Improvement of the cold startability of common rail injection system by pilot injection in a HD diesel engine". *SAE paper 1999-08-0355*, 1999.

[44] Girotra M., Zhong L. R., Henein N. A. and Bryzik W. "Split injection strategy for prompt cold starting and low white smoke emissions". In *Proceedings of the Spring Technical Conference of the ASME Internal Combustion Engine Division*, pp. 343–350, 2005.

[45] Zhong Lurun, Gruenewald Steve, Henein Naeim and Bryzik Walter. "Lower temperature limits for cold starting of diesel engine with common rail fuel injection system". *SAE paper 2007-01-0934*, April 2007.

[46] Chartier Clèment, Aronsson Ulf, Andersson Öivind and Egnell Rolf. "Effect of Injection Strategy on Cold Start Performance in an Optical Light-Duty DI Diesel Engine". *SAE Paper 2009-24-0045*, 2009.

Chapter 3

Tools and methodology

Contents

3.1 Introduction

The methodological approach presented in this work is an answer to the existing needs reviewed and discussed in Chapter 2. Three different information sources have been combined in order to gain understanding on cold start combustion, as sketched in Figure 3.1. The main source is the experimental combustion analysis performed in an optical engine which reproduces low speed and low temperature cold start conditions. All engine-related experimental information presented in this thesis has been obtained at this facility, consisting of classical in-cylinder pressure analysis and high-speed

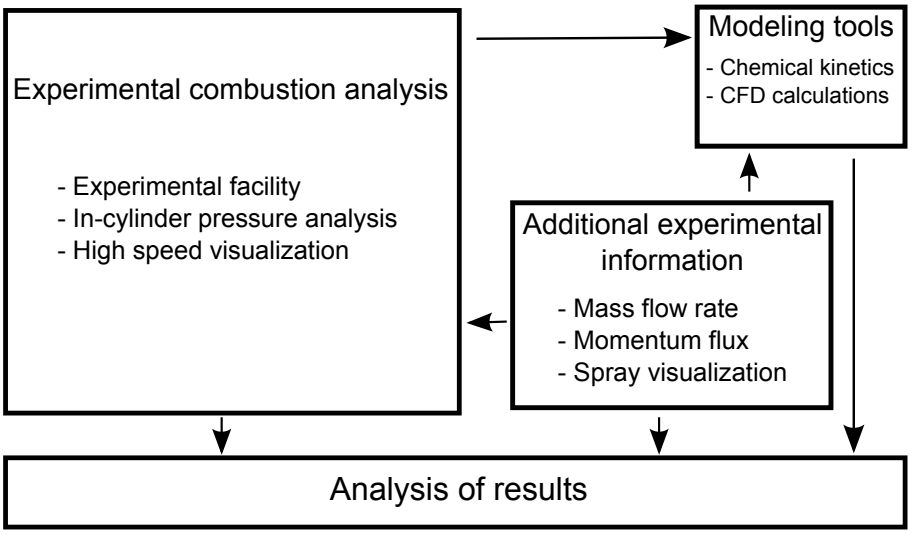

Figure 3.1. *Sketch of the general methodological approach employed in this thesis.*

combustion visualization. In a second place and as support information, nozzle characterization (namely mass flow rate, momentum flux and spray visualization tests) is presented. Nozzle characterization results are used mainly for the analysis of the results in Chapter 6. They are also used as input to the CFD calculations and to the thermodynamical model employed to process in-cylinder pressure, and to control the amount of fuel injected during the tests. The third source employed consists of two modeling tools, chemical kinetics and CFD calculations. These modeling tools have been employed in order to add aditional analysis information which could not be obtained from experimental tests.

3.2 Tools for experimental combustion analysis

This section presents, the definition of the specific conditions to be reproduced in the optical engine and a description of how the facility has been adapted. Then, the thermodynamical model used to calculate the rate of heat release is presented. Finally, the image acquisition system and post-processing procedures are detailed.

3.2.1 Experimental facility

The start phase of the starting sequence is a critical, transient and uncontrolled engine operation mode, especially at low temperature. This phase is illustrated in Figure 3.2, in which in-cylinder pressure and engine speed are plotted as a function of time for a 4-cylinder HSDI diesel engine during a test in a climatic chamber at

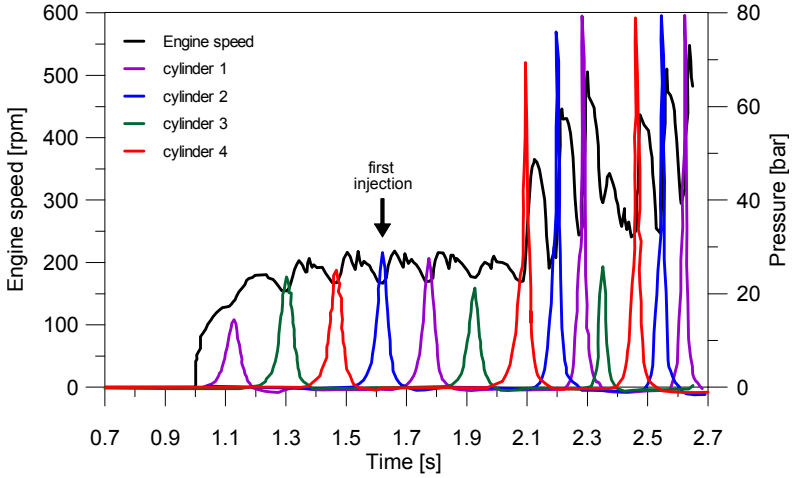

Figure 3.2. *Example of the cold start sequence of a 16:1 compression ratio engine in climatic chamber at* $-20°C$*. Engine speed and in-cylinder pressure for the four cylinders are plotted as a function of time. The cycle at which the first injection is performed is signaled with an arrow.*

$-20°C$. The figure shows that injection starts after a short cranking period but combustion does not appear in any of the first three injection cycles. As combustion appears, the engine speeds up but misfiring happens again in cylinder number three, which results in decelerating of the engine. This Figure evidences how critical this phase is. It is a transient period in which engine speed and in-cylinder conditions are continuously changing in dependency of combustion success. But at the same time, ignition conditions depend on these small changes of in-cylinder conditions in each of the cylinders. The nature of this process makes it difficult to be accurately controlled and monitored. The approach presented in this work aims at reproducing the first injection cycle of the whole starting sequence, due to the fact that it is a representative and reproducible cycle. In-cylinder conditions for the first injection cycle were estimated following the same methodology presented in [1] (as explained in Section 2.4) for a 16:1 compression ratio engine at $-20°C$. These conditions have been estimated to be 608 K and 27 bar, which can be considered representative of low temperature cold start condition for being below the threshold conditions shown in Table 2.1.

A fully equipped test cell has been adapted to allow experiments to be performed in an optical engine at room temperature, as sketched in Fig. 3.3. The figure shows the final configuration of the intake and exhaust lines, each of them is equipped with two air flow meters and a settling chamber. The intake line has also been equipped with electrical heaters commanded via PID in order to control intake temperature. Both lines, intake and exhaust, have been connected with a duct that by-pass the engine. The exhaust line has also been equipped with a filter in order to clean exhaust

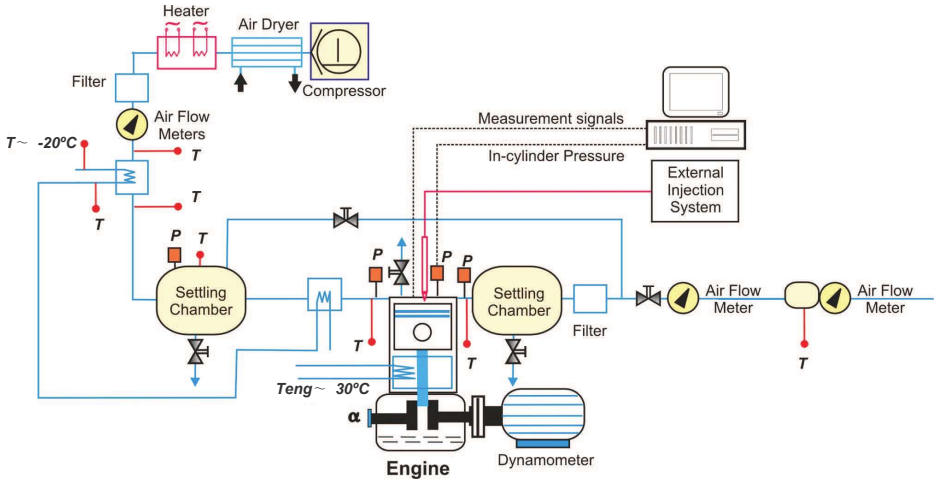

Figure 3.3. *Sketch of the experimental facility used to reproduce the cold start conditions.*

gases before they pass the flow meters. Temperature and pressure sensors have been installed along the whole circuit in order to perform proper control of the fluids.

The engine used is a 4-valve, 0.55 l displacement single cylinder engine with optical access through the bowl. The optical access is sketched in Figure 3.4 and engine specifications are shown in Table 3.1. An elongated piston is used, with a cylindrical bowl with dimensions of 45 x 16 mm ($diameter\ x\ depth$), allowing optical access to the combustion chamber through a sapphire window. The engine is equipped with a standard four-cylinder cylinder head, from which only cylinder number two is used. As compared with a conventional single cylinder engine test bench, some important adaptations have been made to reproduce cold start in-cylinder conditions at room temperature. Major modifications concern those made for reaching the peak compression temperature: engine compression ratio reduction, engine cooling system adaptation, and intake and exhaust lines modification in order to measure the blow-by mass. Other modifications concern peak compression pressure: supercharging and intake pressure stabilization in the intake manifold. Additionally, the electrical motor had to be adapted to set the desired engine speed and other measurement devices were installed and data acquisition systems were modified as required. More details about the modifications performed in the facility and important remarks on its final configuration and operation are described in the following items:

- **Engine geometry:** The solution sketched in Figure 3.4 was adopted to fulfill a two-fold objective: reducing engine compression ratio and allowing the simultaneous use of a glow plug and a pressure transducer.
  - The purpose of reducing compression ratio is to reach a target peak compression temperature of 608 K at room temperature. A first estimation

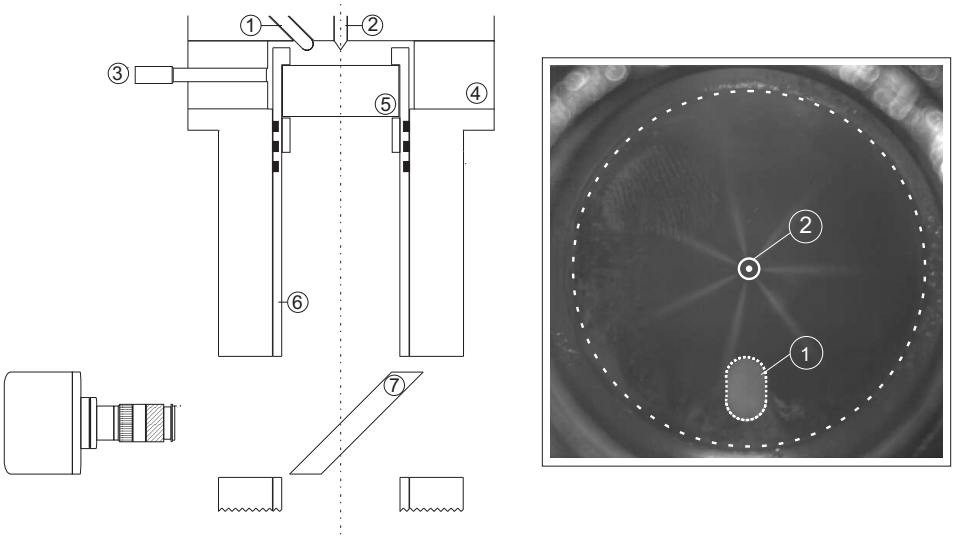

Figure 3.4. *Sketch of the optical access in the single cylinder engine and an image showing how the combustion chamber is seen from the camera point of view. 1.- Glow plug, 2.- Injector nozzle, 3.- Pressure transducer, 4.- Aluminum piece, 5.- Sapphire window, 6.- Elongated piston, 7.- Elliptical UV mirror.*

Table 3.1. *Technical data of the optical engine used during experiments.*

Parameter	Value
Type	Diesel, single-cylinder, 4 strokes
Manufacturer	AVL (Basic unit)
Nominal speed	4200 rpm
Maximum speed	5000 rpm
Maximum in-cylinder pressure	150 bar
Diameter x stroke length	85 mm x 96 mm
Connecting rod length	152 mm
Crank length	48 mm
Swept volume	545.8 cm^3
Compression ratio	18.4 : 1
Bowl diameter	45.0 mm
Bowl depth	16.0 mm
Bowl volume	25.45 cm^3

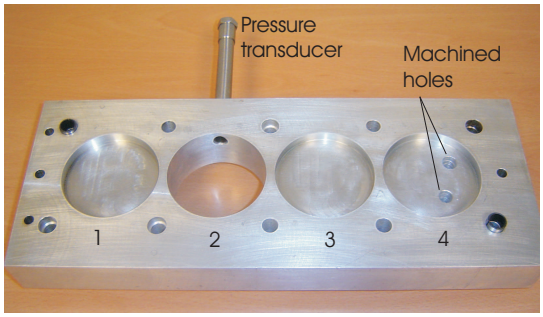

Figure 3.5. *Block elongation piece elaborated to reduce CR and house a pressure transducer.*

was made using the polytropic model presented previously in Equation 2.1, assuming that the polytropic exponent is within the range: $1.33 - 1.35$ and keeping the intake temperature value fixed at 303 K. Target compression ratio resulted to be 8 : 1. This reduction was performed placing an aluminum piece (shown in Figure 3.5), with 42 mm height and internal diameter slightly larger than the engine bore, between the cylinder head and the engine block. It allows to reduce compression ratio but the minimum distance between the piston and the cylinder head and, as a consequence, air movement during compression stroke are not changed considerably.

- Figure 3.5 also shows the volumes left in the other three cylinders to allow normal valve train operation.
- Two holes were machined on cylinder number four to allow real valve lift measurement by means of proximity sensors under motored conditions (independent tests), since the engine uses hydraulic tappets.
- The pressure transducer used is a Kistler 6067C1 type and it was installed on one side of the aluminum piece as shown in Figures 3.4 and 3.5.

- **Engine speed and fluid conditioning:**
  - The optical engine was motored at a constant engine speed of 250 rpm so that real engine time scales during cold starting can be reproduced as close as possible. In order to ensure stable operation at such low speed, the electronics of the electrical motor was modified. Figure 3.6 shows the change in engine speed due to compression and the quick signal stabilization thanks to the electrical motor.
  - An external cooler is used for engine cooling, so that engine water and oil temperature can be set and regulated at $30°C$. Lower temperatures are possible but water condensation problems on the engine surfaces may appear.

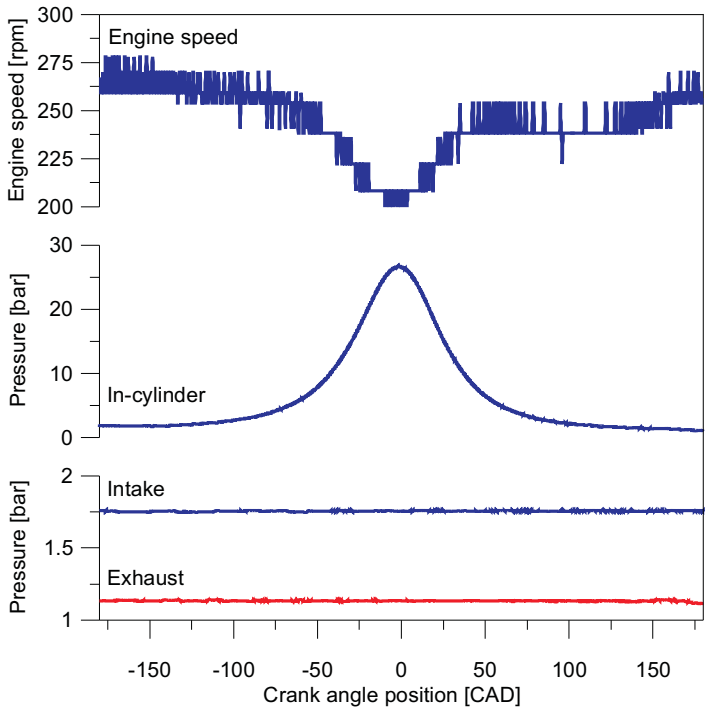

Figure 3.6. *Engine speed (top), in-cylinder pressure (middle) and intake and exhaust manifold pressure (bottom) as a function of the crank angle position for a motored cycle.*

- **Intake air conditioning:**
  - Intake flow measurements are performed simultaneously with two flow meters. A hot wire flow meter (Siemens 5WK9 621 PBT-GF-30), which has been selected to allow proper measurement of the low mass flow of the single cylinder engine operating at low speed, is used as main device. A second volumetric mass flow meter is located downstream of the former for a two-fold reason: on the one hand it allows on-line control of the proper behavior of the hot wire meter, and on the other hand, it allows a further reduction of pressure fluctuations in benefit of the measurement accuracy of the main flow meter.
  - Main intake pressure at the inlet plenum chamber can be set between 1.2 and 2.2 bar. Figure 3.6 also shows in-cylinder pressure and intake and exhaust manifold pressure for a motored cycle as a function of crank angle position. It shows that there are practically no fluctuations in the intake and exhaust pressure signals.
  - Intake air temperature is controlled via PID and measured with a thermocouple placed few millimeters upstream of one of the intake valves.

  - As sketched in 3.3, intake air is supplied by means of a screw compressor, and passes through a dryer, a filter, two mass flow meters, a liquid gas heat exchanger, a plenum chamber and a second heater exchanger before entering the engine. Although very low values of air temperature in the plenum chamber can be reached, it was observed that, due to the low intake mass flow under current operation condition (very low speed), the final temperature at intake valve closing increases up to values close to engine temperature. So, intake air temperature (controlled just upstream of one of the intake valves) was set constant at $30°C$ for all tests. Both oil and water temperature were also set at the same temperature.

- **Exhaust flow control and blow by measurement:**

  - As sketched in 3.3, a hot wire instantaneous gas flow meter (Siemens 5WK9 628 PBT-GF-30) was installed at the engine exhaust, downstream of a plenum chamber, in order to allow determination of real blow-by as the difference between intake and exhaust mass flow rate measurements. To avoid deterioration of the sensor due to fuel deposition (an important part of the fuel injected is not burnt), a filter was installed in the exhaust line upstream the flow rate measurement device. An additional duct connects the intake and exhaust systems for calibration and periodic verification of the proper behavior of the exhaust flow meter. Calibration was carried out under steady flow conditions by means of a by-pass duct that connects intake and exhaust lines. To double check proper exhaust flow measurement, a diaphragm type flow measurement device was installed at the exhaust line end.
  - A valve has been located upstream of the exhaust flow meter for regulation of the exhaust back-pressure.

- **Injection:**

  - A common rail injection system is operated externally so that stable behavior is ensured, avoiding uncertainties associated to ECU (Engine Control Unit) corrections. Injection takes place at a reduced frequency (of the order of one injection every 40 cycles) to avoid any engine temperature increase, speed instability in case of ignition and to reduce window fouling.
  - The cylinder head was slightly modified to allow installation of the injector, which is a piezo electric microsac one. The injector is centered in the cylinder and vertically mounted. In that way, orientation of the sprays relative to the glow plug can be modified by rotating the injector.
  - Commercial diesel fuel was used for all the tests in the present thesis.

- **Ignition aid:** The glow plug used is the standard for the cylinder head [2], which operates at a maximum tension of 11V. With the standard configuration, the glow plug tip penetrates 3mm from the cylinder head plane and is located at 11.5mm from the cylinder axis.

Engine operation and measurement methodology

With the aim of reproducing the first injection cycle in a repeatable and controllable way, the engine is operated at motored steady state conditions. Once all relevant parameters are stabilized (engine temperature, intake gas temperature, intake and exhaust pressures, engine speed,...) and the acquisition systems are ready, injection is performed at a reduced frequency (1 injection every 40 cycles)

The configuration of the acquisition system was specifically modified to allow selection of the measurement temporal windows conveniently. In such way, recording starts in the motored cycle immediately before to an injection cycle and concludes when the injection cycle is completed. In that way, a motored cycle is recorded before every combustion cycle as a reference to control engine repeatability and verify off-line representativeness of the results. Signal acquisition is performed in a temporal base, not angular, due to the low engine speed, at a constant frequency of 50 kHz.
In every test, the following signals are recorded with high temporal resolution:

- Instantaneous in-cylinder pressure.
- Instantaneous intake/exhaust flow meters signals.
- Instantaneous air pressure at the intake/exhaust manifold.
- Instantaneous crankshaft angular position (to calculate engine speed).
- Signal triggering the injection system.
- Command pulse of the injection system.

Other control parameters are recorded on average values, such as: water and oil temperature, temperature at different intake and exhaust systems points, injection pressure, timing values, glow plug tension, etc.

3.2.2 In-cylinder pressure analysis

The one-zone model described by Armas [3] (CALMEC) and recently improved by Martín [4] is the tool employed to perform the combustion analysis. This diagnosis tool allows to calculate the heat released within the cylinder due to combustion. It uses the measured in-cylinder pressure as main input. Then, the first law of thermodynamic is applied between Intake Valve Closing (IVC) and Exhaust Valve Opening (EVO) considering the chamber as an open system because of blow-by and fuel injection. The ideal gas equation of state is used to calculate the mean gas temperature within the chamber. Along with these two basic equations, other sub-models are used to calculate instantaneous volume and heat and mass transfer.

Crank angle-resolved and global cycle parameters can be obtained from CALMEC. Regarding the temporal-resolved parameters, the model main result is the Rate of Heat Release (ROHR) but the temporal evolution of other parameters like the Heat

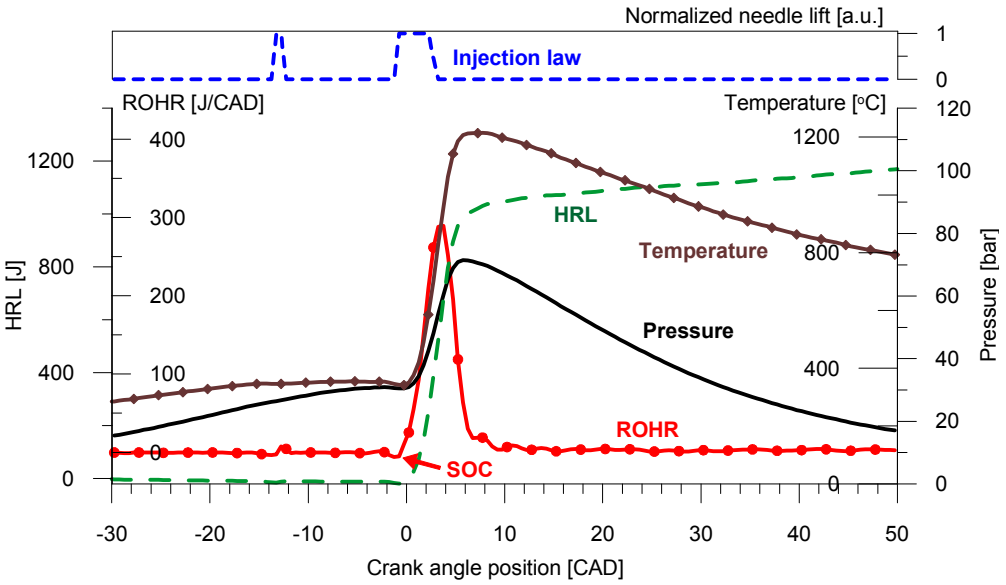

Figure 3.7. *Main parameters obtained from CALMEC plotted as example for a given combustion cycle.*

Release Law (HRL, which is the time-integral of ROHR) or the mean gas temperature can be calculated (they are shown in Figure 3.7). Temporal resolution for these variables depends on the crank angle encoder configuration, which is 0.5 CAD for the present work. With regard to global cycle parameters, Indicated Mean Effective Pressure (IMEP), Start of Combustion (SOC) and Combustion Efficiency (CE) are used in the present study to characterize combustion. SOC has been defined as the crank angle position where the beginning of the strong rise in ROHR due to combustion is detected (see Figure 3.7). And CE has been defined as the ratio between the total energy released in one cycle and the total energy available in the fuel injected. It is calculated by equation 3.1:

$$CE = \frac{100}{m_f \cdot LHV} \cdot \int_{IVC}^{EVO} ROHR(\alpha)\, d\alpha \tag{3.1}$$

where the energy released in one cycle is the integral of the ROHR calculated between IVC and EVO, m_f is the mass of fuel injected and LHV is the fuel lower heating value.

Despite CALMEC was elaborated for systematic use in practically any Diesel engine configuration, it had to be adjusted for cold start studies due to the high cycle to cycle variability. In this case, CALMEC analysis was performed for each one of the firing cycles recorded, instead of calculating a mean in-cylinder pressure trace from a given number of cycles. In this way, each test consists of 20 to 30 separated repetitions to which statistical analysis can be performed. This procedure also enables

Table 3.2. *Engine parameters and in-cylinder conditions reached in the optical engine for a motored test.*

Variable/engine configuration	Commercial	Optical
Compression ratio [-]	16:1	8.1:1
Ambient temperature [$^{\circ}C$]	-20	30
Mass at IVC [mg]	n/a	1197
Temperature at IVC [K]	n/a	312.6
Pressure at IVC [bar]	n/a	1.193
Peak pressure [bar]	27	26.8
Peak temperature [K]	608	607.2
Blow-by level [%]	n/a	1.66

the comparison of cycle-resolved ROHR with simultaneous information from the high speed camera and to detect different possible patterns that occur under the same engine conditions.

Final engine configuration

Tests for validation of the facility operation were performed. A set of motored tests was carried out to determine actual engine compression ratio, verify that target in-cylinder conditions have been achieved, and determine the range of variation achievable in the facility for the main variables. Table 3.2 shows the target commercial engine conditions and the measured and estimated magnitudes of a sample from the motored tests performed for adjustment of CALMEC parameters (mainly thermodynamic delay and heat transfer coefficients). Target pressure (27 bar) and temperature (608 K) were reached with a CR 8.1:1. It was also verified that, in the same way as for the real engine at $-20^{\circ}C$, ignition does not occur in the optical engine without glow-plug aid at the target in-cylinder conditions. These engine conditions are going to remain unchanged along this thesis.

3.2.3 Image acquisition and post-processing

Images have been recorded using a Photron Ultima APX high speed image system with two camera heads. Each camera head is equipped with a 10-bit CMOS sensor and all images in the study have been recorded at an acquisition frequency of 6000 fps with a 512 x 512-pixel image size. The non-intensified camera head, coupled with a

$135 - 400\ mm$ focal length Helmut APO objective with a number 1 close-up lens, was used to record broadband natural luminosity in two ways. First, a set of images was acquired illuminating with an external light source and with long exposure time ($166\ \mu s$) in order to visualize at the same time the Mie-scattering from the liquid spray and flame radiation coming from the first ignition locations. Secondly, combustion radiation images have been recorded without external illumination and camera settings have been adjusted to avoid sensor saturation. Due to the high intensity, this radiation source is assumed to stem from high-temperature reaction locations, where probably soot is present. Most of the quantitative results that will be shown throughout this thesis have been recorded with this optical configuration. For some cases, an intensified camera head was used coupled with a 100 mm focal length UV objective and a 310 nm wavelength interference filter (10 nm FWHM); camera gain was set to its maximum value and the intensifier gate time to 150 μs. The radiation obtained with this configuration was assumed to be OH^* chemiluminescence, as soot radiation is much higher. A discussion on the application of both broadband or OH^* radiation is provided in Chapter 4. A better approximation could be done by proving the existence of OH^* chemiluminescence by means of an spectroscope but the difficulties of the technique applied in such conditions did not allow to make such corroboration.

In order to simplify combustion analysis, time resolved parameters are obtained for every image sequence by means of post-processing. The camera starts recording at the rising edge of the first injection trigger. According to that, if the camera internal delay (few microseconds) is neglected, the first picture corresponds with the injector start of energizing. From here and on, images are acquired every $166\mu s$ during a period which covers the whole combustion event. Each image is saved as a grayscale-*png* image file. With post-processing purposes, a developed software reads every single image, performing the subtraction of a reference background image as sketched in Figure 3.8 and calculates instantaneous and global cycle parameters. In order to separate the flame luminosity from the background, the original picture (left image in Fig. 3.8) is multiplied by a mask delimited by the limits of the piston window, having as a result the image in the middle in Fig. 3.8. Then, segmentation is performed by calculating a threshold value which is equal to the minimum digital level in the image (found in a zone without combustion radiation) plus 15% of the difference between the maximum and the minimum. This percentage has been chosen as a compromise to eliminate light reflected on the liquid spray and the chamber walls without losing much information from the combustion event. The resulting image after segmentation is shown on the right-hand side of Fig. 3.8. Different quantitative parameters have been defined from the processed images. After segmentation, the digital levels of all pixels containing the combustion radiation (with digital levels above the threshold) are added in a single parameter named Cumulative Intensity (I_{cumul}). From the temporal evolution of I_{cumul}, for the whole sequence, the integral is calculated and it is named IL (Integrated Luminosity) and the first luminosity is detected and it is named LD (Luminosity Delay), as shown in Figure 3.9. Finally, pilot probability is defined as, from an ensemble of pilot injection cycles, the percentage of cycles that show any luminosity.

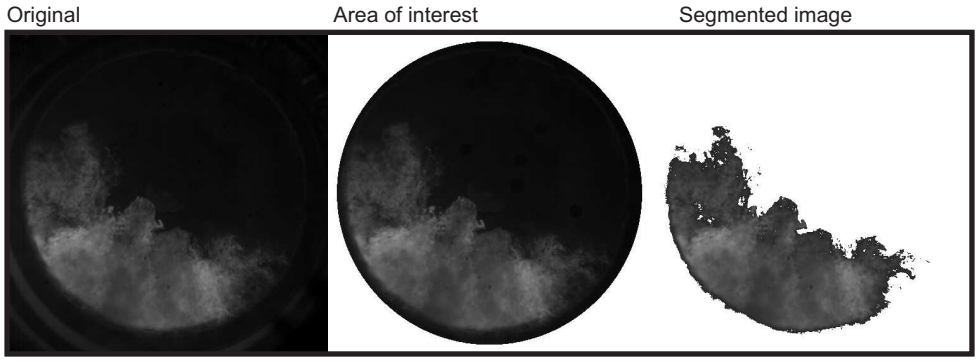

Figure 3.8. *Sketch of the image post-processing routine followed to separate the combustion radiation from the background.*

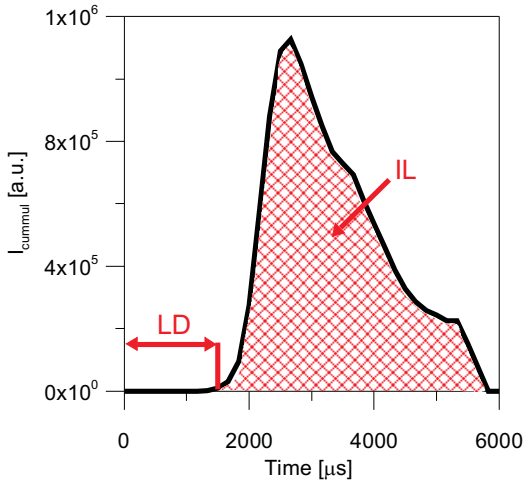

Figure 3.9. *I_{cumul} as a function of time for a pilot injection test. The LD is defined as the time from SOE to flame appearance. And, IL is defined as the area under the I_{cumul} trace.*

3.3 Additional experimental information

Nozzle characterization and spray visualization tests were carried out in order to know the fuel flow characteristics resulting from each one of the nozzles used along this work. These tests consist of nozzle mass flow rate and momentum flux measurements, together with non-vaporizing spray visualization. The information obtained from these tests is going to be used mainly in Chapter 6, where the influence of four different nozzle geometries is studied. In the rest of the thesis, two of those nozzles are used. The nominal characteristics of these nozzles are summarized on Table 3.3.

Table 3.3. *Nominal characteristics of the four multi-orifice injection nozzles selected for the study.*

Parameter/Nozzle	N1	N2	N3	N4
Number of orifices [-]	6	6	7	9
Bosch flow number [$cc/30s$ $100bar$]	250	400	450	450
Included angle[deg]	155	150	153	153
Diameter [mm]	0.121	0.145	0.142	0.125
K-factor [-]	0	1.5	1.5	1.5

These nozzles are representative of those employed nowadays on passenger car diesel engines. The Bosch flow number values range from 250 to 450 cc, the number of orifices from 6 to 9 and the orifice diameters from 0.121 to 0.145 mm.

3.3.1 Mass flow rate

Measurements of injection rate were carried out with an Injection Discharge Rate Curve Indicator (IDRCI) commercial system. This device makes it possible to display and record the data that describes the chronological sequence of an individual fuel injection event. The measuring principle used is the Bosch method [5], which consists of a fuel injector that injects into a fuel-filled measuring tube. The fuel discharge produces a pressure increase inside the tube, which is proportional to the increase in fuel mass. The rate of this pressure increase corresponds to the injection rate. A pressure sensor detects this pressure increase, and an acquisition and display system processes the recorded data for further use. For these tests the fuel temperature was kept at room temperature ($30°C$) and the IDRCI back pressure was set at 27 bar, both values are representative of the engine tests conditions (fuel temperature and in-cylinder pressure at SOI). The fuel temperature value of $30°C$ is a boundary condition in this thesis, the influence of the fuel temperature on fuel injection has been studied with detail in a separated work by Bracho [6].

Injected mass is measured with a precision scale with a two-fold objective. First, it enables the conversion between measured injection rate signal (in volt) and total injected mass. Secondly, it provides with a relationship between duration of injector energizing pulse and the amount of injected mass, which is used to process in-cylinder pressure from engine tests.

Figure 3.10(a) shows the instantaneous mass flow rate as a function of time After Start of Energizing (ASOE) for one of the operating conditions tested. According to this plot, the injection event can be divided in four different periods. First, the hydraulic delay, which lasts from start of energizing to start of injection (approximately $200\mu s$). Secondly, the transient needle lift injection period. In third place, the stationary injection period which is the period during which the needle is

fully open. Finally, the falling transient of the mass flow rate trace which is the needle closing period. For pilot injections, the nozzle needle starts closing during the opening transient injection period and stabilization is never reached (for pilot injections of less than $10mg$). For longer pulses (main injections), stabilization is reached and the average value during the stationary injection period (horizontal dashed line) is used to calculate different discharge parameters.

3.3.2 Momentum flux

Spray momentum flux was measured in a pressurized chamber filled with nitrogen, at the same pressure as in the optical engine at SOI. The nozzle is located within this chamber so that one of the sprays impacts on a piezo-electric pressure sensor, which is placed at 5 mm from the hole exit. This sensor has been calibrated to measure force. The sensor frontal area and position are selected so that spray impingement area is much smaller than that of the sensor. Due to the conservation of momentum, the force measured by the sensor will be the same as the momentum flux at the hole outlet or at any other axial location, since the pressure inside the chamber is constant and surrounds the entire spray, and fuel deflected is perpendicular to the axis direction. A more detailed explanation of the momentum flux measurement test rig and the method principle is shown in [7]. For these tests the chamber back pressure was set at 27 bar and the temperature of the fuel was $30°C$, both values are representative of the engine tests conditions (fuel temperature and in-cylinder pressure at SOI).

Following this methodology, the momentum induced by one spray during the stabilized injection period is measured (transients are not measured properly). All the orifices for the same nozzle are tested in order to check hole-to-hole dispersion, but for the analysis in this thesis only hole-averaged value are used. An example of one of the measurements performed is shown in Figure 3.10(b), where the horizontal dashed line shows how the momentum flux is averaged during the stationary injection period.

3.3.3 Non-vaporizing spray visualization

Spray visualization tests were carried out to characterize the spray evolution (mixing process) during the injection event under well controlled and constant conditions. These tests were carried out using a test rig able of reproducing the same gas density as in the optical engine when injection starts. It is a constant-volume vessel filled with nitrogen at high pressure and at room temperature, thus fuel evaporation is avoided. The test rig is equipped with three optical accesses. Two opposite windows are located on the sides of the injector for illumination purposes, and the other optical access is used for visualization and it is placed in front of the injector, which is horizontally mounted. A PixelFly CCD color camera (12 bit - dynamic range) has been used to record the Mie-scattering signal from the liquid sprays, which are illuminated by means of a flash lamp synchronized with the camera. These tests have been carried out using the camera full resolution of 1280 x 1024. Due

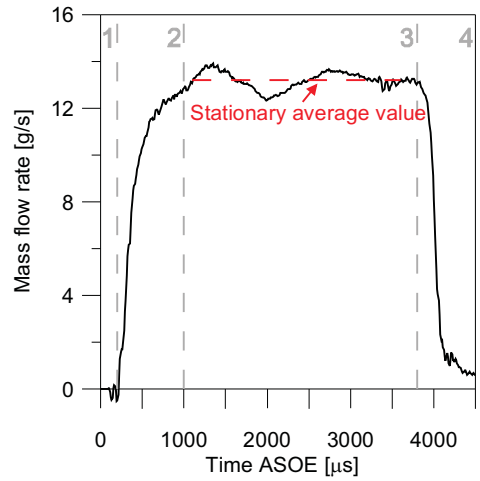

(a) Mass flow rate

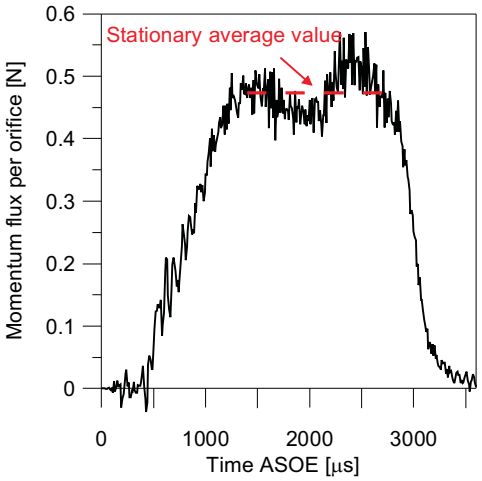

(b) Momentum flux

Figure 3.10. *Injection characterization results sketches. Mass flow rate (a) and momentum flux (b) as a function of time ASOE for one of the conditions tested. Stationary average values are signaled with red lines. In (a), four periods are differentiated: (1) hydraulic delay, (2) rising transient, (3) stationary injection period and (4) injector closing..*

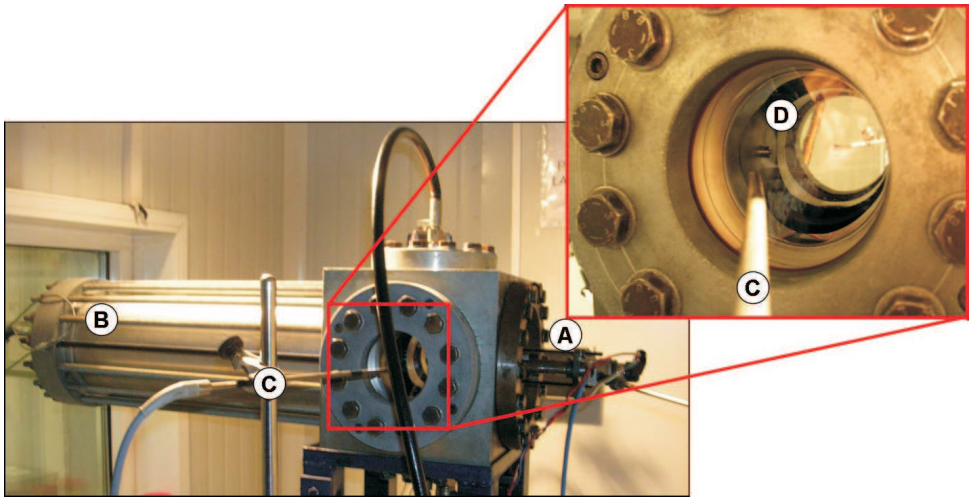

Figure 3.11. *Constant volume vessel used for the non-vaporizing spray visualization tests. (A) injector, (B) N_2 constant-volume vessel, (C) illumination fiber, (D) zoom of the nozzle tip seen through one of the illumination windows.*

to the camera low acquisition velocity only one picture per injection can be taken. Therefore, the spray event was scanned by recording images with a 50 μs interval starting at injector start of energizing. For each time instant five repetitions were recorded.

Images have been digitally processed using the software developed by Palomares [8] and improved by Zapata [9]. This software carry out several tasks in order to deliver the length of each of the sprays for every single picture. First, each original image is read in order to handle the image as a 1280 x 1024-size matrix in which each cell contains the mie-scattering information in terms of digital levels (from 0 to 4096). One of the recorded original images is shown in the top of Figure 3.12 as an example. Secondly, a background image (first of the sequence) is subtracted from each picture in order to get rid of all possible light spots that are normally within the camera field of view and are not caused by sprays. Then, the image is divided in as many sectors as holes has the injector, see Figure 3.12. For each sector, segmentation is performed and the liquid spray is isolated. At the bottom of Figure 3.12 a sketch shows how the spray penetration s is measured for each isolated spray. Further detailed explanations about the processing software are available in references [8, 9].

3.4 Modeling tools

Two modeling tools have been employed as support information for the experimental combustion analysis: chemical kinetics and CFD. Chemical kinetics

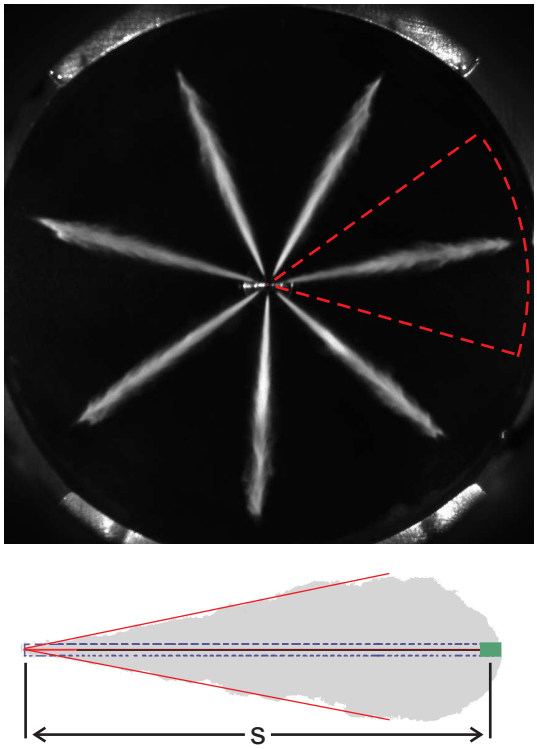

Figure 3.12. *Original image recorded during the non-vaporizing visualization tests (top) and an sketch explaining how spray penetration s is measured (bottom).*

calculations have been carried out in order to have an estimation of the ignition delay times. And CFD calculations have been carried out to provide with information about the flow evolution during and after the injection event.

3.4.1 Chemical kinetics

In order to have an estimation of the delay caused solely by the development of chemical reactions, closed homogeneous reactor conditions have been simulated by means of CHEMKIN-PRO software [10]. This code has been set to solve the time evolution of temperature and species composition for a closed reactor filled with a given fuel and air homogeneous mixture, at a given initial temperature and at constant pressure conditions. The fuel oxidation kinetic mechanism is from n-Heptane [11], which is considered as suitable diesel fuel surrogate in terms of ignition characteristics. From the temperature evolution, ignition delay can be calculated as the time period from start of calculations until a steep rise in temperature is detected (400 K above initial temperature). This simulation can actually serve as an estimation of the chemical delay times obtained within the engine, since in-cylinder pressure remains

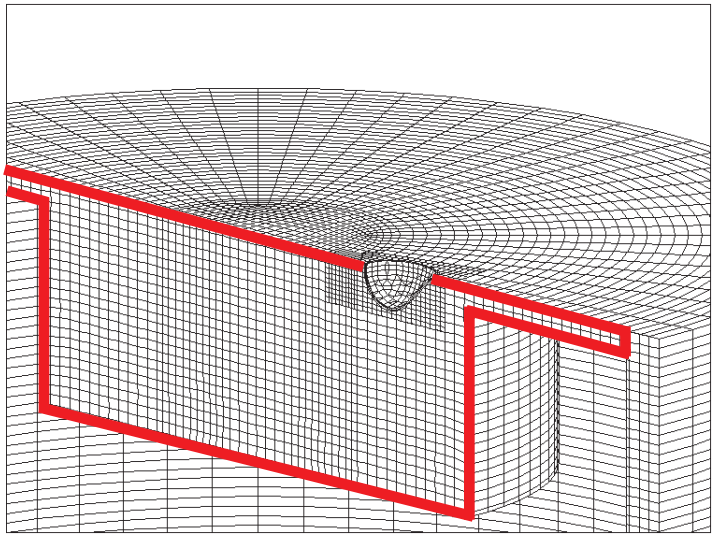

Figure 3.13. *3D view of an axial cut of the computational mesh built for the CFD calculations. The red lines represent the limits of the combustion chamber. The further refined volume around the glow plug can also be observed.*

more or less constant during injection and the first ignition reactions. This constant pressure has been set at 27 *bar* which is the same in-cylinder pressure when injection starts. Equivalence ratio and initial temperature have been swept within wide ranges that cover the conditions expected within the engine. Initial temperature ranges from 600, which is approximately average in-cylinder temperature in a motored test with no glow plug aid, to 1200 K, which is around the temperature reached by the glow plug surface. Equivalence ratio ranges from 0.2 to 2, which is a range that cover expected equivalence ratio values in the ignition zone according to CFD calculations.

3.4.2 CFD calculations

A complete model of the combustion chamber has been built by means of StarCD [12] code with the purpose of supporting experimental information. The main role of this model is to fill an important gap in which no information can be obtained by the experimental tools, from SOI until flame appearance. A computational grid has been carefully developed that resolves accurately the combustion chamber, crevice volumes and the glow plug surface as similar as possible to the real engine geometry. Typical grid size is around 1 mm, and it has been further refined around the glow plug region due to the relevance of this volume during first ignition stages, as shown in Figure 3.13.

Regarding the models employed, a standard lagrangian approach (DDM [13]) is used for fuel spray modeling. Huh-Gosman [14] and Reitz-Diwakar [15] models are

applied for primary and secondary break-up, respectively. Fuel physical properties are given by the so-called DF1 [16] diesel fuel surrogate. Turbulent flow is modeled with the RNG $k-\epsilon$ model and standard wall functions. And no combustion model has been used.

Concerning initial and boundary conditions, spray outlet, mass flow and velocity boundary conditions are obtained from injection mass flow rate and momentum flux measurements. Both, initial conditions at IVC and wall temperatures, have been estimated by means of CALMEC [4, 17] from experimental data. A wheel-flow velocity profile with swirl number 2.2 is used for air-flow initialization, and a constant temperature boundary condition (1373 K) is applied on the glow plug surface.

The flow solver uses the PISO algorithm [18] in order to solve pressure-velocity coupling. A second order scheme is used for momentum and turbulence equations, while first order upwind is applied for enthalpy and species equations. Calculations run from IVC until SOI with 10-5 s time-step and 10-6 s from SOI onward.

3.5 Conclusions

The tools and methodology employed in this work have been described in this chapter. They have been developed, set up and validated with the purpose of allowing to perform systematic studies for understanding cold start combustion processes.

Different experimental and theoretical tools are employed, but the main tool is an experimental facility that, operating at room temperature, can reproduce in-cylinder thermodynamic conditions representative of those of real passenger car engines during start at very low ambient temperatures. This facility is based on a conventional single cylinder research engine with optical access through the piston bowl adapted in order to simulate real engine cold start. Major modifications concern (a) compression ratio reduction and intake temperature control to achieve in-cylinder peak temperature. (b) Engine speed control at a very low range as in the real engine. (c) Control of all engine fluids temperature (water, oil and fuel) to the minimum value achievable to avoid moisture condensation problems on engine surfaces. (d) Measurement of instantaneous intake and exhaust mass flow rate to indirectly measure blow-by. Under its final configuration, the facility is capable of reproducing, systematically and repeatably, a difficult to simulate regime under well controlled low speed and low temperature conditions. Such conditions are repeatably reproduced thanks to the fact that the engine is used in skip-fire mode (1 injection every 40 engine cycles), which is not common in this kind of studies. Thermodynamic in-cylinder conditions are set to values where ignition probability is low, *i.e.* in the borderline between ignition and misfiring, so that the effect of the different individual geometrical and operation parameters upon ignition success can be assessed. The main engine variables can be measured reliably in order to perform in-cylinder pressure analysis and it can be combined with high-speed visualization.

Other tools have been employed to give support and complement the information given by the experimental combustion analysis performed in the optical engine, *i.e.* nozzle flow characterization and specific modeling tools.

It can be concluded that the facility and methodology presented are certainly useful tools to improve understanding on cold start process of passenger car Diesel engines with glow plugs at very low ambient temperature. The influence of the main parameters controlling the cold start process can be isolated on the basis of systematic experiments in an optical engine. Studies reported in the present study aim to shed some light on this complex process and on the relevance of main engine parameters and physical processes affecting ignition success.

Bibliography

[1] Broatch A., Ruiz S., Margot X. and Gil A. "Methodology to estimate the threshold in-cylinder temperature for self-ignition of fuel during cold start of Diesel engines". *Energy*, Vol. 35, pp. 2251–2260, March 2010.

[2] Lindl Bruno and Schmitz Heinz-Georg. "Cold-start equipment for diesel direct-injection engines". *SAE Paper 1999-01-1244*, 1999.

[3] Armas Octavio. *Diagnóstico experimental del proceso de combustión en motores diesel de inyección directa.* Tesis Doctoral, Departamento de Máquinas y Motores térmicos. Universidad Politécnica de Valencia, Valencia, 1998.

[4] Martín Díaz Jaime. *Aportación al Diagnóstico de la combustión en motores diesel de inyección directa.* Tesis Doctoral, Departamento de Máquinas y Motores térmicos. Universidad Politécnica de Valencia, Valencia, 2007.

[5] Bosch W. "The fuel rate indicator: a new measuring instrument for display of the characteristics of individual injection". *SAE Paper 660749*, 1966.

[6] Bracho León Gabriela. *Experimental and theoretical study of the direct diesel injection process at low temperatures.* Tesis Doctoral, Departamento de Máquinas y Motores térmicos. Universidad Politécnica de Valencia, July 2011.

[7] Gimeno Jaime. *Estudio de la inyección diesel mediante la medida del flujo de cantidad de movimiento del chorro.* Editorial Reverté, 2011.

[8] Palomares Alberto. *Análisis de imágenes de chorros diesel.* Tesis Doctoral, Departamento de Máquinas y Motores térmicos. Universidad Politécnica de Valencia, Noviembre 2000.

[9] Zapata Luis Daniel. *Caracterización de los procesos de inyección-combustión diesel mediante visualización y procesado digital de imágenes.* Tesis Doctoral, Departamento de Máquinas y Motores térmicos. Universidad Politécnica de Valencia, Noviembre 2010.

[10] REACTION-DESIGN. *CHEMKIN-PRO, Reaction Design: San Diego, 2008.*

[11] Curran H. J., Gaffuri P., Pitz W. J. and Westbrook C. K. "A comprehensive modeling study of n-Heptane oxidation". *Combustion and Flame*, Vol. 114, pp. 149–177, 1998.

[12] CD-Adapco. *Star-CD Methodology, Version 3.26.* CD-Adapco, 2005.

[13] Dukowicz John K. "A particle-fluid numerical model for liquid sprays". *Journal of Computational Physics*, Vol. 35 n^o 2, pp. 229–253, 1980.

[14] Huh K. Y. and Gosman A.D. "A Phenomenological Model of Diesel Spray Atomization". In *Proceedings of the International Conference on Multiphase Flows*, September 1991.

[15] Reitz R. D. and Diwakar R. "Structure of High-Pressure Fuel Sprays". *SAE Paper 870598*, 1987.

[16] Habchi Chawki, Lafossas Francois A., Beard Philippe and Broseta D. "Formulation of a One-Component Fuel Lumping Model to Assess the Effects of Fuel Thermodynamic Properties on Internal Combustion Engine Mixture Preparation and Combustion". *SAE Paper 2004-01-1996*, June 2004.

[17] Lapuerta M., Armas O. and Hernández J.J. "Diagnosis of DI Diesel combustion from in-cylinder pressure signal by estimation of mean thermodynamic properties of the gas". *Applied Thermal Engineering*, Vol. 19 n^o 15, pp. 513–529, May 1999.

[18] Issa R. I. "Solution of the implicitly discretized fluid flow equations by operator-splitting". *J. Comp. Phys*, Vol. 62, pp. 40–65, 1986.

Chapter 4

Phenomenological description of the low temperature cold start combustion process

Contents

4.1 Introduction

This Chapter presents a phenomenological description of the most relevant events that occur during cold start combustion. The objective is to provide with a mental picture of the events that will be used throughout the thesis to guide the analysis of subsequent parametric studies. According to the methodology presented in the previous chapter, ignition and combustion development are characterized by means of high speed visualization and in-cylinder pressure analysis. After that, first parametric variations are presented with the purpose of understanding the mechanisms that control ignition and combustion progress. At the end of the chapter,

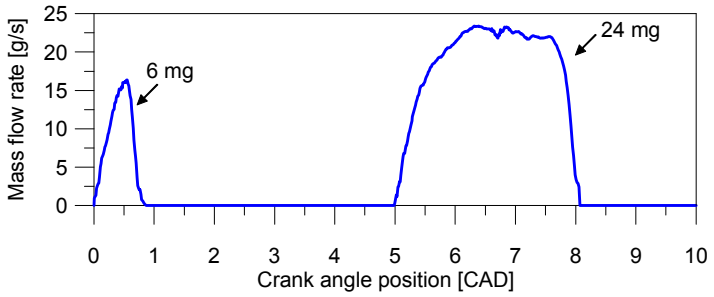

Figure 4.1. *Example of the nominal injection strategy. 6mg of fuel are injected at TDC and 24mg are injected at 5CAD with a rail pressure of* 250 *bar.*

a phenomenological description is actually built and presented as a summary of the events that are believed to occur during the cold start combustion sequence. The phenomenological description, combustion characterization and parametric variations shown in this chapter are the result of a synthesis process applied to a larger number of tests performed in the optical engine, including those presented in Chapters 5 and 6.

According to the methodology described in Chapter 3, in-cylinder conditions are chosen to be representative of the first injection cycle during the starting sequence of a real engine. This establishes fixed in-cylinder thermodynamic conditions, with 27 *bar* and 600 K at TDC. Regarding hardware settings, injector position is such that one of the sprays is oriented at 10° from the glow plug in down-swirl direction, and the glow plug is supplied with nominal voltage (11 V). Regarding injection settings, a pilot + main injection strategy, which is sketched in Figure 4.1, is used. This strategy consists of a first 6 mg injection pulse injected at TDC and a 24 mg one injected at 5 CAD. Injector nozzle N3 (see Table 3.3) has been employed for most of this study. It is a 7-hole nozzle with nominal orifice diameter of 0.142 mm and K-factor equal to 1.5. An exception is made in Sub-section 4.3.2, in which results obtained with nozzle N1 complement the explanation given in this chapter. It is a 6-hole nozzle with cylindrical orifices with diameter equal to 0.121 mm. Differences between nozzles N1 and N3 will be investigated in Chapter 6, but they should not affect this description.

Regarding the parametric variations, rail pressure and the amount of fuel injected have been changed and the specific values tested are presented in Table 4.1. Two levels of rail pressure were tested. The lower one is the minimum value for stable behavior at short injection pulses, while the higher one is a value close to the limit above which ignition cannot be achieved in the optical engine. A difference of 50 *bar* in the lowest level of rail pressure exists between both nozzles used, but it should not affect this phenomenological description. For both levels of rail pressure, three different amounts of mass were tested when isolating pilot injection, and four different amounts of mass were tested for the main pulse, keeping the pilot injection mass constant.

Table 4.1. *Test matrix of conditions tested in Chapter 4.*

Rail pressure bar	Nozzle -	$m_{f,pilot}$ mg	$m_{f,main}$ mg
Nominal strategy			
250/370	N3	6	24
Pilot injection			
250/370	N3	3	-
250/370	N3	6	-
250/370	N3	12	-
Main injection			
200/370	N1	6	24
200/370	N1	6	44
200/370	N1	6	64
200/370	N1	6	84

4.2 General description of the combustion event

This section comprises a detailed description of how combustion progresses for the full (*i.e.* pilot + main) injection strategy. After that, the main characteristics of the pilot injection flame are investigated by injecting a single pilot pulse. The full injection strategy description starts from the observation of global cycle combustion parameters and it is completed with the study of cycle-resolved information by means of visualization and in-cylinder pressure. Pilot characterization is presented at the end of the section by means of visualization.

In agreement with what has been observed in the literature, the performance of a firing cycle under the engine conditions reproduced in this study is difficult to predict. It is believed that these kind of conditions are in the borderline between combustion and misfiring. Accordingly, variation of local conditions due to turbulence or to cycle-to-cycle scattering can prevent combustion from starting or progressing. A sample of 30 firing cycles was obtained under this borderline conditions and their global combustion characteristics as derived from pressure-signal analysis (Indicated Mean Effective Pressure IMEP, Start of Combustion SOC and Combustion Efficiency CE) are presented in Figure 4.2. In this plot, IMEP represents the work obtained from the high-pressure loop of the pressure-volume diagram. SOC is defined as the crank angle position where heat release rate becomes larger than zero. Although visualization results show the presence of a pilot flame for some of the cycles, heat release is within the level of noise of the ROHR curve, and therefore SOC on the plot is always linked to the start of combustion of the main injection. Finally, CE is a measure of the percentage of energy that has been released as heat during the working cycle. In these

firing cycles, pilot injection starts at 0 CAD and the main pulse starts at 5 CAD. Start of combustion was detected with a certain delay with respect to SOI_{main} but before the EOI_{main}, which has been plotted in the figure with a dashed line. The most remarkable fact about SOC is the scattering. Under the same engine conditions, combustion start can be distributed from close to the start of injection to close to the end. This evidences certain ignition difficulties in spite of the fact that ignition is achieved for all the repetitions. Regarding IMEP, values are low and disperse. They are within the range between 2.5 and 4 bar, which can be considered low for the start phase of the starting sequence of a real engine (load must be in the range $8-11$ bar [1] since in addition to the work devoted to speed-up the engine, mechanical losses have to be overcome). Dispersion is also high for IMEP, the coefficient of variation of IMEP (COV_{IMEP}) being equal to 8.77%. Under stable engine situations, this coefficient is around-below 1% [2] and according to Heywood [3] driveability problems results if it exceeds 10%. This dispersion in IMEP seems to be related to some extent with SOC, higher IMEP values are obtained if SOC occurs close to SOI_{main}. Finally CE values attained are low. In general, only around 50% of the fuel is burnt during the whole expansion stroke. Such incomplete combustion conditions should be causing the extra emissions of UHC and CO reported previously by Bielaczyc *et al.* [4]. Under conventional diesel conditions, combustion efficiency is normally above 98% [3] since diesel engines usually operate with lean mixtures. Lower efficiency values are usually reached in gasoline engines for mixtures richer than stoichiometric, as lack of oxygen prevents complete combustion of the fuel carbon and hydrogen. In this case, low combustion efficiency is mainly a result of the poor combustion development for the pilot injection, as well as the large quantity of fuel deposited on the bowl wall, as a result of the poor vaporizing conditions. This non-conventional result is also evidenced in the linear relationship observed between CE and IMEP, namely cycles with high IMEP correspond to cycles with high CE and vice-versa. Although not shown in the plot, a linear relationship between IMEP and CE has been found, with $R^2 = 0.96$, which confirms the link between combustion efficiency and engine performance under these operating conditions. In general, IMEP depends on combustion efficiency and temporal distribution along the cycle. The second factor is usually more important than the first one under conventional engine conditions. For cold start combustion, the previous link between IMEP and CE indicates that any improvement in fuel combustion will directly improve engine performance under cold start conditions.

In order to have a qualitative picture of how combustion progresses within the cylinder, Figure 4.3 shows an image sequence that corresponds to a high performance (high IMEP and early SOC) combustion cycle. In spite of the fact that saturation in the images eventually occurs, this sequence was recorded with the high speed camera with long exposure time and using external illumination with the purpose of providing as much detail as possible of the ignition process. This temporal sequence of events starts at 133 μs, when pilot injection has already begun. During pilot injection, sprays penetrate rapidly into the chamber reaching the bowl wall within a short time (at 300 μs). From this moment until EOI_{pilot}, liquid fuel is seen to impinge on the walls. After the EOI, at 633 μs, liquid fuel is observed to vanish from the injector toward the chamber walls. Up to this moment, no reaction has been observed in any of the sprays.

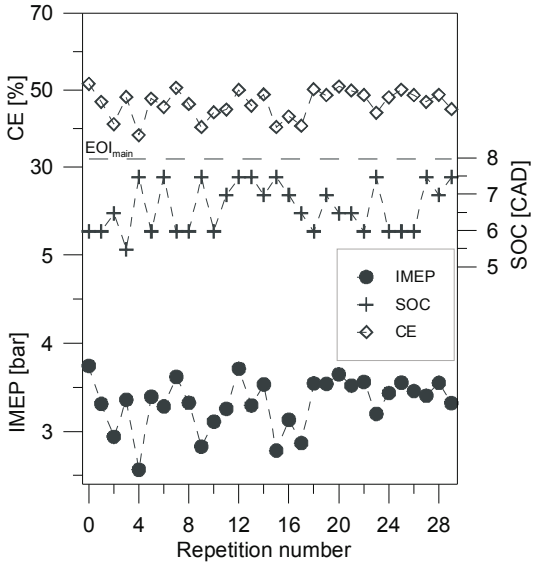

Figure 4.2. *IMEP, SOC and CE versus the repetition number for a 30 repetitions test. Rail pressure is* 250 *bar and a pilot + main injection strategy,* 6 *mg at* 0 *CAD and* 24 *mg at* 5 *CAD, is used.* EOI_{main} *is plotted on the SOC axis as a reference of the injection duration.*

Only some time after EOI_{pilot}, at 1633 μs, some small radiation spots are detected by the camera on the down-swirl side of the glow plug. Subsequent images show how these ignition sites travel toward the bowl wall and a small flame is formed. Due to the location of the first luminosity spot, and also to the later path followed by this small flame, it can be stated that the fuel burnt corresponds to the spray closest to the glow plug. Pilot flame remains attached to the bowl wall during the period between both injection pulses. Main injection combustion starts as soon as the closest spray to the glow plug reaches the pilot flame (at 4467 μs). The flame starts propagating toward the rest of the chamber, as shown in the image acquired at 5467 μs. The other sprays, illuminated by the light source or by the flame radiation, are seen to impinge on the bowl wall, and some liquid fuel is seen to flow on the window wall toward the center of the image, although no visual indication of the autoignition of any other sprays further away from the initial reaction zone is obtained. After a short period (at 5800 μs), the initial flame has spread over the two adjacent sprays, and burns the fuel in those zones. At this time, the main injection finishes but the flame can still be seen to propagate a little further in subsequent instants (6800 μs). From here and on, camera saturation prevents from understanding any further progress in combustion.

With the same purpose and the same camera settings, a similar image sequence (shown in Figure 4.4) was acquired for a low performance combustion cycle (low IMEP and late SOC). In this sequence, pilot injection occurs similarly as in the high performance cycle but no flame radiation is observed coming from the fuel injected in this first pulse. Subsequently, the main injection starts and the first luminosity spots

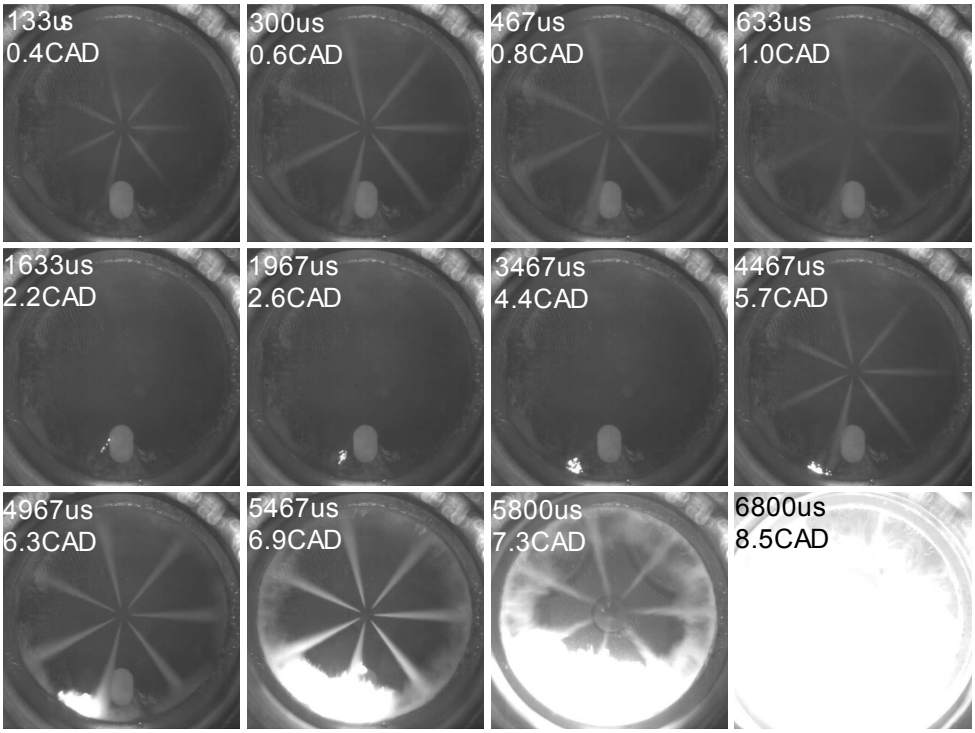

Figure 4.3. *Image sequence for a high performance combustion cycle. Pilot injection (6 mg) starts at 0 CAD and main injection (24 mg) starts at 5 CAD. Rail pressure 370 bar. In the top-left corner of each image the acquisition time ASOI and the crank angle position are shown.*

are observed to appear in the glow plug vicinity before the end of injection. After some time, main injection finishes and images show that the flame has not progressed as much as in the previously analyzed cycle. In fact, at this time the visible flame is similar in intensity to the pilot flame in Figure 4.3. After end of injection, this flame grows at a slower rate burning a small zone within the chamber close to the glow plug. The comparison between Figures 4.3 and 4.4 indicates that main combustion is developing later as a consequence of the absence of a pilot flame. This is a first indication of the link between pilot and flame combustion, which will be observed in subsequent studies along this thesis.

To provide with information on events happening when saturation occurs in previous image sequences, camera settings have been modified to reduce sensor exposure time. As a consequence, camera sensitivity to low intensity events is lower, but processes during main combustion can be adequately observed. The selected cycle, shown in Figure 4.5(a), corresponds to the repetition zero of the test presented previously in Figure 4.2. The combustion sequence begins with the injection of the

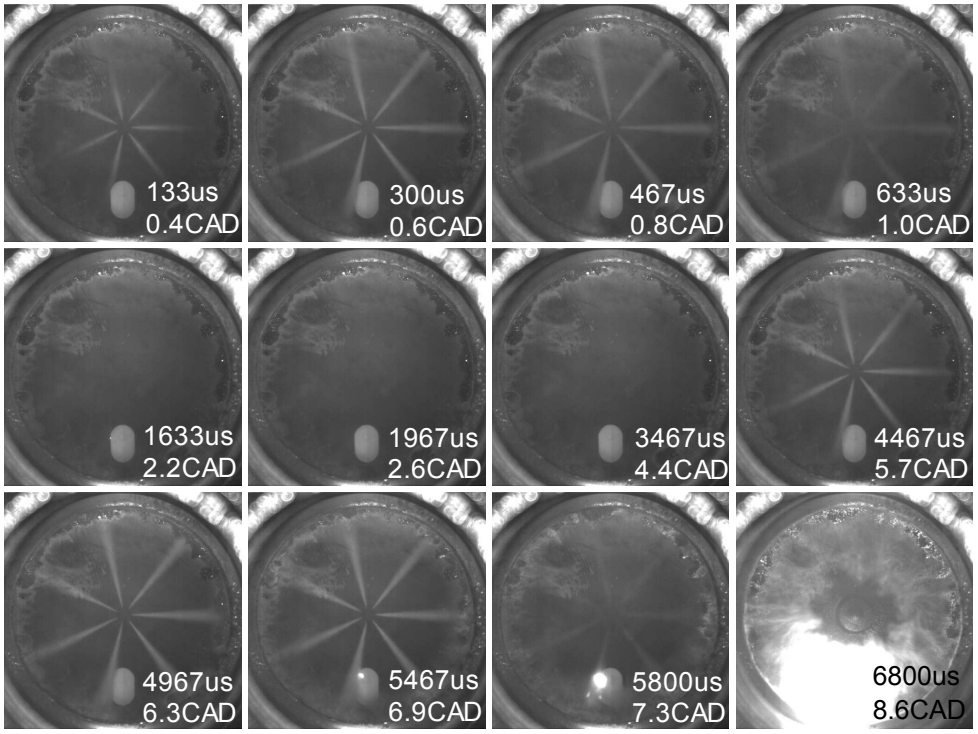

Figure 4.4. *Image sequence for a low performance combustion cycle. Pilot injection (6 mg) starts at 0 CAD and main injection (24 mg) starts at 5 CAD. Rail pressure 370 bar. In the bottom-right corner of each image the acquisition time ASOI and the crank angle position are shown.*

pilot pulse at TDC. From here until SOC of main injection little information is available, since the ROHR signal is on noise level and the luminosity detected is also low due to the camera settings. Main combustion starts at 4770μs, which is the moment when the main injection pulse reaches the pilot flame. Subsequently, visible flame grows in size and luminosity (I_{cumul}), which also corresponds to a more intense heat release (ROHR). The reaction zone maintains a compact appearance with high-intensity radiation. During this initial period, flame propagation is interacting with the injection event from the initial spray (1) to the adjacent ones (2 and 7) and toward the center of the chamber (images at 6437 and 6937 μs). After EOI, flame propagation interacts with the decelerating flow; thus both ROHR and I_{cumul} still increase at a lower rate until the first peak in ROHR trace is reached. Later, at 7937 μs, flame appearance is not as compact as before and increasing number of unconnected bright zones can be seen over the previous flame limits (between sprays 3 and 6). Then, at 9770 μs, these highly disperse bright zones extend to the zones where combustion was not seen before. The next paragraph will show that this is an indication of non-visible chemical activity out of the compact flame, since during

this period the ROHR still reaches a second maximum. Meanwhile, the bulk compact flame is still observed in the zone where ignition started (between sprays 2 and 7). In the later part of the cycle, the ROHR decreases and combustion seems to be located both at the initial zone where it appeared and also attached to the bowl wall forming a kind of flame ring that lasts for a long period. This is a diffusion flame that most probably occurs due to the high amount of liquid fuel that is deposited on the wall as a result of the low in-cylinder temperature and density. The fact that it burns fuel during an important fact of the expansion stroke does not guarantee that all fuel is burnt, so this indicates that fuel deposition on the wall may explain low combustion efficiency obtained under these operating conditions (Figure 4.2)

To further clarify the part of the combustion sequence after EOI, Figure 4.5(b) compares OH^* and broadband radiation for two cycles obtained at an independent test but under the same in-cylinder conditions and using the same injection strategy. Both cycles presented a very similar ROHR evolution. In this sequence, the first pair of images corresponds to SOC, at 4916 μs, in which luminosity is only observed in the broadband radiation images, probably due to limitations in sensitivity for OH^* radiation. The second pair, which corresponds to the moment at which the main injection is finishing (7572 μs), shows that the reaction structure in both pictures is very similar, with a relatively compact flame that is spreading across the combustion chamber. Later on, the bulk visible flame is seen to stop growing, and the less compact zones progress throughout the remaining parts of the combustion chamber. Nevertheless, OH^* radiation images do show the reaction extending over zones beyond the visible flame, while still keeping a relatively compact appearance. This is shown in the last two pairs of images, indicating that there exists a non-visible combustion process that sweeps the combustion chamber. This non-visible combustion activity may also be related with the small bright spots seen on the less compact zones in the broadband-luminosity images, which seem to advance together with the non-visible flame front. During the injection event, this process emits a strong radiation, most probably due to soot presence, but after EOI the further progress of this combustion zone emits non-visible radiation. In this sense, recent results [5] under more conventional engine operating conditions have shown that EOI produces a fast deceleration of the spray flow, as well as a rapid leaning of the mixture. This could explain that radiation becomes much lower in intensity.

4.2.1 Pilot combustion characteristics

According to the results in the previous subsection, pilot combustion can be observed in cycles with better performance, whereas no indication of pilot flame is obtained in cycles with lower IMEP. This seems to indicate that pilot ignition success is linked to main combustion progress, and hence to the work produced in the cycle. This sub-section shows the main characteristics of the pilot injection flame appearance and progress for the reference conditions treated in this chapter. In this case, no illumination source was used and only a pilot pulse has been injected with the purpose of adjusting the camera settings to take advantage of the whole

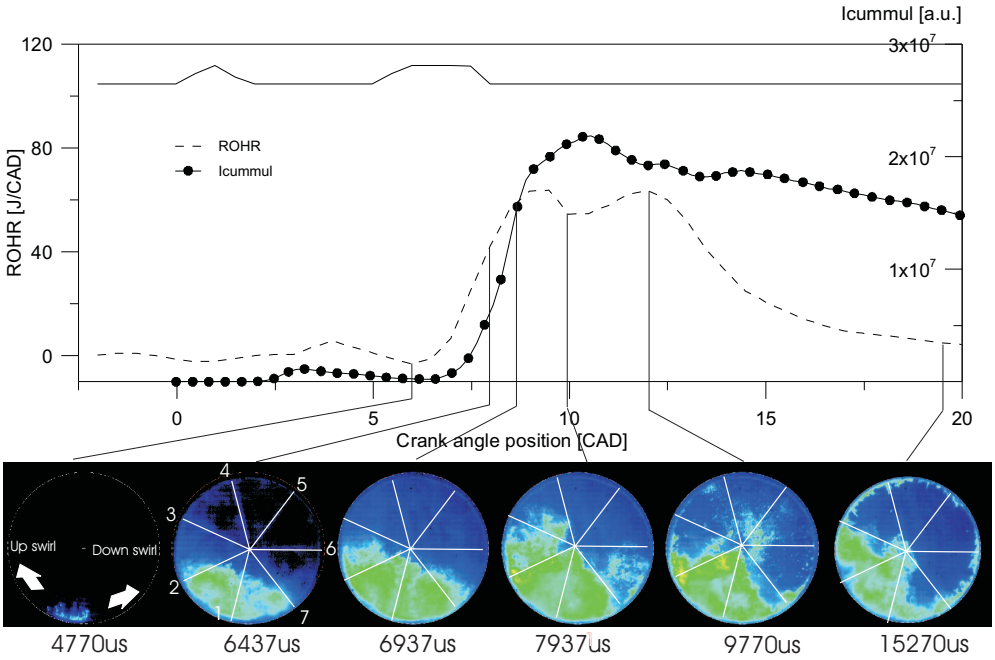

(a) Injection pulse, ROHR and I_{cumul} as a function of the crank angle position

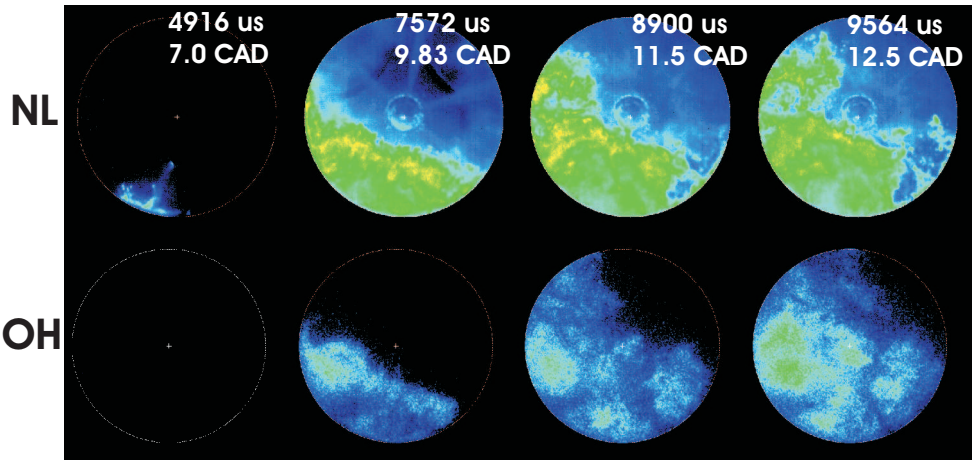

(b) broadband luminosity (NL) and OH^* radiation selected images of similar injection cycles

Figure 4.5. *(a) Injection pulse, ROHR and I_{cumul} as a function of the crank angle position with selected images of a combustion cycle with 250 bar of rail pressure, pilot injection of 6 mg injected at 0 CAD and main pulse of 24 mg at 5 CAD. White straight lines on the images correspond to the approximate location of the sprays. (b) Images corresponding to two combustion sequences: on the top, images of broadband luminosity (NL); and on the bottom, images of OH^* radiation. Acquisition time (ASOI) and its corresponding crank angle position are shown in the top-right corner of each image.*

camera dynamic range avoiding saturation due to the intense radiation released by the combustion of the main injection pulse.

Main characteristics of pilot ignition and subsequent development can be observed in Figure 4.6. In this figure, the results concerning a pilot injection test of 20 repetitions recorded with the high speed camera are shown. These results are synthesized in terms of LD, IL and the location of the first luminosity spot in the 2D view of the camera. The first noticeable fact is that flame luminosity is not detected for all repetitions. Cycles 5 and 14 do not reach conditions to release visible light, showing that cycle dispersion, observed for the full injection strategy in Figure 4.2 in terms of performance parameters, is also occurring for the pilot injection. Secondly, luminosity appearance for all cases always occurs well after EOI_{pilot}, as already shown in Figure 4.3. The timing of these first luminosity spots is distributed between a minimum value, around 1400 μs, and a maximum of 2500μs. No radiation is observed for either shorter or longer timings, which could be the indication that the time period in which fuel ignition should be reached is limited, and out of this period combustion may be inhibited. Similarly, IL also exhibits strong scattering with certain correlation with LD: repetitions with longest LD generally show lowest IL, and vice-versa. This correlation should be caused by the temporal fuel availability close to the glow plug and not due to piston expansion cooling, since even for the longest ignition delay (2500 μs) piston is still close to TDC (around 4 CAD). Finally first luminosity spots appear always on the glow plug side closest to the spray in agreement with results in [6]. The fuel burnt in the pilot flame should correspond to the fuel injected in the closest to the glow plug spray, since it does not seem feasible that fuel from any other spray further away reaches the glow plug.

4.3 Effect of rail pressure and total injected mass

Due to the fact that in-cylinder thermodynamic conditions are somehow fixed in cold start sequence, injection settings are the most basic parameters to be changed in order to improve startability. This section comprises the variation of two injection settings: rail pressure and the total amount of injected mass. These variations are shown first for the isolated pilot injection pulse and subsequently for the full injection strategy.

4.3.1 Pilot injection

In order to shed some light on the mechanisms that lead to ignition under glow plug-assisted cold start conditions, this sub-section presents a combined study in which three different amounts of injected mass per orifice (0.43, 0.86 and 1.71 mg per orifice) have been tested at two levels of rail pressure (250 and 370 bar, see Table 4.1). These results are shown in terms of injected mass per orifice, since ignition occurs only due to the fuel injected by the spray closest to the glow plug. Nozzle characterization results indicate that, within the range of injection conditions used in

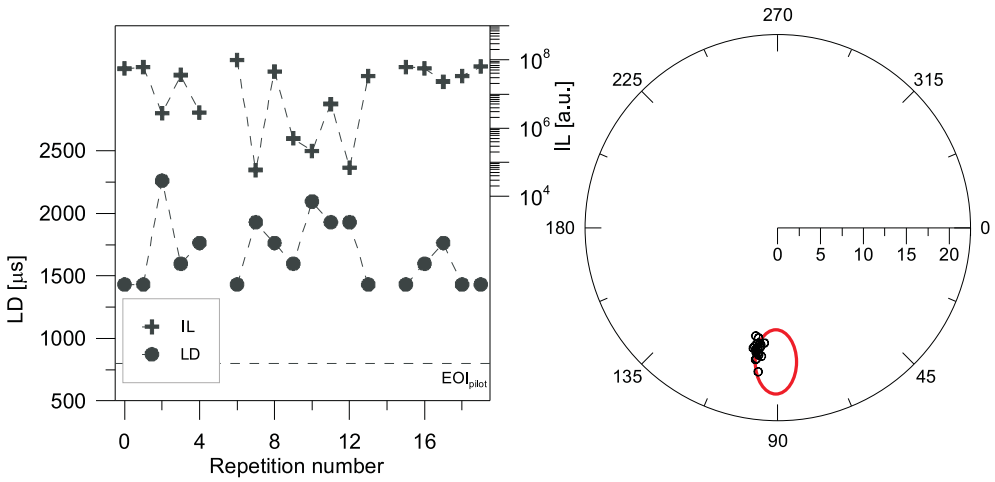

Figure 4.6. *Left: LD and IL versus repetition number for a single pilot injection test with* 20 *repetitions.* 6 *mg are injected at TDC with a rail pressure of* 250 *bar. Right: Location of the first luminosity spot detected plotted in polar coordinates; the red ellipse is a sketch of the glow plug.*

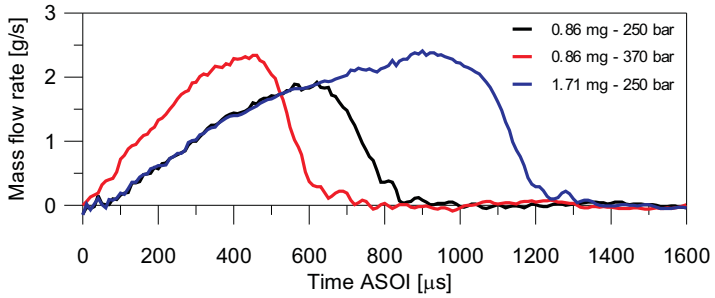

Figure 4.7. *Injection rate per orifice as a function of time ASOI for three different pilot injection strategies:* 0.86 *mg at* 250 *and* 370 *bar, and* 1.71 *mg at* 250 *bar.*

this study, a change in any of both, rail pressure or fuel mass involves a change in the shape of the injection rate, as shown in Figure 4.7. This is due to the short duration of pilot pulses, for which needle never reaches full lift and hence injection rate is never stabilized. As a consequence, a change in pulse duration modifies both injected mass and momentum of the spray, whereas a change in pressure only modifies the latter variable.

The effects of rail pressure and fuel injected mass are shown in terms of pilot probability (percentage of cycles of the sample where luminosity is observed), LD and IL in Figures 4.8(a) and 4.8(b), respectively. To start with, pilot probability is

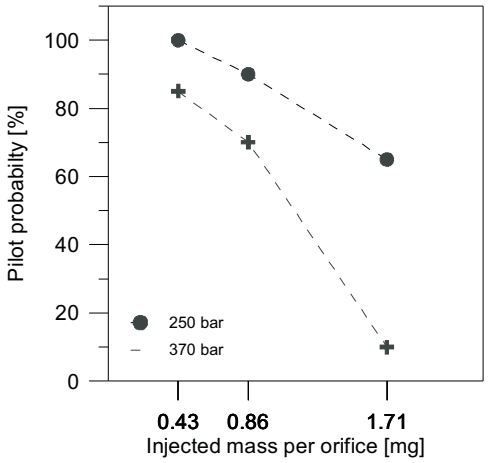

(a) Pilot probability as a function of the injected mass per orifice for two levels of rail pressure.

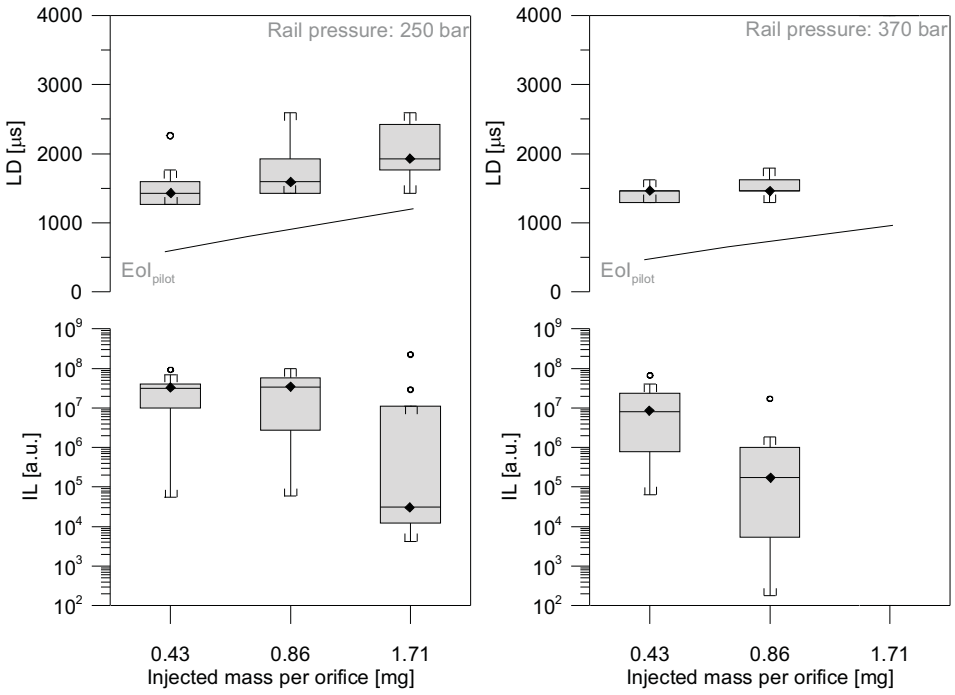

(b) Injection pulse, ROHR and I_{cumul} as a function of the crank angle position

Figure 4.8. *Pilot injection tests results for both levels of rail pressure,* 250 *and* 370 *bar. (a) Pilot probability as a function of the injected mass per orifice. (b) Box-Whisker plots for LD (top) and IL (bottom) as a function of the injected mass per orifice. Unfilled dots represent the outliers which have been calculated with a factor of* 1.5 *times the interquartile range.*

shown in Figure 4.8(a) as a function of injected mass per orifice for both levels of rail pressure. This plot shows how pilot probability decreases with increasing rail pressure and/or injected mass. This situation is specially critical at 370 *bar* and 1.71 *mg* per orifice, since only two cycles show pilot flame, evidencing the poor conditions for autoignition. For this particular condition, subsequent results obtained for LD and IL (Figure 4.8(b)) cannot be considered statistically significant, as confirmed by the high dispersion in the measured parameters. These results indicate that a strategy with a single long main injection would not burn under the conditions tested in this thesis, which is coherent with problems reported in the literature (Chapter 2). Figure 4.8(b) shows LD as a function of the injected mass per orifice for both levels of rail pressure. This Figure shows how LD increases the larger the injected mass and, to a lower extent, the lower the rail pressure. Pilot ignition is also shown to occur well after EOI for all cases. Actually, it is remarkable the fact that both characteristic times (LD and EOI) follow the same trend, *i.e.* LD increases with injected mass at the same rate as EOI timing does. This fact hints at the hypothesis that EOI processes may also play a role on pilot injection ignition. It seems that the rapid leaning occurring in the cylinder could be important in the autoignition sequence of a glow plug-assisted engine. Finally, IL is also shown in Figure 4.8(b) to quantify the overall luminosity released during one pilot injection cycle. IL is observed to reduce with an increase in either injected mass or rail pressure. This result confirms for the parametric study presented here the inverse trend between IL and LD, which was observed in Figure 4.6 for a single condition. Summarizing, increasing the injected mass and/or the rail pressure for the pilot injection diminishes the probability of ignition and growth of the pilot flame. More insight into this result will be provided in Chapter 7, when comparing experimental results with information obtained from modeling.

4.3.2 Full injection strategy

Rail pressure influence

Regarding the influence of rail pressure on the full injection strategy, results at 370 *bar*, presented in this section, will be compared with previous results at 250 *bar*. The first comparison is made in terms of global cycle parameters, results at 370 *bar* are presented in Figure 4.9(a), while the corresponding results at 250 *bar* have been shown in Figure 4.2. By comparing both levels of rail pressure important differences arise. First, there is a clear difference in terms of combustion probability. At 250 *bar*, all 30 repetitions show positive work. Meanwhile, at 370 *bar*, 5 out of 30 cycles show IMEP lower than zero, evidencing ignition problems at higher rail pressure. Secondly, if combustion occurs, IMEP and CE are significantly higher at 370 *bar*. According to the previous description, combustion under cold start conditions seems to be limited by fuel evaporation. A higher injection pressure results in a higher momentum in the spray, and consequently a faster mixing and evaporation process. If ignition occurs, more fuel will be prepared, and therefore CE and IMEP are higher than those achieved at 250 *bar*. This seems to be a consequence of higher velocity or momentum induced by injection, which improves mixing and evaporation. Finally,

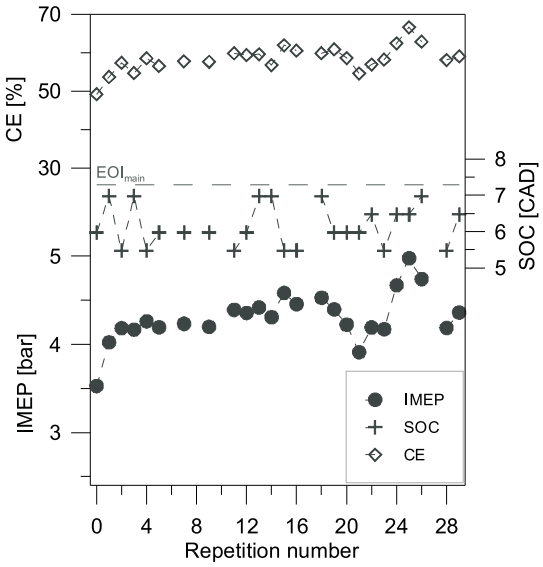

(a) CE, SOC and IMEP vs repetition number

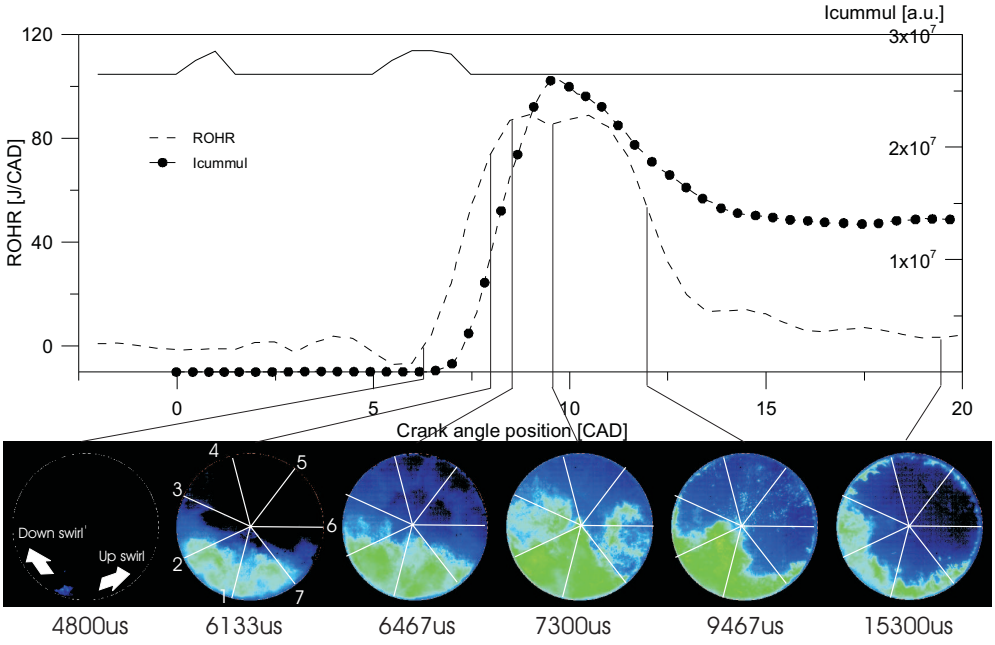

(b) Injection pulse, ROHR and I_{cumul} as a function of the crank angle position

Figure 4.9. *Main combustion engine results for the* 370 *bar rail pressure case using the nominal injection strategy,* 6 *mg at* 0 *CAD and* 24 *mg at* 5 *CAD. (a) IMEP, SOC and CE versus the repetition number for a 30 repetitions test. (b) Injection pulse, ROHR and* I_{cumul} *as a function of the crank angle position with selected images. White-radial lines on the images correspond to the approximate location of the sprays.*

there is a small difference in terms of SOC which is in the order of the crank angle encoder resolution. At 370 *bar* SOC is detected around 0.5 CAD earlier for some cycles. This is most probably due to the fact that at higher rail pressure the spray reaches the pilot flame approximately 200 μs (*i.e.* 0.3 CAD) earlier.

The next comparison is presented in terms of propagation of the main combustion. The temporal evolution of one cycle with high IMEP at 370 *bar* is shown in Figure 4.9(b) in the same way as in Figure 4.5(a) for the cycle at 250 *bar*. The main combustion characteristics (initiation of main combustion at the spray the closest to the glow plug, spatial development of visible flame during injection, later deceleration after EOI and final drop in ROHR) are coincident with the results at 250 *bar*. Differences are related to the duration and intensity of the combustion process. At 370 *bar*, combustion is shorter in duration, in agreement with the shorter injection pulse, but more intense as well. This is evidenced in the slope of both, ROHR and I_{cumul}, traces and their peak values. As a conclusion, increasing injection pressure results in better mixing and more efficient combustion process, but also in more difficulties to reach ignition.

Influence of the amount of injected mass

Regarding the influence of the amount of injected mass on the full injection strategy, four different strategies have been tested. The main pulse has been increased from 24 mg (nominal) to 84 mg in 20 mg steps, for a constant pilot injection of 6 mg. As pilot injection mass is kept constant and pilot ignition is not under study here, only cycles with visible pilot flame, as a consequence with positive IMEP, are taken into account. In this particular case, results from a different nozzle are shown (N1, see Table 3.3). In spite of the fact that nozzle geometry does have some influence on combustion under cold start conditions, as will be shown in further detail in Chapter 6, the general description of the combustion progress, which is the objective of the present chapter, should not depend on the nozzle type.

Performance results derived from the analysis of the pressure signal are shown in Figure 4.10(a), in which IMEP and CE are plotted as a function of the total amount of fuel injected (only cycles with positive IMEP). IMEP is shown to increase monotonically with injected mass, but the rate of change is observed to change, with a steep increase from 30 to 50 mg, and a lower slope for higher values. On the other hand, combustion efficiency is observed to have an optimum value at 50 mg, with both lower and higher injected mass values resulting in lower efficiency. Both results are obviously coupled: increasing mass up to 50 mg increases largely the amount of energy released by combustion, and therefore also IMEP, but further increases of mass are offset by the decreasing combustion efficiency, which results in a lower rate of increase of heat supplied to the cycle, and therefore a lower rate of increase of IMEP above 50 mg. Similar conclusions have been obtained for both injection pressure values.

In Figure 4.10(b) selected ROHR traces for each one of the strategies tested have been selected with the purpose of understanding the change of slope detected at 50 mg. Each ROHR trace is accompanied by an image of the moment at which injection

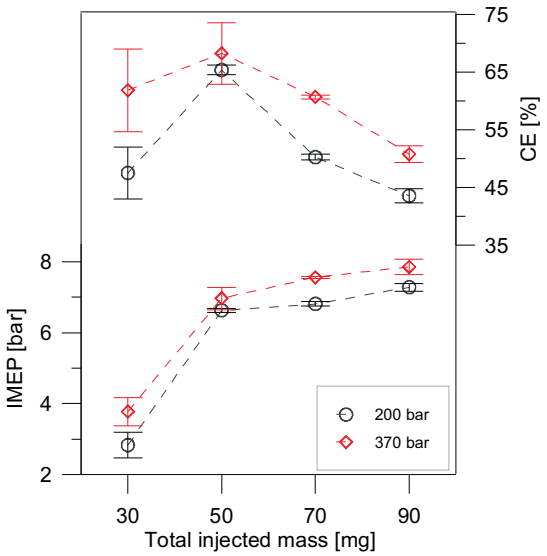

(a) CE and IMEP vs the total amount of fuel injected

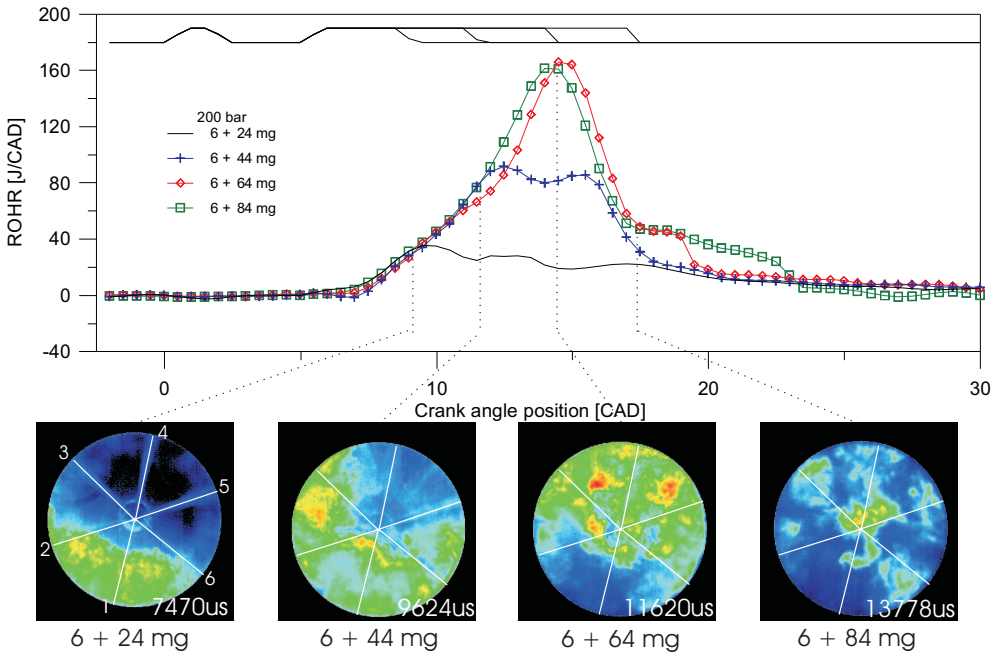

(b) ROHR and images at nozzle closing

Figure 4.10. *Influence of the main injected mass on combustion global parameters and flame progress for the full injection strategy, 6 mg are injected at* 0 *CAD and the main pulse is increased from 24 mg to 84 mg in 20 mg steps. (a) IMEP and CE as a function of the total amount of fuel injected mass for both levels of rail pressure. (b) ROHR as a function of the crank angle position for four selected cycles with different amount of fuel injected at 200 bar. Images in the bottom correspond to the moment at which the injector nozzle closes for each case.*

finishes. These images indicate the location of the visible flame front when nozzle closes. Previous visualization results for the nominal injected mass (30 mg) indicate that visible flame extends throughout the combustion chamber as long as injection proceeds, while after end of injection the rapid leaning throughout the chamber results in the evolution of a non-visible flame front sweeping the rest of the combustion chamber and collapsing on the location opposite to the original ignition site, after which heat release strongly decreases. In any of both phases, the reaction front consumes the available fresh mixture within the combustion chamber, after which an atmosphere of hot combustion products and low oxygen concentration can be found.

Changing the injected mass shifts the timing between both stages of the reaction evolution. For 30 mg injected mass, the visible flame front has not even reached half of the combustion chamber before end of injection, so the second phase is really significant. For 50 mg, injection finishes shortly before the visible flame has swept the whole combustion chamber, but still the second phase should occur. If more fuel is delivered, images indicate that the first phase manages to sweep the whole combustion chamber, and heat release shows a single maximum which is located at the same time instant for both 70 and 90 mg. Therefore, even if more mass is injected, combustion rate decreases abruptly after this maximum, and proceeds at a much lower rate. This is probably due to the fact that local conditions within the chamber are poor for combustion development. These conditions will be mainly high temperature and low oxygen concentration. While the first should improve the vaporization process, which should act positively for combustion development, the second one has a negative effect on combustion, and it seems to be the limiting factor for the development of the combustion process at higher injected masses.

Oxygen availability is obviously linked to the equivalence ratio within the bowl. Simple estimations can help understand this effect: in-cylinder air mass is around 1 g, which results in the possibility of burning around 70 mg of fuel if stoichiometric fuel-air ratio is assumed to be 1/14.5. Therefore, for cases with fuel mass higher than 50 mg oxygen availability within the chamber is very low after the flame front sweeps the whole combustion chamber, and this explains the drop both in heat release rate after the maximum and the subsequent reduction in CE when going to very long injections.

As a conclusion, increasing the injected mass has confirmed the two phases in the evolution of the combustion process, with the first one being sustained by injection, with a strong visible flame, and the second one occurring after end of injection, with a much lower luminosity and a flame front that sweeps the rest of the combustion chamber. Increasing injection duration shifts the timing for the change from one mode to the other, but it is limited by oxygen availability within the chamber. An optimum should exist in CE, which probably depends on different engine operating conditions.

4.4 Synthesis: Phenomenological model of the cold start combustion process

Before presenting the conclusions of this chapter, this section synthesizes the sequence of phenomena that is believed to occur during cold start combustion process. With this purpose, a phenomenological model has been built based on the experimental evidences shown and discussed in this chapter for the nominal pilot + main injection strategy (6 + 24 mg). This phenomenological model does not intend to explain how the complex physical and chemical processes develop under these conditions. Instead, it only aims at describing a sequence of the phenomena observed and presented previously to set a guiding mental description for the rest of the document.

The phenomenological model is sketched in Fig. 4.11. Schematics represent a view from the piston window, in a way that they help explain the information presented throughout the study from both images and pressure signal. This sequence starts with pilot injection, liquid spray is injected at high speed within the combustion chamber and due to the low in-cylinder density it rapidly impacts against walls forming a liquid film on them. Due to the low in-cylinder density and temperature, vaporization and mixing occur but resulting in a lean and local vapor fuel-air mixture. This fresh mixture is located only in limited areas which have been reached by the spray, as well as close to the bowl walls. After end of pilot injection, further evaporation, mixing and chemical reactions take place. It is during this period when chemical reactions fight against the dissipation, caused by local temperature differences and the turbulent motion within the chamber, in order to remain exothermic and achieve autoignition. As a consequence of these processes, and depending on factors that will be studied along this document, pilot flame appears on the glow plug area.

First reactions appear really near to the glow plug (probably on the glow plug) but they grow in size resulting in a reaction zone that burns the fuel available on its surroundings. As the flame grows, it travels from the glow plug to the wall dragged by swirl motion. The small amount of burnt fuel and the lean local conditions prevent the flame from propagating to other sprays. At this point and depending on the amount fuel burnt, pilot flame can either remain within the chamber, probably attached on the walls, or it can extinguish before the main injection starts. In any case, it can be concluded that the pilot injection process is very poor and inefficient process in terms of evaporation and combustion, since the fuel burnt corresponds to only one of the sprays and it is not even all the fuel injected in that spray, resulting in very low heat released.

Later, the main injection event starts and the liquid fuel delivered in the main pulse interacts with the glow plug and the remaining pilot reaction zone. If the pilot flame (*i.e.* a hot combustion zone) is still present, main combustion starts as soon as one of the sprays reaches the pilot flame. In the other case, main combustion start is delayed since autoignition has to occur once again but in an hotter atmosphere for the combustion products of the pilot flame. After ignition, main combustion propagates with the shape of a flame/reaction front from the glow plug area to the rest of the

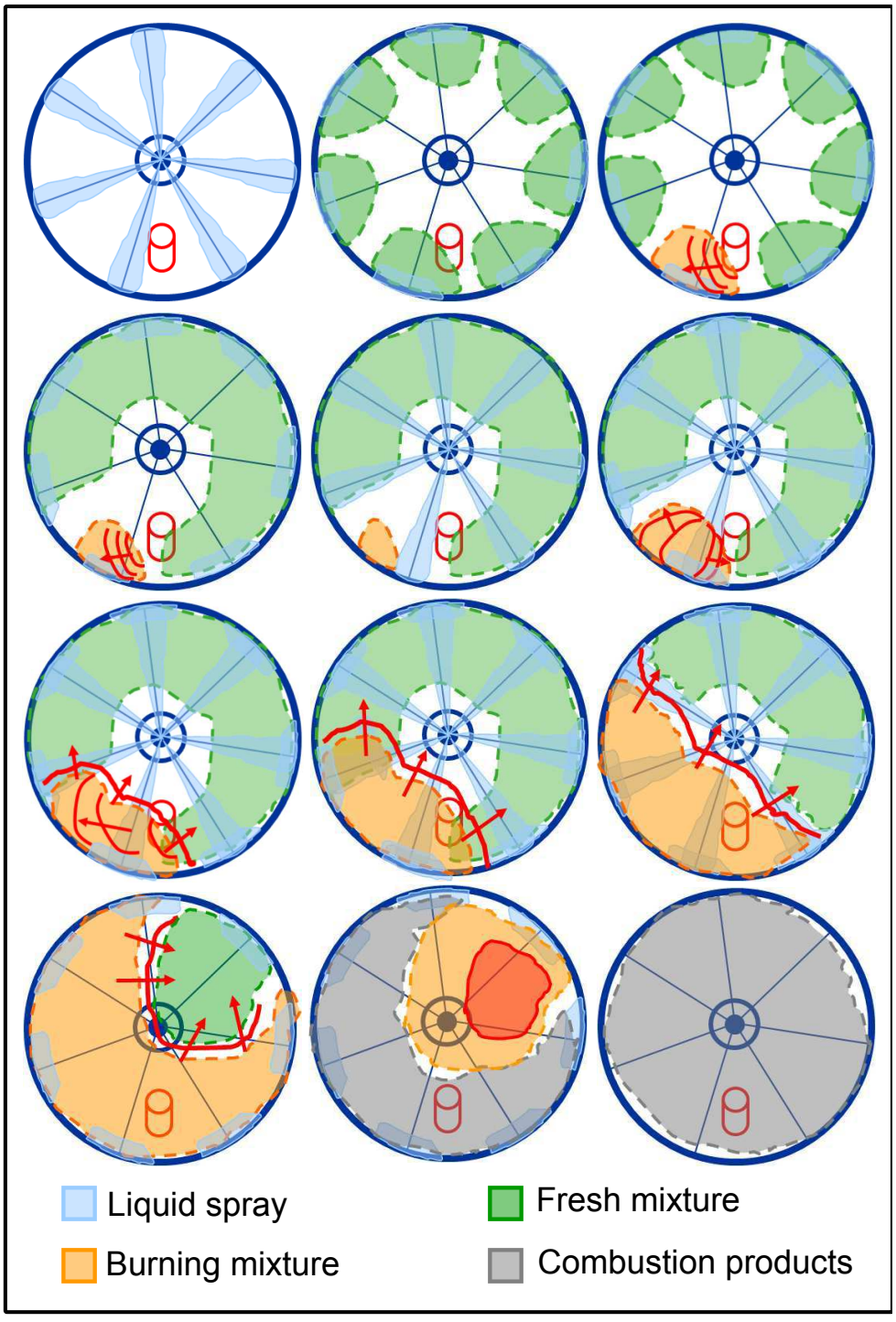

Figure 4.11. *Sketch of the sequence of processes that occur during cold start combustion.*

chamber. This front grows first in the swirl direction but after some instants it starts growing in all directions: down-swirl, up-swirl and to the center of the chamber. No signs of autoignition occur in any of the sprays outside the reaction zone. This reaction front sweeps the combustion chamber rapidly promoted by the injection event and divides the chamber in two zones. The first zone, upstream of the reaction front, is composed of combustion products, some possible remaining oxygen and the fuel that has been injected after the front has gone by. The second zone, ahead of the reaction front, is composed of fresh mixture with very different local fuel to air ratio, oxygen and liquid fuel. Depending on the injection duration, the flame front manages to burn different portions of the chamber with leaner or richer zones. At the end, the reaction front usually finishes sweeping the combustion chamber close to maximum heat release.

4.5 Conclusions

The main combustion characteristics for a pilot + main injection strategy under low temperature cold start conditions have been presented in this chapter. In addition to characterize the combustion event, this study has made it possible to present the general methodology that will be used throughout this thesis. For example, in-cylinder pressure analysis has been performed based on single-cycle pressure traces, since ignition conditions are in the limit between combustion and misfiring. High speed visualization has been used systematically, since low intensity, local and transient phenomena strongly affect combustion development, and this information cannot be provided by in-cylinder pressure. Single pilot injection pulses have been tested to characterize pilot ignition, since the difference in intensity with respect to the main combustion does not allow to adjust the camera settings to quantify both combustion events.

From the results it has been observed that cold start combustion is characterized by low combustion efficiency and high cycle-to-cycle dispersion, evidenced in both IMEP and SOC. Under such conditions, injection settings, specifically rail pressure and injection duration, do have an influence on combustion progress.

Pilot ignition is probably the most critical stage in the whole combustion process since it is in charge of promoting an early and controlled start of the main combustion. It occurs around 1200 to 1500 μs after the end of pilot injection in the glow plug vicinity. It has been found that a change in the injection rate, produced by a change in rail pressure or the amount of fuel injected, directly affects the conditions for autoignition in the glow plug vicinity. Specifically, injection strategies with low pressure and short duration are favorable to create a strong pilot flame on the spray closest to the glow plug. Ignition of pilot injection has been found to happen for cycles with higher IMEP and earlier SOC, whereas for those cases where pilot ignition failed, lower IMEP values were obtained. These results allow to explain the difficulties presented by single injection strategies in the past and justify the use of pilot injection strategies.

Main combustion starts mainly from pilot flame, and propagates from the pilot flame location sweeping the rest of the combustion chamber and promoted by the turbulent motion generated by the injection event. During injection, a strong visible flame is observed due to high local equivalence ratios, most probably due to soot. After end of main injection, the rapid leaning of the mixture suppresses the typical strong soot radiation, and OH^* UV radiation is observed to end the combustion process in regions far from the glow plug. Under these conditions, even for the best case, not all the injected fuel is burnt, as indicated by the presence of a flame attached to the bowl walls well after the end of the main heat release. Regarding the parametric variation, an increase in rail pressure increases cycle work, most probably due to the increase in the rate at which fuel is mixed and burnt. However, higher injection pressures are also correlated with lower probability of the cycle to ignite. On the other hand, an increase in the amount of fuel injected means an increase in the work obtained per cycle but a maximum in combustion efficiency is attained due to oxygen availability.

Altogether, the cold start problem can be sub-divided into two main issues: ignition and combustion progress. Ignition depends on the interaction between one of the sprays and the glow plug. Such interaction depends on several factors, among which fuel motion driven from the injector nozzle and the role of the glow plug as a hot spot are probably two of the main issues. Combustion progress is promoted by the injection event in terms of injection duration and the momentum induced during such process. Based on these facts, more specific studies about the role of the glow plug (Chapter 5) and the nozzle effect (Chapter 6) should be carried out in order to gain deeper insight, which could lead to a better understanding about the controlling mechanisms. After those parametric variations, discussion on these phenomena will be provided in Chapter 7.

Bibliography

[1] Chartier Clèment, Aronsson Ulf, Andersson Öivind and Egnell Rolf. "Effect of Injection Strategy on Cold Start Performance in an Optical Light-Duty DI Diesel Engine". *SAE Paper 2009-24-0045*, 2009.

[2] Payri F., Broatch A., Salavert J. M. and Martín J. "Investigation of diesel combustion using multiple injection strategies for idling after cold start of passenger-car engines". *Experimental Thermal and Fluid Science*, Vol. 34 n^o 7, pp. 857–865, 2010.

[3] Heywood John B. *Internal Combustion Engine Fundamentals*. McGraw-Hill, Inc., 1988.

[4] Bielaczyc Piotr, Merkisz Jerzy and Pielecha Jacek. "Investigation of exhaust emissions from di diesel engine during cold and warm start". *SAE paper 2001-01-1260*, 2001.

[5] Musculus M. "Entrainment waves in decelerating transient turbulent jets". *J. Fluid Mech.*, Vol. 638, pp. 117–140, 2009.

[6] Perrin H., Dumas J. P., Laget O. and Walter B. "Analysis of Combustion Process in Cold Operation with a Low Compression Ratio Diesel Engine". *SAE Paper 2010-01-1267*, April 2010.

Chapter 5

Influence of hardware configuration

Contents

5.1 Introduction

As shown in Chapter 4, the interaction between one of the sprays and the glow plug is certainly one of the main factors influencing ignition in cold start combustion. The present chapter aims to study such interaction in two sections. First, the influence of the relative distance between one of the strays and the glow plug is presented. And then, the influence of the glow plug temperature will be shown. The chapter closes with a brief summary of the main outcomes. The whole test matrix developed for this chapter is shown in Table 5.1. In this study, nozzle N1 was used with a minimum rail pressure of 200 *bar* and the same nominal injection strategy as in the previous chapter. In order to study the influence of the relative distance between one of the sprays and the glow plug three parameters were changed: orientation angle, glow plug protrusion and nozzle tip protrusion. On the other hand, the glow plug temperature effect was also investigated by changing the glow plug supply voltage.

Table 5.1. *Test matrix of conditions tested in Chapter 5.*

Rail pressure bar	Orientation °	GPP mm	NTP mm	Voltage V
Nominal strategy				
200/370	10	3	2.1	11
Orientation				
200/370	-30/-20/-10/0/10/20	3	2.1	11
GPP				
200	10	3/4.4/5.8	2.1	11
NTP				
200	10	3	1.1/2.1/2.9	11
Supply voltage				
200/370	10	3	2.1	8.3/9.2/10/11

Table 5.2. *Distance between glow plug and the spray closest to the glow plug for the conditions tested in Chapter 5.*

NTP mm	GPP mm	d mm
1.1	3	2.81
2.1	**3**	**3.51**
2.9	3	4.15
2.1	4.4	2.22
2.1	5.8	1.78

5.2 Influence of glow plug position relative to spray

Starting from the nominal configuration, which is the same as in previous chapter, three parametric variations regarding the glow plug-spray arrangement have been performed, as summarized on Table 5.1 and illustrated in Figure 5.1. First, the orientation angle between the sprays and the glow plug has been changed by rotating the injector around its axis. This angle grows with positive values in swirl direction and the position at which the spray impacts directly against the glow plug corresponds to 0°. On the other hand, glow plug and nozzle tip protrusion have been modified by changing their respective spacer rings. All such variations provoke a change in the distance (d) between the glow plug surface and the spray axis, which has been estimated and it is shown in Table 5.2. The nominal configuration is printed in bold.

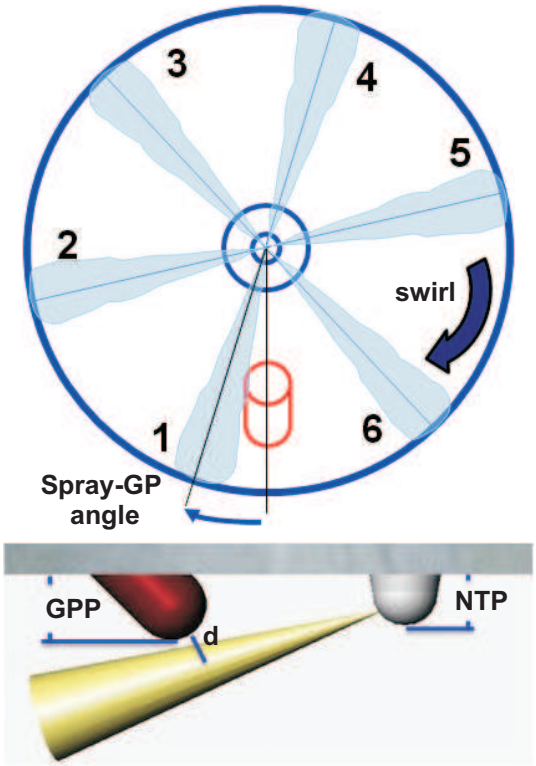

Figure 5.1. *Sketch of the relative position between the glow plug and one of the sprays. In the top, the figure shows the direction of the swirl and how the orientation angle is measured. In the bottom, the variation of the NTP and GPP are shown.*

Results corresponding to the glow plug arrangement variation have been divided according to the injection strategy, namely pilot and full injection strategy. As concluded in Chapter 4, the full injection strategy comprises two different but related problems, pilot ignition and main combustion progress. Pilot flame is closely linked to the ignition of the main injection. This statement has been confirmed for the conditions tested in this parametric study, as evidenced in Figure 5.2. In this figure, the appearance probability of early burning cycles ($IMEP > 0$ and $SOC < EOI$) is plotted as a function of the probability of pilot flame appearance ($I_{cummul} > 0$) before 5 CAD. These tests were performed independently but keeping constant pilot injection settings; combustion probability corresponds to full injection strategy tests and pilot probability is for single pilot tests. Good correlation is shown between the percentage of pilot injection tests with flame and the percentage of cycles with high IMEP. These results are representative sample of the conditions tested in this section (two levels of rail pressure and six different orientation angles). Such results, together with the description presented in Chapter 4, evidence that pilot flame creates a high

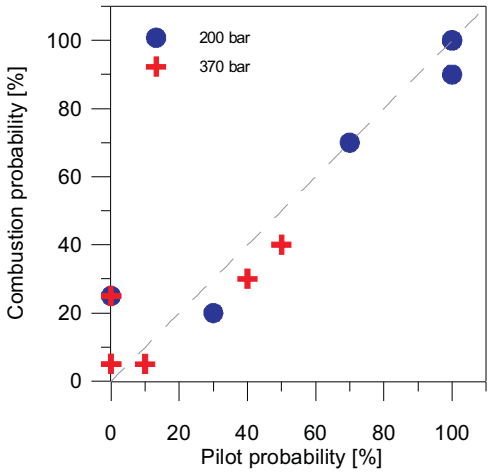

Figure 5.2. *Combustion probability, calculated for the full injection strategy, of early burning cycles ($IMEP > 0$ and $SOC < EOI$) as a function of pilot probability, measured for the pilot single injection in independent tests. The tests presented in this figure corresponds to the six orientation configurations tested at both levels of injection pressure.*

temperature reactive zone close to the glow plug that, if adequately located in time, ensures favorable conditions for the ignition of the main injection event.

5.2.1 Pilot injection

Due to its proved relevance as the main combustion promoter, pilot injection is isolated and shown in this sub-section in order to shed some light on its ignition mechanisms. Figure 5.3 shows LD and IL as a function of the spray-glow plug orientation angle for two very different ignition stability situations, low and high rail pressure. Each test consists of 20 recorded repetitions and the plots are built with the cycles that show any luminosity. Regarding the orientation angle parametric variation, it is observed that shorter LD values with higher IL are detected when the distance between the glow plug and one of the sprays is shorter (similar results were reported in [1, 2]). It is also shown that shorter LD values and higher IL intensities are obtained if the spray is located on the up-swirl direction from the glow plug, compared to the down-swirl direction, for the same absolute angle value. These results confirm that swirl motion plays a role on ignition, in agreement with results from Pacaud *et al.* [1]. It is also shown in the figure how the first luminosity is detected in all cases after EOI, confirming that ignition occurs not due to the contact between the spray and the glow plug but due to the convection of fuel after EOI. More insight into these processes will be shown in Chapter 7. Finally, the strong effect of the rail pressure is shown again: at higher rail pressure, IL values are lower, and the first luminosity for orientation absolute angles larger than 20° is detected after 4000 μs (SOI_{main}

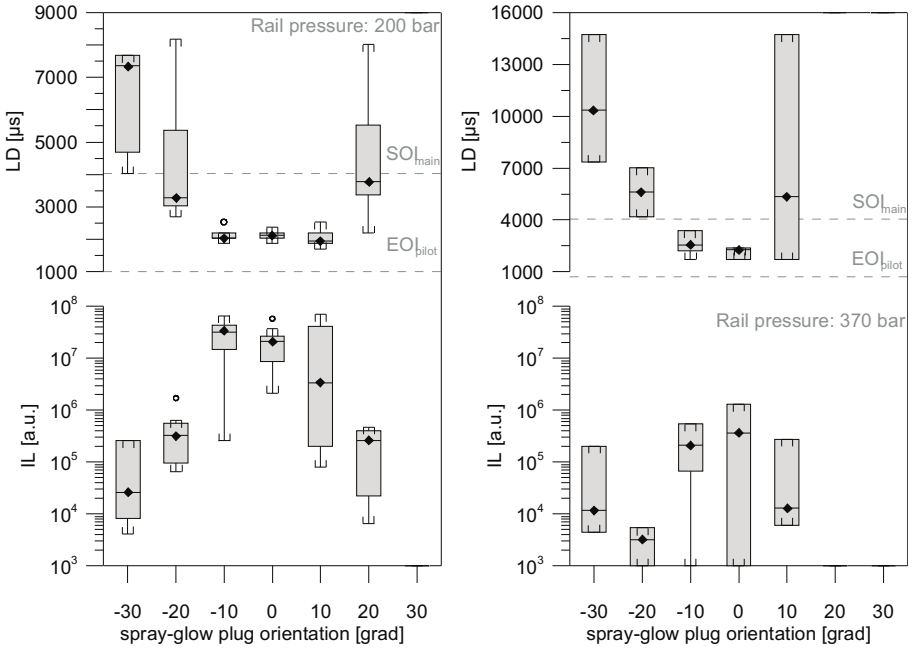

Figure 5.3. *LD (top) and IL (bottom) as a function spray-glow plug orientation angle for both levels of rail pressure. In the LD plot the EOI_{pilot} and SOI_{main} are marked with a dashed line as a reference to the injection event. The outliers (unfilled dots) are points out of the range defined by 1.5 times the interquartile range.*

in the full injection strategy) or not detected at all in most of the cases. Dispersion in both parameters increases the larger the absolute value of the orientation angle. These results make it possible to confirm once again two controlling parameters on the mechanisms leading to ignition under cold start conditions, namely rail pressure and the transient processes occurring after end of injection.

5.2.2 Full injection strategy

As a reference to the conditions tested in this section, the importance of an early start of combustion is shown in Figure 5.4. On the left-hand side, IMEP is plotted versus SOC for the 30 repetitions of a test with an orientation angle $-10°$. It can be observed that IMEP values are higher in cycle with SOC earlier than EOI than those cycles with combustion starting after EOI. The crankangle-resolved evolution of ROHR is also shown for two representative cases, namely one cycle where $SOC < EOI$ (blue), and another one where $SOC > EOI$ (red). These ROHR traces show that, for early burning cycles, combustion rates are considerably higher, combustion duration is shorter and better controlled since its progress is promoted by the injection event. On real engine cold start, high IMEP values are compulsory

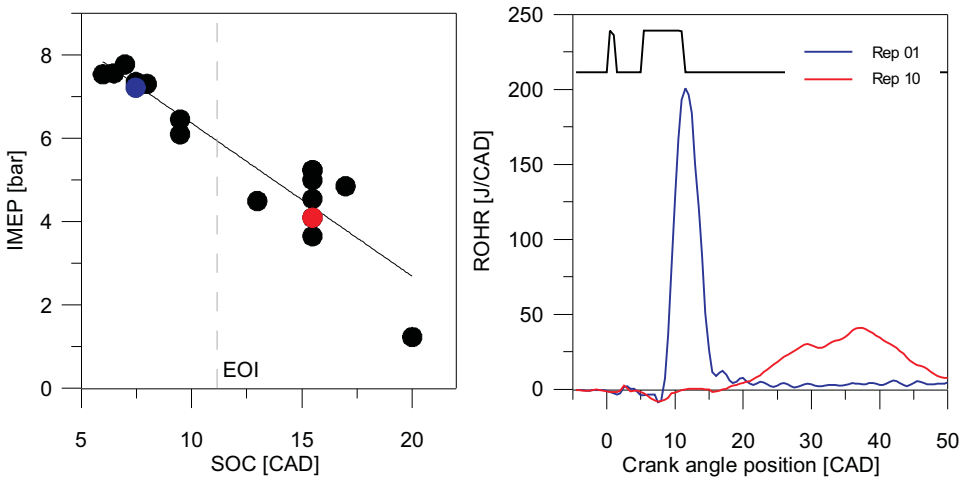

Figure 5.4. *Left: IMEP vs. SOC for the* 30 *repetitions of a full injection strategy test with an orientation angle of* -10 $^{\circ}$ *at the high level of rail pressure. Right: ROHR versus crank angle position for two of the cycles shown on the right side. The injection strategy consists of a pilot pulse of* 6 *mg at* 0 *CAD followed by a* 24 *mg pulse at* 5 *CAD.*

because it is necessary to overcome mechanical losses and speed up the engine. Therefore, it is the repetitive appearance of these kind of cycles which will lead to engine start. For these reasons, the study of the influence of glow plug arrangement presented in this section will be focused only in early-burning of cycles.

The relationship between ignition and combustion progress, explained in the last paragraph, exists under different configurations, as shown in Figure 5.5. This Figure shows IMEP and SOC as a function of the spray-glow plug orientation angle at both levels of rail pressure. Results show that the distance between the spray and the glow plug has an effect on SOC and IMEP, since higher IMEP values are reached for configurations at which the spray is oriented closer to the glow plug. For the high rail pressure case, IMEP values are notably higher if the spray is oriented in up-swirl direction. Furthermore, high IMEP values are linked with low SOC values, which confirms the relationship explained previously and shown in Figure 5.4.

Further evidence on the influence of the distance between the glow plug and the closest spray on combustion is shown in Figure 5.6, where SOC and IMEP are plotted as a function of spray-glow plug distance for the low rail pressure level case. The tests shown in the figure correspond to the NTP and GPP variations at a constant orientation angle of 10°. Figure 5.6 shows that spray-glow plug distance does have an influence on SOC and hence on IMEP. If the distance is short (from 1.78 to 3.51 *mm*), high combustion probability (above 90%) and high IMEP values are observed, with slightly higher values when the glow plug is at 1.78 and 2.22 *mm*. For the longer distance case (at 4.15 *mm*), the situation changes abruptly: combustion probability decreases to 30% and IMEP values become considerably lower. These results confirm

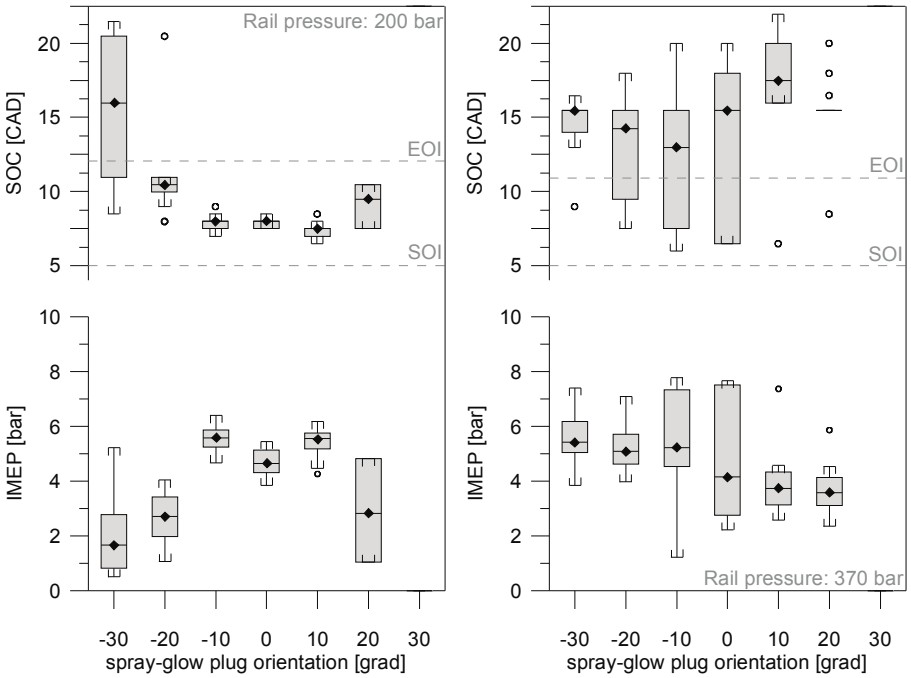

Figure 5.5. *SOC (top) and IMEP (bottom) as a function of the spray-glow plug orientation angle for full injection tests at both levels of rail pressure. The outliers (unfilled dots) are points out of the range defined by 1.5 times the interquartile range.*

that the spray-glow plug distance is an important factor with influence on combustion. But, this influence does not seem to be a consequence of the direct contact of the spray with the glow plug. For a distance value of 3.51 mm, for which ignition conditions are good, contact between the glow plug and the spray is not granted. A discussion on local conditions on the GP enabling ignition will be presented in Chapter 7.

5.3 Influence of glow plug temperature

Influence of glow plug temperature has been investigated by performing a variation of the glow plug supply voltage when performing engine tests. Before that, the glow plug surface temperature was characterized as a function of the supply voltage by means of an approximated method based on the dual-wavelength thermometry. Regarding the conditions tested in this section, the supply voltage has been modified within the range allowed by the glow plug (7, 8.3, 9.2 and 10 V), nozzle N3 was used for these tests and the injection strategy consists of a single pilot injection pulse of 6 mg injected at 0 CAD at the low level of rail pressure (250 bar).

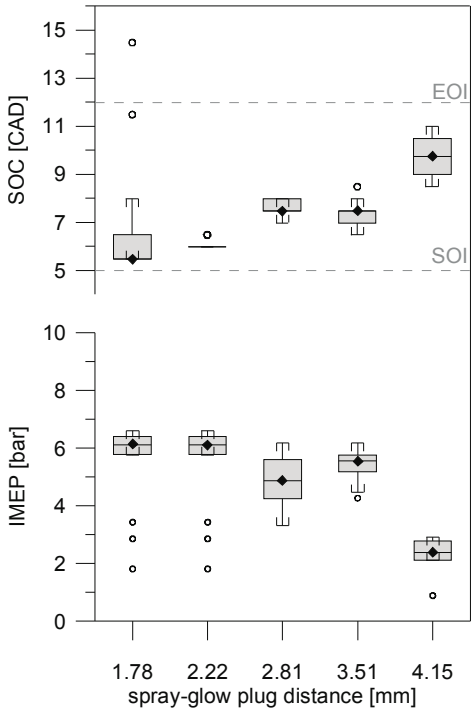

Figure 5.6. *SOC (top) and IMEP (bottom) as a function of the spray-glow plug distance for full injection tests at the low level of rail pressure. The outliers (unfilled dots) are points out of the range defined by 1.5 times the interquartile range.*

5.3.1 Glow plug surface temperature measurement

The glow plug surface temperature has been measured by using a simplified version of the dual-wavelength thermometry method [3]. It is based on the Planck's law for black bodies and it has been extensively used for gray bodies by accounting for the surface emissivity [4, 5]. According to the method, the signal from a photo sensor viewing a radiating surface may be expressed as:

$$R_\lambda = \varepsilon_\lambda \cdot \frac{1}{\lambda^5} \cdot \frac{c_1}{e^{\frac{c_2}{T \cdot \lambda}} - 1} \tag{5.1}$$

where R_λ and ε_λ are the radiation intensity measured by the detector and the surface emissivity at a given wavelength (λ), respectively. T is the surface temperature and c_1 and c_2 are constants with values of $1.191043910^{-16}\ Wm^2/sr$ and $1.438810^{-2}\ mK$, respectively.

The material employed to build the whole glow plug tube, including the tip, is a $NiCr_{23}Fe$ alloy [6]. Specific information of its emissivity as a function of wavelength and temperature was not found, but related information has allowed to choose a range

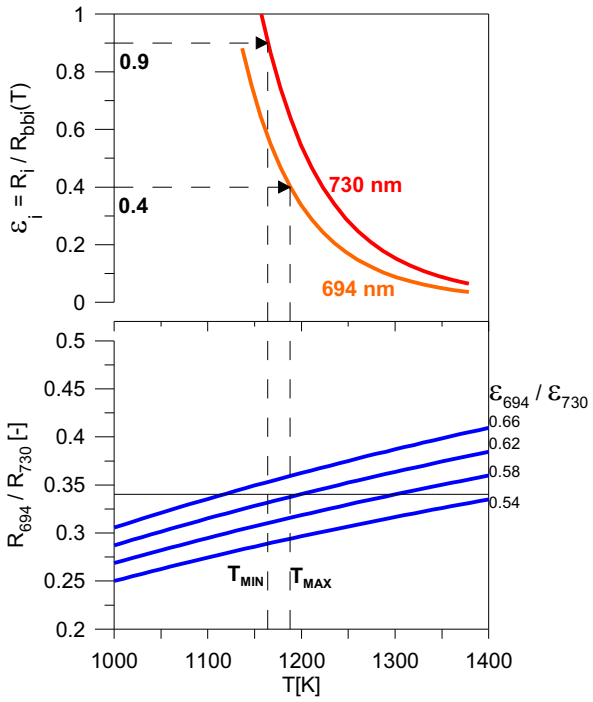

Figure 5.7. *Surface emissivity and radiation ratio as a function of 2-color temperature for two wavelengths, 730 and 694 nm. This plot shows the methodology used to estimate the possible range of temperatures that the glow plug tip has for a supply tension of 11 V.*

of possibilities. According to the material manufacturer [7], for a very similar nickel alloy ($NiCr_{15}Fe$) the total hemispherical emissivity ranges between 0.76 and 0.82 for temperatures from 923 K to 1253 K, respectively. And according to [8], the emissivity of these kind of alloys ranges between 0.42 and 0.58 for temperatures from 922 K to 1033 K. These emissivity values cannot be taken as exact values but they can help to select a range. For the temperatures measurements shown in this thesis, the emissivity values will range from 0.4 to 0.9, which cover the range of possibilities found in the literature.

In the present study, R was measured at 694 and 730nm. Given the uncertainty in emissivity, both radiation values are used to estimate a temperature range for the glow plug temperature. Figure 5.7 shows the main relationships used in the developed algorithm. From eq. 5.1 one can see that, for fixed wavelength, the ratio of R values depends on temperature and the ratio of emissivities. Therefore a first estimation of glow plug temperature was obtained by calculating the ratio of measured intensities ($R694/R730$) and assuming emissivity ratio between 0.54 and 0.66. Fig. 5.7 shows that a relatively wide range of possible temperature values are possible for a given measurement, depending on the emissivity ratio. This wide range is reduced

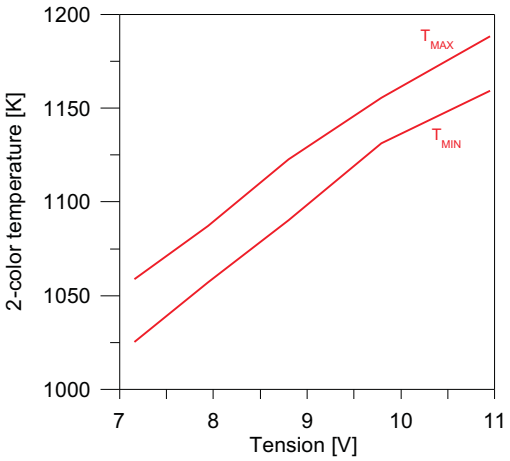

Figure 5.8. *2-color temperature range as a function of the supply tension.*

if one accounts for the surface material emissivity range as from the literature (0.4 to 0.9). These emissivity values can be calculated from the experimental radiation values divided by the corresponding blackbody radiation at a given temperature. As a result, the procedure enables a definition of an interval where glow plug temperature can be found (Tmin to Tmax in Fig. 5.7).

Values of R at each wavelength were obtained after performing experimental measurements, calibration and image processing with the glow plug installed in an identical cylinder head out of the engine. The circuit current was controlled by means of a variable resistor and the supply tension was measured in the terminals of the glow plug, as in the engine tests. The radiation has been measured with an intensified camera installed in front of the glow plug. The camera is a LaVision-Dynamight with a 16 bit CCD sensor at full resolution of 512 x 512. Two interference filters were used to isolate the radiation at each wavelength, namely 694 and a 730 nm, both of them 10 nm in bandwidth. The calibration was performed with a tungsten-ribbon lamp and the procedure is the same as explained by Payri *et al* [9]. The digital levels were observed to be very uniform all over the glow plug tip and an average value have been considered representative. Finally, these average digital levels at each wavelength and supply tension were converted into radiating intensity by means of the calibration function.

Figure 5.8 shows the possible range of temperatures on the glow plug tip as a function of the supply voltage. The plot shows that the relation between both parameters is approximately linear. The uncertainty range of temperature calculated for a given voltage is of only around 35 K. These results actually help to enclose the range of possibilities within the glow plug works, which are very similar to the nominal values expected for a metallic glow plug [10].

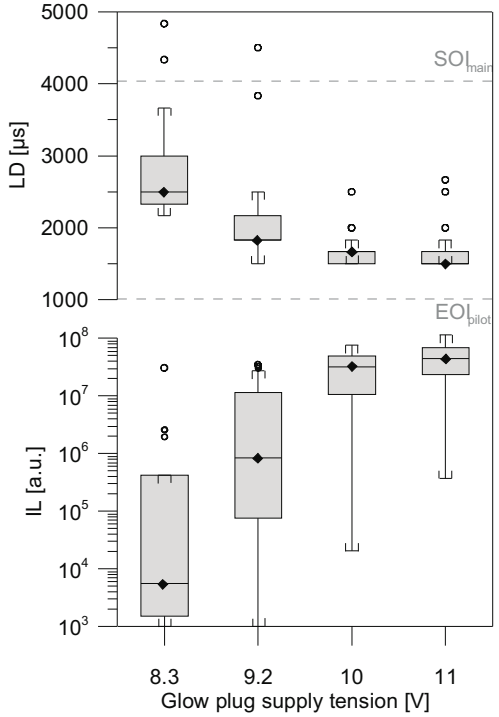

Figure 5.9. *LD (top) and IL (bottom) as a function of the supply glow plug tension at 250 bar of rail pressure. In the LD plot the EOI is marked with a dashed line as a reference to the injection event. The outliers (unfilled dots) are points out of the range defined by 1.5 times the interquartile range. The injection strategy is a single injection of* 6 *mg injected at* 0 CAD.

5.3.2 Engine results

Following the general methodology used throughout this thesis, the engine results enclosing the effect of glow plug temperature are shown separately for the pilot injection and the full injection strategies. With regard to the pilot injection strategy, results showing the influence of the glow plug temperature on pilot ignition are shown in Figures 5.9 and 5.10. In Fig. 5.9, LD and IL are plotted as a function of glow plug supply voltage for a constant injection condition (6 mg injected at 0 CAD). Ignition probability for these tests was observed to be around 100%. This Figure shows a clear reduction in luminosity delay if the supply voltage is increased, as can be expected due to a local temperature increase in the glow plug. Nevertheless, it is observed that this delay is reduced until a minimum value (approximately 500 μs AEOI) from which no further reduction is achieved even when the supply voltage is increased (from 10 to 11 V). This result shows that glow plug temperature is a determinant parameter but it is not the only one. The limited reduction in LD tells that some processes,

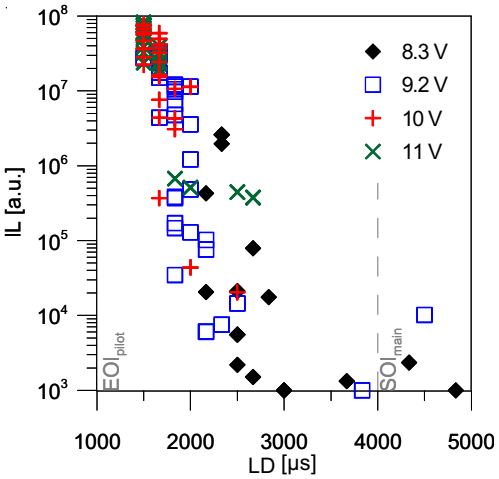

Figure 5.10. *IL as a function of LD for the four supply glow plug tension conditions tested and previously plotted in Fig. 5.9. In the LD axis the SOI of the main injection is marked with a dashed line as a reference to the injection event. The injection strategy is a single injection of* 6 *mg injected at* 0 *CAD.*

independent of the glow plug temperature, have to occur after EOI in order to finally achieve ignition.

In the same Figure, it can also be observed that an increase in voltage brings about also an increase in pilot luminosity. This could be simply the consequence of an earlier autoignition (short LD causes high IL) or a vaporization enhancement due the local increase in temperature. In order to clarify this, the same data has been plotted in Fig. 5.10 but this time as a scatter plot with IL versus LD. Different colors and symbols have been chosen in dependency of glow plug supply voltage. It is shown how all the points follow in some way the same rough trend. It appears that high IL values are achieved due to short LD, since all the points seem to merge within a similar trend independently of the supply voltage.

Finally, full injection strategy results are shown in Fig. 5.11. In this figure, SOC and IMEP are plotted as a function glow plug supply voltage for both levels of rail pressure.

The low rail pressure case is a very stable ignition condition in which all cycles have produced positive work. No effect is observed on main combustion initiation or development if the glow plug voltage is changed within this range. This lack of dependence on main combustion can be understood by considering the pilot injection results shown previously. Glow plug supply voltage has an important effect on pilot ignition. But, within the range of voltages tested pilot ignition occurs before SOI_{main} in a repeatable way. So, in all cases main injection finds pilot flame from which it can start propagating to the rest of the chamber. As a consequence, main combustion start and IMEP do not change if the supply voltage is modified. At higher rail pressure,

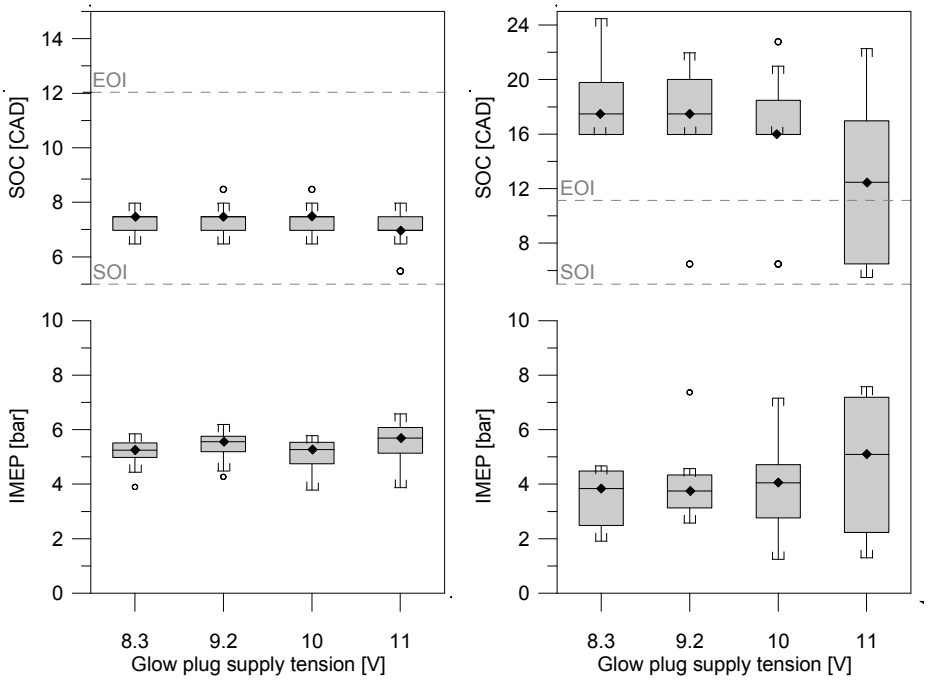

Figure 5.11. *SOC (top) and IMEP (bottom) as a function of the supply glow plug tension for both levels of rail pressure. Left: 200 bar and Right: 370 bar. In the SOC plot the SOI and EOI are marked with a dashed line as a reference to the injection event. The outliers (unfilled dots) are points out of the range defined by 1.5 times the interquartile range. The full injection strategy is used,* 6 mg *are injected at* 0 CAD *and* 24 mg *are injected at* 5 CAD.

which is a more instable ignition condition, advantage is taken from the glow plug surface increase. In this case, autoignition delay is reduced and IMEP is increased if the glow plug tension is increased up to 11 V, most probably due to an earlier and better controlled pilot flame appearance. This leads to the conclusion that the glow plug temperature has a clear has an effect on pilot injection ignition which is the one that controls main combustion initiation.

5.4 Conclusions

Spray-glow plug arrangement has been shown to have a clear influence on ignition of the pilot flame, which at the same time promotes a proper start of combustion a few hundreds of microseconds after start of main injection. This marked influence on pilot ignition does not seem to be caused solely by the direct interaction of the liquid spray with the glow plug surface, since ignition occurs for all cases well after end of injection. It has also been observed that glow plug to spray distance influences

pilot ignition, but it also depends on the orientation angle between the spray and the glow plug. In this sense, it has been corroborated that swirl motion does affect pilot ignition. If the spray is oriented in up-swirl direction with respect to the glow plug, advantage can be taken for the swirl motion effect and ignition improves. These effects are going to be better explained in Chapter 7 in which specific modeling tools have been employed with that purpose.

Glow plug temperature, is another of the pilot ignition controlling parameters. As can be expected, increasing the temperature of the glow plug surface reduces ignition delay and increases the luminosity of the pilot flame. However, above a given temperature value this reduction starts to be negligible and other processes (most probably physical) start to be the controlling ones. For the conditions tested, an increment of the glow plug temperature above 1200 K does not mean a noticeable improvement for pilot injection ignition. The effect on main combustion is indirect, since increasing glow plug temperature can reduce main combustion delay and increase the work obtained per cycle as a consequence of the presence or not of the pilot flame. This means that the real effect of glow plug temperature is solely on pilot ignition.

Bibliography

[1] Pacaud P., Perrin H. and Laget O. "Cold Start on Diesel Engine: Is Low Compression Ratio Compatible with Cold Start Requirements?". *SAE Paper 2008-01-1310*, April 2008.

[2] Walter B., Perrin H., Dumas J. and Laget O. "Cold operation with optical and numerical investigations on a low compression ratio diesel engine". *SAE paper 2009-01-2714*, November 2009.

[3] Meriaudeau F. "Real time multispectral high temperature measurement: Application to control in the industry". *Image and Vision Computing*, Vol. 25, pp. 1124–1133, 2007.

[4] Maswadeh Waleed, Tripathi Ashish, Arnold Neil S., DuBow Joel and Meuzelaar Henk L.C. "High speed, two-wavelength radiation thermometry of single micro particles during CO2 laser heating". *Journal of Analytical and Applied Pyrolysis*, Vol. 28 n^o 1, pp. 55 – 70, 1994.

[5] Tago Yuichiro, Akimoto Fumie, Kitagawa Kuniyuki and Arai Norio. "Measurements of surface temperature and emissivity by two-dimensional four-color thermometry with narrow bandwidth". *Energy*, Vol. 30 n^o 2-4, pp. 485 – 495, 2005.

[6] Eller Martin (DE). *Patent: Protection tubes for sensors or glow elements*, ep0945724 edition, September 1999.

[7] SPECIALMETALS. *http://www.specialmetals.com/products/inconelalloy600.php*.

[8] Wilson Jon S. *Sensor technology handbook*. Elsevier Inc., 2005.

[9] Payri F., Pastor J. V., García J. M. and Pastor J. M. "Contribution to the aplication of two-colour imaging to diesel combustion". *Measurement Science and Technology*, Vol. 18, pp. 2579–2598, 2007.

[10] Lindl Bruno and Schmitz Heinz-Georg. "Cold-start equipment for diesel direct-injection engines". *SAE Paper 1999-01-1244*, 1999.

Chapter 6

Influence of nozzle geometry

Contents

6.1 Introduction

This Chapter is devoted to study the influence of nozzle geometry on pilot ignition and main combustion progress under glow plug-assisted cold start conditions. Starting from the results presented in Chapter 4, in which a description of pilot ignition combustion progress was presented, this chapter is aimed at validating previous hypothesis and to gain more insight on the role of injection on ignition and combustion. Within this frame, nozzle geometry is a very interesting parameter, since it allows to understand fundamental physical phenomena, and at the same time it is an important and interchangeable engine part for which no dedicated studies under cold start conditions have been found in the literature. Four different multi-orifice and micro-sac injector nozzles have been used in the present study, their nominal characteristics are summarized on Table 3.3.

In this chapter, characterization tests results are shown first. These results have allowed to know the main flow characteristics induced by the different nozzles

Table 6.1. *Test matrix of conditions tested in Chapter 6.*

Rail pressure	m_f	Nozzle	Hole diameter	Number of orifices
bar	mg	-	mm	-
Pilot ignition				
200/370	6	N1	0.121	6
250/370	6	N2	0.145	6
370	6	N2	0.145	6
370	6	N3	0.142	7
370	6	N4	0.125	9
Main combustion				
200/370	6+24	N1	0.121	6
250/370	6+24	N2	0.145	6
200/370	6+24	N3	0.142	7
200/370	6+24	N4	0.125	9

geometries. From characterization results, combustion-visualization results have been analyzed and understood properly. Engine results are divided according to the injection strategy, namely pilot or full injection strategy. Table 6.1 also summarizes the conditions tested. The pilot injection tests are sub-divided in two studies according to two parameters that could be isolated after the characterization tests: fuel speed (nozzles N1 and N2) and injected mass (nozzles N2, N3 and N4). For the full injection strategy, tests results of all nozzles are used together.

It is remarkable the fact that the minimum level of rail pressure is lower for nozzle N1. This difference has been taken into account, and characterization tests have allowed to make comparisons in terms of flow parameters instead of engine parameters. For example, pilot injection is shown as a function of fuel speed and injected mass which are two flow parameters that depend on the engine parameters and the nozzle geometry. In the same way, main injection results have been treated in terms of momentum flux, instead of engine or geometry parameters. In this way, the analysis of the results can be performed by looking at physical variables and the explanation can be extended to different configurations.

6.2 Nozzle characterization results

Nozzle characterization results are presented in this section. These results have allowed to understand the differences between the four nozzles in terms of fuel flow physical variables. This information has been used later to understand and analyze

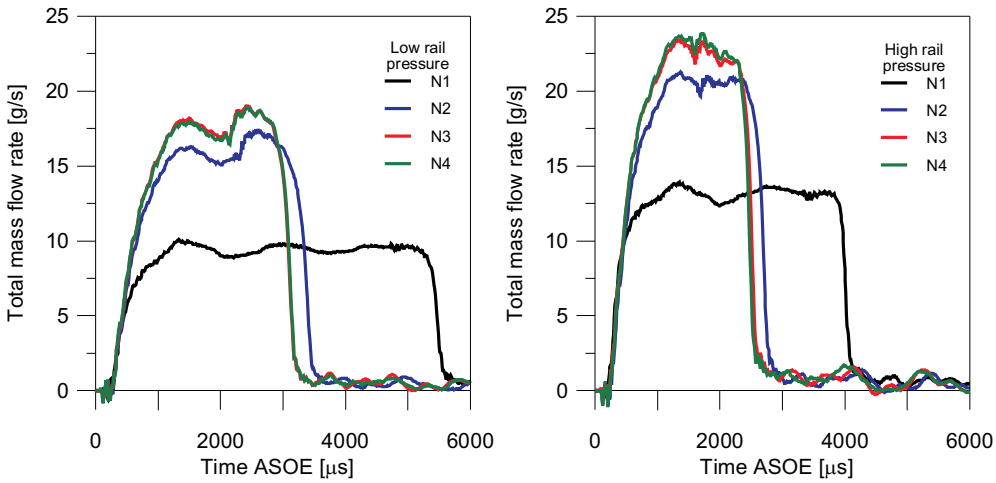

Figure 6.1. *Fuel mass flow rate as a function of time for each one of the nozzles tested using a single injection strategy of 44 mg at both levels of rail pressure.*

engine results presented in the following sections. The most important sources of information are the fuel mass and momentum flux measurements, which deliver information about the fuel flow characteristics at the nozzle exit. Additionally, macroscopic spray visualization results are shown to check specific issues of the spray temporal and spatial evolution under such low density conditions.

6.2.1 Mass flow rate and momentum flux tests results

Based on flow characterization, this section intends to show how fuel is delivered during two differentiated periods, stabilized and transient injection period. The stabilized period is the time lap during which the injector nozzle is fully open and, as a consequence, the mass flow rate and momentum flux signals reach maximum and stabilized conditions. Such conditions are reached only if the amount of fuel injected (controlled by means of the injector energizing time) is large enough. During this period momentum flux measurements can be performed properly and effective values of nozzle hole area and fuel speed at the nozzle exit can be calculated. How fuel is delivered during this period is closely related with the combustion rates during main combustion. The transient period during which the nozzle hole is opening also has special interest for being directly related with how fuel is delivered in pilot injection strategies. Using the available methodology, momentum flux measurements cannot be performed for transient injection evolutions, which has forced to make an estimation of the fuel speed for pilot injections.

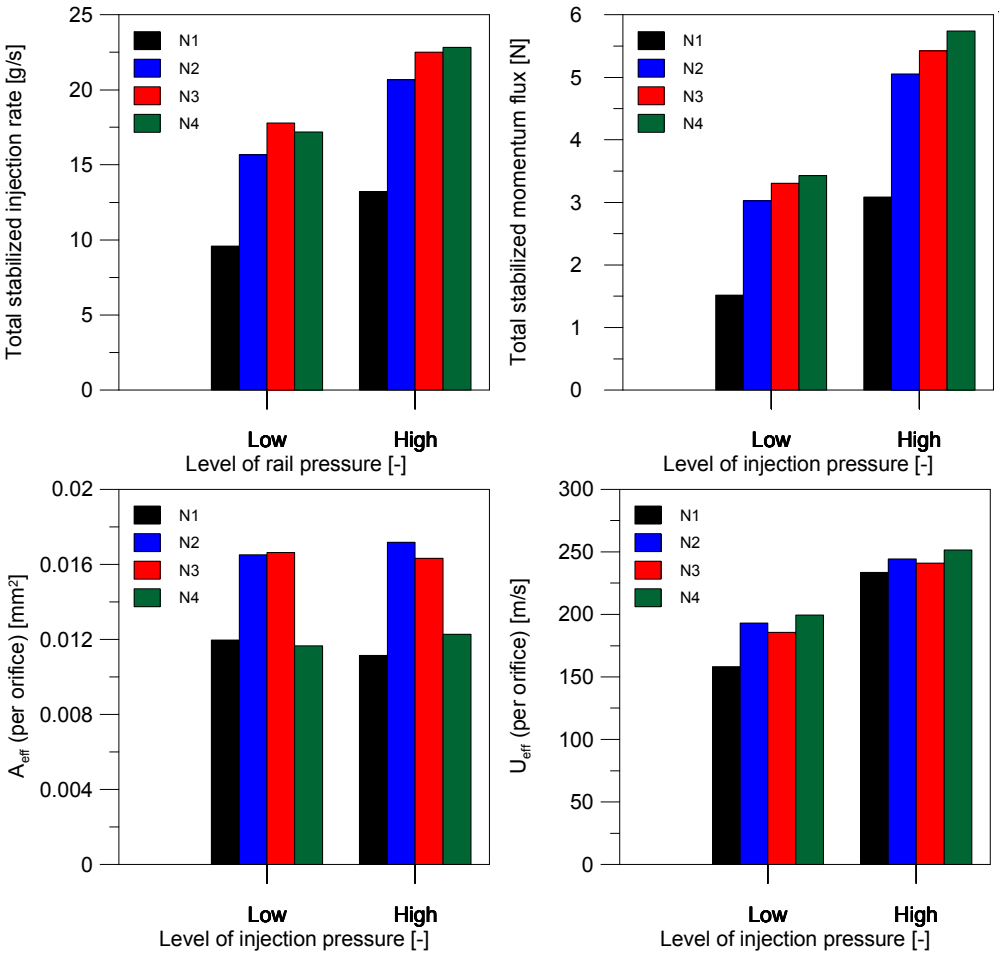

Figure 6.2. *Total stabilized mass flow rate and momentum flux, $A_{eff-max}$ and $U_{eff-max}$ at both levels of rail pressure for the four nozzles.*

Regarding the stabilized injection period, mass flow rate and total[1] stabilized values are shown in Figures 6.1 and 6.2, respectively. The conditions showed correspond to a single injection of 44 mg for the four nozzles at both levels of rail pressure. The mass flow rate traces plotted in Figure 6.1 show how nozzles N2, N3 and N4 follow a different evolution in comparison with nozzle N1. It is shown how the maximum values are reached according to the Bosch flow number values given in Table 3.3. That is, nozzles $N3$ and $N4$ reach the highest mass flow rate, closely followed by nozzle $N2$. On the other hand, nozzle $N1$ is considerably different, this nozzle reaches a maximum mass flow rate value which is around the half of those reached by nozzles

[1]In this section, *"total"* (e.g. total injected mass or total momentum flux) refers to the addition over all the nozzle holes

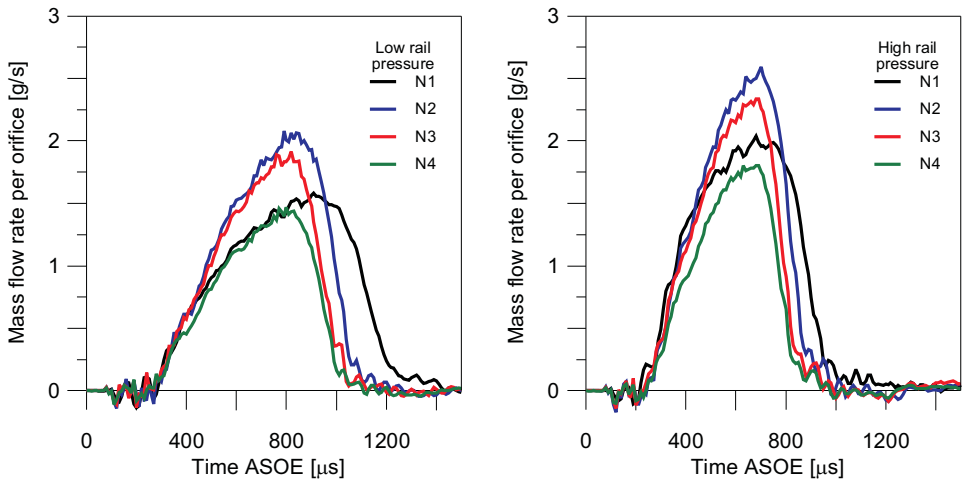

Figure 6.3. *Mass flow rate per orifice as a function of time ASOE for the four nozzles tested at both levels of rail pressure.*

$N3$ or $N4$. And as a consequence, for constant injected mass strategy this nozzle needs a considerably larger injection duration. The maximum-stabilized values are shown in Figure 6.2, namely mass flow rate ($\dot{m}_{0-max}$) and momentum flux ($\dot{M}_{0-max}$) total stabilized values, maximum effective nozzle hole area and maximum fuel speed at the nozzle exit. The nozzle area $A_{eff-max}$ has been calculated according to:

$$A_{eff-max} = \dot{m}^2_{0-max}/(\dot{M}_{0-max} * \rho_f) \tag{6.1}$$

where ρ_f is fuel density. And the maximum fuel speed at the nozzle exit has been calculated according to:

$$U_{eff-max} = \dot{M}_{0-max}/\dot{m}_{0-max} \tag{6.2}$$

The total stabilized momentum values shown in the figure range between 1 and 6 N, it will allow gain more insight on the role of the momentum induced by injection as combustion promoter. $A_{eff-max}$ values shown agree very well with the nominal area values calculated with the diameters given in Table 3.3 and they will be used to estimate fuel velocity during the transient injection period. Finally, $U_{eff-max}$ values shown in Figure 6.2 follow the same trend as the total stabilized momentum flux, the higher values are reached with nozzle $N4$ and the lower with nozzle N1. However, intermediate stratification is not exactly the same as for momentum.

Results concerning pilot injection are shown in Figure 6.3 in terms of mass flow rate per orifice, for a single pilot injection pulse of 6 mg, for the four nozzles and at both levels of rail pressure. In these plots, the mass flow rate per orifice is shown, instead of the total value, since the pilot injection ignition is the result

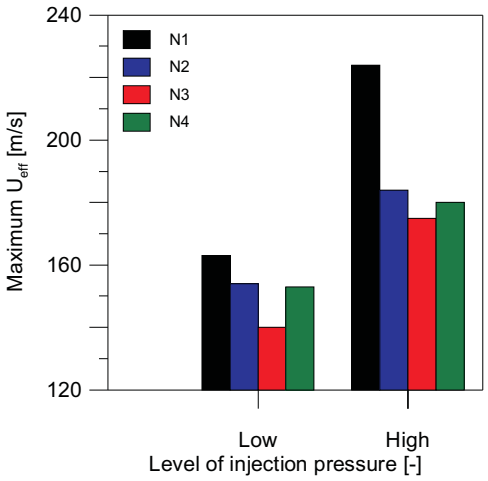

Figure 6.4. *Estimated maximum fuel speed reached during pilot injection for the four nozzles, at both level of rail pressure and for a single injection of* 6 *mg.*

of the interaction between the glow plug and only one of the sprays. It must be taken into account that, as the injection strategy keeps a total injected mass, the amount of fuel injected per orifice is different between nozzles in dependency of the number of holes. Regarding the results, it is clear how the mass flow rate trace never reaches stabilization under these conditions, which makes pilot injection a completely transient phenomena. It is also observed that differences among nozzles are smaller, compared with the differenced observed during the stabilized period, but these small differences could still play a role on pilot ignition.

To further evaluate the transient period, the maximum fuel speed reached during pilot injection has been estimated for all the injection conditions. This speed serves as a reference to the fuel motion after EOI, which, at the same time, has strong influence on pilot ignition (as will be shown in Chapter 7). This speed cannot be directly calculated from mass flow rate and momentum flux measurements, as it has been done during the stabilized period, since reliable momentum flux measurements cannot be performed during transients [1]. Therefore, an effective fuel speed (U_{eff}) has been calculated according to Equation 6.3:

$$U_{eff} = \dot{m}_0/(A_{eff-max} * \rho_f) \tag{6.3}$$

where $\dot{m}_0$ is measured mass flow rate per orifice (as those shown in Figure 6.3), $A_{eff-max}$ is effective nozzle transversal area (shown in Figure 6.2) and ρ_f is fuel density. In this way, by assuming a constant $A_{eff-max}$, which will be equal to the one during the stabilized injection period, the maximum effective speed can be estimated. This approach has been followed previously in [2] and it has been considered quite

acceptable for micro-sac nozzles. Regarding the results, the estimated maximum fuel speed is plotted in Figure 6.4 for the four nozzles at both levels of rail pressure for a single injection of 6 mg. In this graph, it is observed how maximum fuel speed reached with nozzle $N1$ is clearly higher, compared with any of the other three nozzles. Nevertheless, a direct comparison can only be done with nozzle $N2$ for which the same amount of fuel is injected. Between these two nozzles ($N1$ and $N2$), the difference could be due to the fact that the transient period at the start of injection is faster for $N1$ and that the injection rate is closer to reach stabilization for this nozzle. Comparing nozzles $N2$, $N3$ and $N4$, no major differences in fuel speed arise, but it must be taken into account that a different amount of fuel is injected by each of them due to the number of orifices.

6.2.2 Non-vaporizing spray visualization results

Non-vaporizing spray visualization tests have been performed with the purpose of detecting differences between nozzles in terms of spray global evolution. Within this evolution and considering the spray development in the combustion chamber, the time instants at which liquid fuel reach the position of the glow plug and the position of the chamber walls are particularly interesting. For these tests, injections were performed into a volume filled with nitrogen at the same density as in the engine at TDC (16 kg/m^3), as a reference to cold start conditions, and at 40 kg/m^3, as a reference to more conventional high-load diesel conditions. A representative example of the results is shown in Figure 6.5(a), in which spray penetration is plotted as a function of time at both density values and for two nozzles ($N2$ and $N4$) with notably different orifice diameter. At low density, spray penetrates rapidly and linearly (with respect to time) reaching the bowl walls distance in a short time and no differences between nozzles have been detected in spite of the difference in orifice diameter. This lack of dependence on orifice diameter can be better understood by looking at the high density case, for which two periods can be differentiated. From SOI until approximately 800 μs, the spray penetrates quasi-linearly without significant differences between nozzles, as in the low density case. This period corresponds to the time that it takes for the injection rate to reach stabilization. During this initial transient stage, spray size is small, entrainment is not steady and spray penetration depends more on injection velocity (Fig. 6.4) than on momentum flux. In the second period, spray penetrates at a slower rate (approximately with the square root of time) and differences start to be noticeable, spray penetration becomes higher for nozzle $N2$. This is the logical trend according to current knowledge from diesel spray behavior (e.g. Naber and Siebers [3]), the larger the orifice diameter, the larger the spray penetration due to the larger momentum flux (Fig. 6.2). When transferring this information to analyze in-cylinder engine spray evolution, it can be concluded that, at low density, the liquid spray penetrates so fast that it will reach the chamber walls during the first injection period and there should be no differences among nozzles.

The effect of rail pressure on spray penetration is shown in Figure 6.5(b). This effect is shown only for one of the nozzles (N4) since the effect should be similar for the rest of the nozzles. Liquid spray penetration is plotted as a function of time for

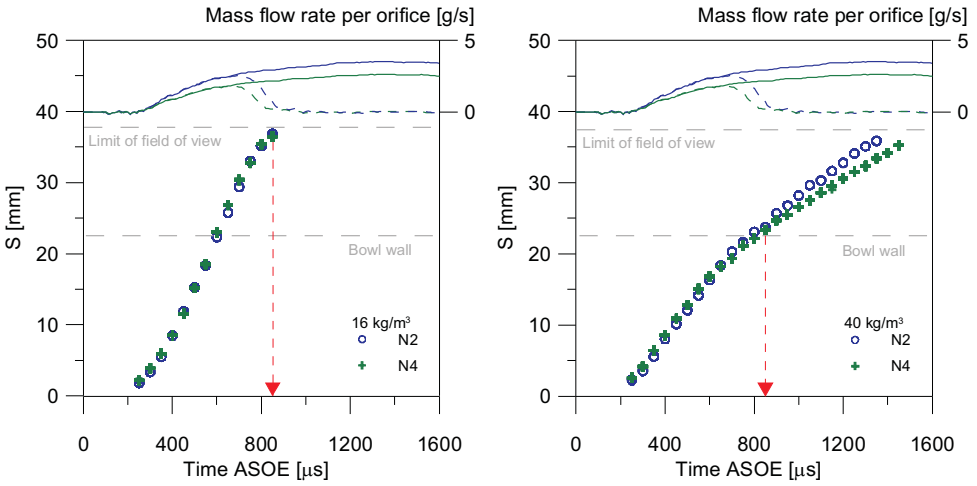

(a) Nozzle geometry influence

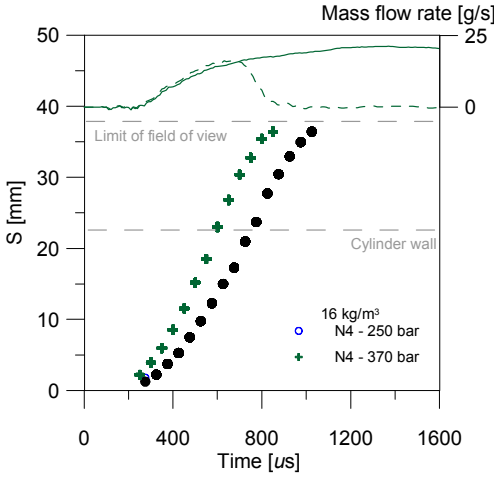

(b) Rail pressure influence

Figure 6.5. *(a) Fuel penetration in mm as a function of time for nozzles* 2 *and* 4 *at high level of rail pressure for two different densities.* 16 kg/m^3 *left and* 40 kg/m^3 *right. (b) Fuel penetration in mm as a function of time for nozzle* 4 *at both levels of rail pressure for the low density condition (*16 kg/m^3*). The mass flow rate for a long and a pilot injection are plotted in the top of each graph. The test rig limit of field of view and the bowl wall distance are signaled with gray lines.*

both levels of rail pressure at the lower density (16 kg/m^3). At higher rail pressure the spray penetrates more rapidly into the combustion chamber due to the higher momentum flux. In this figure, the hypothetic cylinder wall distance is also plotted. The spray reaches this distance with a difference of around 200 μs between both levels of rail pressure. Again, if one thinks of these results in terms of in-cylinder engine spray evolution, a small difference in terms of time of arrival to the wall can be expected between the both levels of rail pressure tested.

6.3 Nozzle influence on pilot ignition

Pilot injection under glow plug-assisted cold start conditions is a remarkably important process due to its role as ignition promoter. In Chapter 4, the first luminosity spots where found to occur in the glow plug close vicinity some time after EOI. The apparition or not of these spots and their luminosity intensity were shown to have dependency on rail pressure and on the amount of fuel injected. Testing different injection nozzles allows to modify fuel flow keeping the rail pressure and/or the total injected mass the same. In other words, it allows to isolate effects in order to gain insight on the pilot ignition controlling mechanisms. In this sense, using a constant injection strategy of 6 mg, changing the rail pressure, number of orifices or orifice geometry provokes differences in injected mass per orifice and the rate at which fuel is injected. The effect of these differences on pilot flame ignition and combustion progress are aimed to be investigated in this section. First, the effect of nozzle geometry is isolated, since nozzles $N1$ and $N2$ inject the same amount of fuel per orifice with a notably different nozzle geometry. Then, the effect of the injected fuel is presented, given that $N2$, $N3$ and $N4$, due to the different number of orifices, deliver a different amount of fuel per orifice.

By keeping a constant injected mass per orifice, the effect of nozzle geometry can be isolated. First, results for two nozzles with the same number of orifices but notably different orifice diameter and conicity will be presented. If a constant total pilot mass is maintained, both nozzles deliver the same injected mass per orifice. Characterization results have shown that the main effect of nozzle geometry and rail pressure observed in the investigated nozzles is a change in the speed at which fuel is delivered. The effect of both, nozzle geometry and rail pressure, has been grouped in this section as a function of the maximum fuel speed and it is shown in Figure 6.3. Results evidence that both pilot probability and IL depend on fuel speed. Actually, they are observed to drastically decrease when fuel speed is increased. Besides, LD does not depend on fuel speed, while it seems to correlate with EOI, since the time between EOI and the appearance of the first flame spots is very similar for these four different injection conditions. The present results agree with previous trends reported in Chapter 4 for a single nozzle where an increase of rail pressure was shown to decrease both ignition probability and IL. Under those conditions, pilot mass was kept constant when changing rail pressure (*i.e.* higher fuel velocity). Present results hint at the fact that changing fuel velocity by modifying either rail pressure or nozzle geometry have similar consequences.

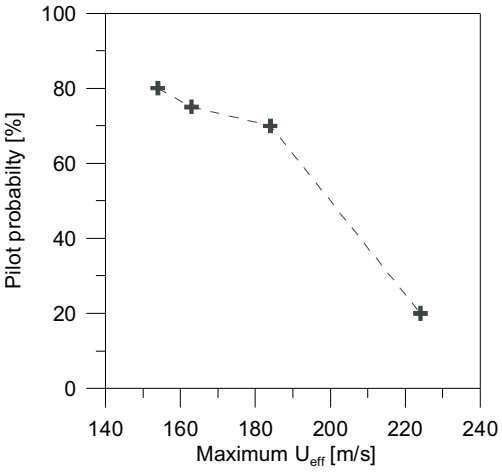

(a) Pilot probability

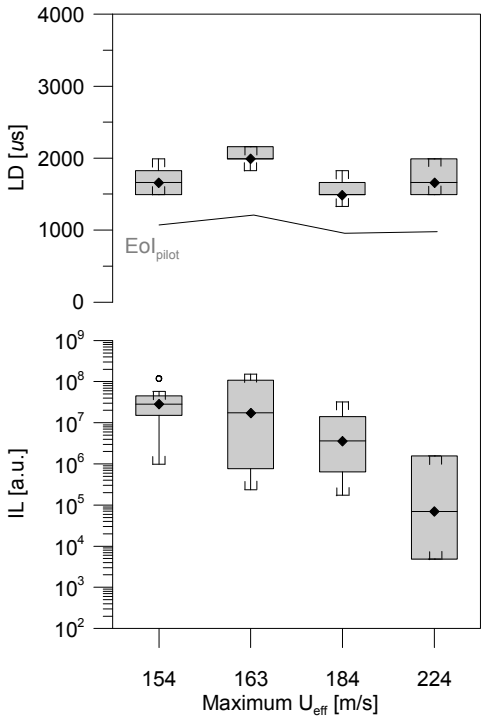

(b) LD and IL

Figure 6.6. *Pilot probability (a), LD and IL (b) as a function of maximum fuel speed at both levels of rail pressure, for nozzles $N1$ and $N2$ with a constant injection strategy of* 6 *mg at TDC.*

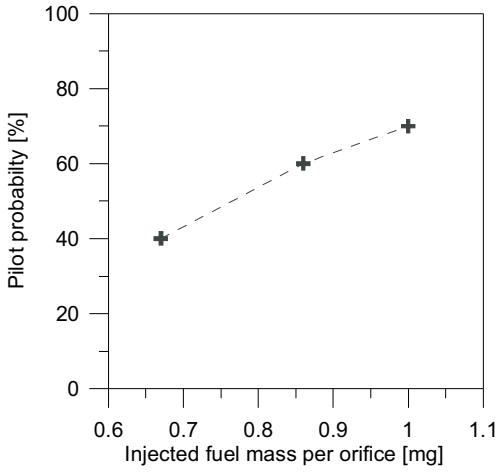

(a) Pilot probability

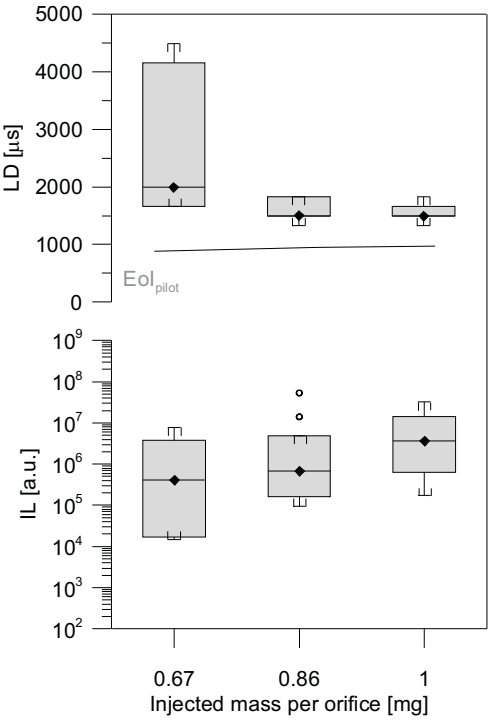

(b) LD and IL

Figure 6.7. *Pilot probability (a), LD and IL (b) as a function of the injected fuel mass per orifice. These results correspond to a rail pressure of* 370 *bar, for a single injection pulse of* 6 *mg for nozzles* $N2$, $N3$ *and* $N4$.

The influence of injected mass per orifice is shown for nozzles N2, N3 and N4 at a constant total injected mass of $6mg$. Results from injection characterization have shown that maximum fuel speed for such conditions will be very similar. According to that, the main effect introduced by these nozzles is the amount of fuel injected. Figure 6.3 shows pilot probability, LD and IL as a function of the injected mass per orifice at the high level of rail pressure. Increasing injected mass per orifice, under these conditions, has a positive effect on the appearance probability of the pilot flame and on flame intensity (IL). Regarding LD, no large variation is observed when increasing the injected mass per orifice. In agreement with previous results (Figure 6.3), the time between EOI and the first appearance of flame seems to remain constant for these three nozzles. These results hint at the fact that increasing injected mass per orifice with similar maximum fuel speed improves conditions for ignition noticeably, probably due to an increasing amount of fuel reaching the glow plug.

Results shown in this section have allowed to isolate the positive effect of increasing the amount of injected mass per orifice and the negative effect of increasing the fuel speed during the injection event. These two effects are combined when the total pilot injection mass is increased keeping the injection nozzle and rail pressure the same, which has been previously presented in Sub-section 4.3.1. In that case, increasing the total pilot injected mass made autoignition more difficult, delayed the apparition of flame and diminished the amount of light radiated by burning fuel. These trends can now be explained due to the fact that the negative effect of increasing fuel speed is more important than the positive effect of increasing the amount of injected mass per orifice.

6.4 Nozzle influence on main combustion

The injector nozzle influence on the main combustion event is presented in this section according to the test matrix for *"Main Combustion"* in Table 6.1. Specifically, the initiation of the combustion process, the total work obtained per cycle and the efficiency of that process are discussed in this section for the four nozzles. Results for each nozzle are presented at both levels of rail pressure. It will allow to detect, if any, possible cross effects and to validate hypothesis for a wider range of possibilities.

Figure 6.8 shows, for a wide range of conditions (four nozzles at two levels of rail pressure), combustion probabilities of full injection tests plotted versus the pilot flame appearance probabilities measured in independent tests. Although the match is not perfect, this figure shows that the probability of combustion at a given condition (a given nozzle at a given rail pressure) is quite similar to the probability of appearance of the pilot flame. This trend is very similar to that shown in Fig. 5.2 in which the same result was obtained when testing different orientation angle configurations. These results prove that, for the conditions tested, pilot ignition strongly influences the full-strategy success. For this reason, the factors that control main combustion start are the same factors that determine pilot injection success, which have been discussed in the previous section.

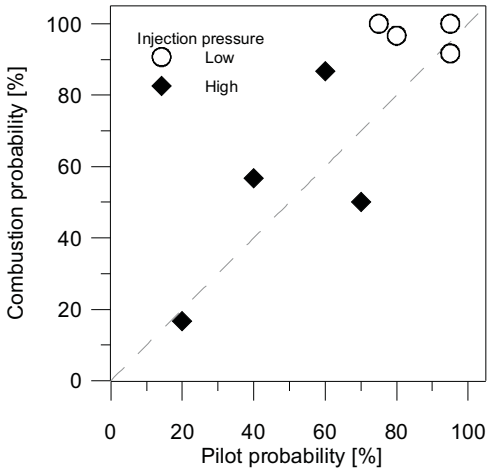

Figure 6.8. *Full combustion probability as a function of the pilot injection appearance probability. In this plot, results of the four nozzles at both levels of rail pressure are shown.*

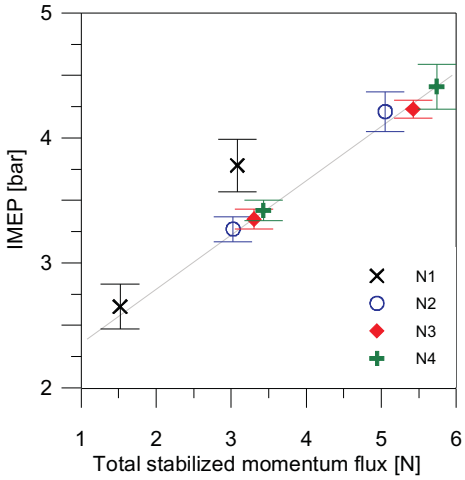

Figure 6.9. *Average IMEP for cycles with positive work and early SOC of 30 repetitions tests as a function of total momentum multiplied by the number of orifices. The confidence interval of the mean (with a confidence level of 95%) is plotted with error bars.*

Regarding the fact that injection is the main combustion progress promoter, it was also reported in Sub-section 4.3.2 that increasing rail pressure has a positive effect on IMEP probably due to a higher momentum induced by the injection event. This statement can be reinforced by looking at Figure 6.9, in which average IMEP values are plotted as a function of the total momentum for full-strategy combustion tests. This average has been calculated only for the cycles with positive work and early SOC from 30 repetitions tests for the four nozzles at both levels of rail pressure. The total momentum has been calculated multiplying the measured momentum flux by the number of orifices of a given nozzle. Figure 6.9 shows a very good correlation between IMEP and the total momentum, evidencing the strong influence of rail pressure and the weak effect of the nozzle geometry. This result leads to the conclusion that combustion rates are controlled by the momentum flux introduced by the sprays.

6.5 Conclusions

The influence of the nozzle geometry on ignition and combustion development has been studied for four nozzles with characteristics similar to those that current injection technology present nowadays. For these nozzles, important fuel flow characteristics were observed by means of characterization tests in two differentiable injection periods. On the one hand, during the transient period at the beginning of injection, which concerns to pilot ignition, noticeable differences in fuel speed were detected in dependency of the nozzle geometry. On the other hand, important differences were also detected between nozzles during the stabilized injection period in terms of momentum flux induced by the sprays, which promotes combustion progress.

For conditions under investigation it was shown how combustion initiation is promoted, almost exclusively, by pilot injection flame. This clear dependence allows to split the combustion problem in two parts. On the one hand, ignition, which is controlled by pilot injection and can only be monitored by means of visualization. And on the other hand, main combustion progress which is promoted by the injection event and can be measured with classical in-cylinder pressure analysis.

Regarding pilot ignition, this study has allowed to separate two different injection parameters that are sensitive to different nozzle geometries, namely the amount of fuel injected and fuel speed. Increasing the amount of fuel injected per orifice, keeping the fuel speed the same, has a positive influence on ignition, since more fuel is available to be burnt. On the contrary, increasing the fuel speed worsen considerably conditions for ignition. These two effects were shown together in Chapter 4 when the pilot injected mass was modified using the same nozzle. In that chapter and in the present one, the effect of fuel speed has proved to be more determinant that the effect of the amount of fuel injected. For this reason, pilot ignition probabilities are enhanced at low rail pressure, by using short injection pulses. More detail on the explanation of the effect of fuel speed on ignition will be presented in Chapter 7.

Regarding main combustion development, a clear dependence between the momentum induced by the injection event and the amount of work obtained per cycle

has been observed. The higher the momentum, higher is the work obtained per cycle. For this reason, both parameters, rail pressure and nozzle geometry, have shown to have influence on main combustion progress. Comparatively, the effect of rail pressure is stronger than the effect introduced by different nozzle geometry. Summarizing, the present study concludes that a compromise must be done, under this conditions, in order to find optimum settings for both, ignition and combustion progress.

Bibliography

[1] Gimeno Jaime. *Estudio de la inyección diesel mediante la medida del flujo de cantidad de movimiento del chorro.* Editorial Reverté, 2011.

[2] Payri R., Salvador F. J., Gimeno J. and De la Morena J. "Influence of injector technology on injection and combustion development. Part 1: Hydraulic characterization". *Applied Energy*, 2010. In press.

[3] Naber Jeffrey D. and Siebers Dennis L. "Effects of gas density and vaporization on penetration and dispersion of diesel sprays". *SAE Paper 960034*, 1996.

Chapter 7

Discussion on cold start ignition mechanisms

Contents

7.1 Introduction

From the experimental results presented previously, the ignition sequence can be summarized according to the conceptual model presented in Section 4.4. This sequence starts with the injection of a relatively short pilot injection pulse. Fuel exits from the nozzle hole and reaches the piston walls within a few hundred microseconds (300 μs at 370 bar rail pressure), as seen in Fig. 4.3. The time of arrival to the wall does not depend on nozzle geometry, but it does depend on rail pressure (as shown in Figure 6.5(b)). In fact, the difference in time of arrival to the wall provoked by a change in rail pressure (between the two levels tested in this thesis) was measured to be around 150 μs. Injection finishes and first ignition spots appear between 500 and 1000 μs later on the glow plug vicinity, as shown in 4.2.1. If pilot ignition occurs with a short delay and the reaction zone remains active until main injection start, combustion progresses within the chamber and a relatively large amount of total fuel injected could be burnt depending on rail pressure (Chapter 4), injection duration (Chapter 4) and nozzle geometry (Chapter 6).

This Chapter is devoted to piece together an explanation of the processes that lead to ignition under glow-plug assisted cold start conditions. The most relevant experimental results regarding pilot ignition that have been presented along this thesis are grouped with specific modeling results with the purpose of showing a single and coherent explanation.

This Chapter is focused solely on pilot injection ignition due to its direct influence on main combustion initiation and indirect influence on main combustion development. Regarding main combustion initiation, strategies with high pilot flame appearance probability have also been shown to have high combustion probability (Figures 5.2 and 6.8). Regarding main combustion development it has been shown that if main combustion initiation occurs early, during injection event (starting from pilot flame), the work obtained per cycle and the combustion efficiency can be also high, as shown in Fig. 5.4.

In order to know the controlling parameters that lead to pilot ignition more information is needed, since it is very difficult to obtain reliable experimental information from the end of injection until first ignition spots appearance on the glow plug. This is the blank that this chapter aims to fill. Specifically, different questions regarding pilot injection ignition arise. First, knowing that in the nominal case the spray is oriented so that its radial limit contacts the glow plug and that the spray reaches the glow plug area approximately after 133 μs after start of injection, why is ignition always delayed with respect to end of injection? Such delay is observed even when the closest spray is directed toward the glow plug, as shown in Section 5.2.1. Another question arises of the relationship between LD and IL , since higher IL is usually obtained for cases with short LD (as observed in Figures 4.6, 4.8(b), 5.3, 5.9, 6.6(b) and, 6.7(b)) Regarding glow plug surface temperature, it would be interesting to know until which extent this temperature is determinant for pilot injection ignition. And regarding the parametric variations, it would be interesting to find out why the effect of increasing fuel velocity is negative. And finally, it would be interesting to know about the effect of swirl, since conditions for ignition are better if the spray is oriented in up-swirl direction. Can swirl, at its low speed compared with injection, drag fuel toward the glow plug? The aim of this chapter is trying to provide additional discussion arguments to clarify these questions.

The chapter has been divided into five sections. After this introduction, the following section is devoted to explain two main parameters that lead to ignition, namely local glow plug temperature and mixture preparation. After this description, some of the parametric variations results are explained. The chapter closes with the main outcomes of the discussion.

7.2 Study of the processes that lead to pilot ignition

From a general point of view [1], in order to reach ignition conditions liquid fuel must evaporate, mix with air and react chemically promoted by the mixture temperature. All these processes must occur rapidly since in-cylinder conditions

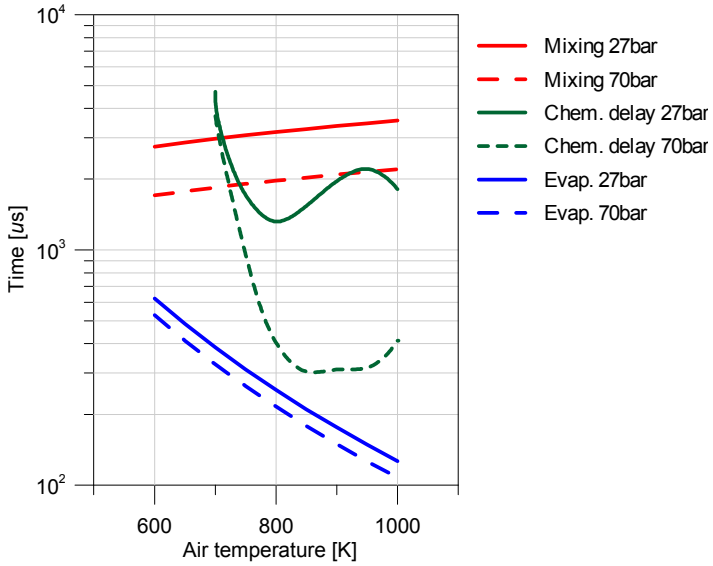

Figure 7.1. *Characteristic combustion times, namely evaporation, mixing under stoichiometric conditions and chemical delay, as a function of air temperature. Low temperature cold start conditions (27 bar) are compared with "Normal" diesel conditions (70 bar).*

change both spatially along the combustion chamber and temporally with piston evolution. The slowest process would be the one that controls ignition. As a reference of the rate at which each of these processes occur, Figure 7.1 shows the characteristic times for steady full evaporation, mixing and chemical ignition delay for a stoichiometric mixture as a function of air temperature. The first two ones have been obtained from quasi-steady mixing-controlled vaporizing spray analysis. The latter one is derived from chemical kinetics calculations that will be fully analyzed in 7.2.1. Calculations have been performed for two different values of in-cylinder pressure, 70 and 27 *bar*. It must be mentioned that, while physical times change monotonically from low to high temperature, chemical times show a different behavior. As temperature is increased, there is a range within which chemical delay is reduced but above certain value chemical delays are increased. This is due to the negative temperature coefficient effect and it can be better observed for the 27 *bar* condition.

Under conventional diesel conditions [2], *e.g.* 70 *bar* and around 900 K, mixing characteristic times are considerably much more important that chemical ignition delay or evaporation characteristic times. Hence, combustion under such conditions is known to be *mixing-controlled* [3]. Nevertheless, at cold start conditions, 27 *bar* and around 600 K, chemical times are much longer than any physical time, being chemistry the controlling process. For this reason, it becomes necessary to use ignition aids as intake heaters or glow plugs in order to reduce chemical times to reasonable values to allow ignition. Using a glow plug, mixture temperature could be increased

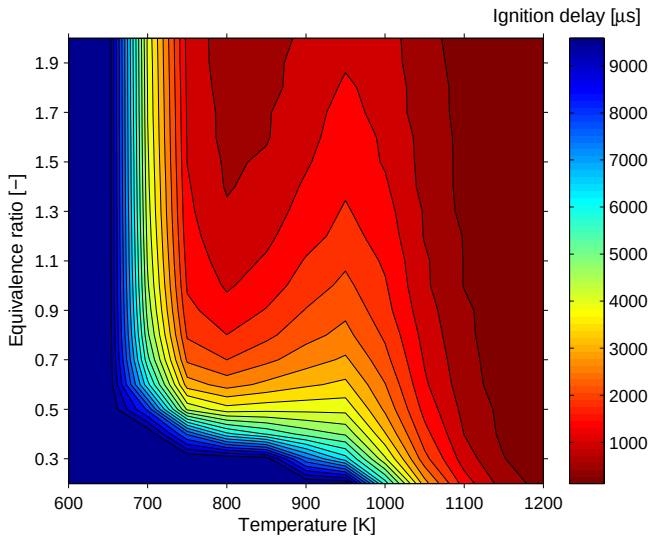

Figure 7.2. *n-Heptane predicted ignition delay as a function of equivalence ratio and temperature at a constant pressure of* 27 *bar*.

up to approximately 1000 K, temperatures at which chemical delay times are reduced to values slightly lower than those of mixing times allowing ignition in a reasonable time period.

This explanation has given an overall picture of how important physical and chemical delays are for the combustion of fuel-air mixtures under different conditions of temperature and pressure. Next in this section, more insight on how these processes develop to reach ignition is aimed to be gained but applied to the particular problematic of this thesis (geometry and thermodynamic conditions). The contribution of the chemical processes and vaporization will be presented together due to their common dependency on local temperature. Next, an explanation of mixture preparation in the glow plug area is given.

7.2.1 Effect of local temperature

To start with, the ignition delay caused solely by the chemical processes is represented as a function of temperature and equivalence ratio in Figure 7.2 for a constant pressure of 27 *bar*. This pressure value corresponds to the peak in-cylinder pressure at TDC, which can be considered a representative value during the ignition process since small pressure variations do not have considerable effect on autoignition. These calculations clearly show how strong the effect of temperature stratification on autoignition delay under these conditions is. At temperatures similar to those that can be reached far from the glow plug (in-cylinder bulk temperature of approximately

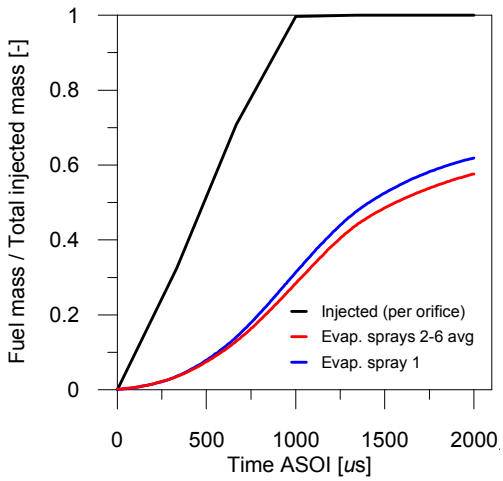

Figure 7.3. *Injected mass per orifice, evaporated mass in the closest spray to the glow plug (spray 1) and average of the evaporated mass in the other sprays (sprays 2-6) as a function of time. These calculations have been performed by means of CFD for each one of the sprays during the pilot injection event for a six-holes nozzle.*

600 K), autoignition delay is independent of the equivalence ratio and it is longer than 10 ms, which is well above experimental values. On the contrary, at temperatures as high as those that can be reached on the glow plug surface (near 1200 K), autoignition delay decreases to a few hundred microseconds with some dependency on equivalence ratio, namely ignition delay is shorter for higher equivalence ratio values. Experimental luminosity results presented in 4.2.1 show that autoignition is limited to the glow plug vicinity, and the shortest LD values were in the range between 1200 and 1500 μs, which falls between both limiting cases mentioned before. This indicates that both, temperature and equivalence ratio, will have an influence on ignition delay.

Another remarkable result regarding glow plug temperature is the one presented in Section 5.3.2, in which it was shown that an increase in glow plug temperature provokes reductions in LD but above certain value its contribution is negligible. Glow plug temperature affects two important processes, chemical kinetics and vaporization. Regarding chemical kinetics, Figure 7.2 shows that at temperatures near 1200 K chemical ignition delays are reduced to very low values. Any further temperature increase would not provoke substantial reductions in chemical delays. Regarding vaporization, the heating effect of the glow plug on the closest spray can be observed in Figure 7.3. In this figure, the injected mass per orifice, the evaporated mass in the closest to the glow plug spray (spray 1) and the average of the mass of fuel evaporated in the other sprays (sprays 2-6) are plotted as a function of time for a 6 mg pilot injection. All these parameters have been obtained from CFD calculations. First, it is observed that at the end of injection only around 30% of the injected mass has been evaporated due to the low temperature conditions within the chamber. And

regarding the effect of the glow plug, it is observed that more fuel is evaporated in the closest spray but the difference is less than 5% with respect to the others sprays, which does not really make a significative difference. All these, leads to the conclusion that the true role of the glow plug is to accelerate chemical reactions rather than to enhance vaporization. However, chemical reactions can be accelerated only until one point from which any temperature increase will not bring about a chemical ignition delay reduction. This addresses one of the questions that arose at beginning of this chapter, glow plug temperature controls ignition but it is not the only controlling parameter and its effect is limited since above 1200 K no chemical ignition delay reductions are provoked.

7.2.2 Effect of mixing process

After locating the only possible ignition spot on the glow plug close vicinity, mixing local properties have been evaluated and they are plotted in Figure 7.4 as a function of time. Figure 7.4 combines experimental data with detailed numerical information about mixing and fuel motion. The experimental data consists of mass flow rate per orifice, which is a reference to the injection event, and I_{cummul} evolution of five different repetitions, which serve as a reference of the start of luminosity. On the other hand, the numerical information consists of fuel and air speeds (maximum and minimum for each of them) on a plane that contains the spray and cylinder axes, which can give an idea of the governing motion as a function of time, and the average equivalence ratio in a small volume with an approximate thickness of 1 mm around the glow plug, which together with the glow plug temperature governs ignition. The condition shown in the figure corresponds to a 6 mg pilot injection at 250 bar for a seven-holes nozzle.

From the equivalence ratio evolution, one can observe that there is a minimum delay for the injected fuel to travel from the nozzle to the glow plug area, *i.e.* no fuel vapor is observed in the glow plug area before 500 μs ASOI due to the time needed for the spray to reach this location. After this delay, there is a steep increase in equivalence ratio up to a maximum value, which is reached approximately 700 μs after EOI. Until EOI, fuel supply is due to the ongoing injection event. But after EOI, the evolution is fully governed by the leaning process going on throughout the spray. The reason why fuel (vapor or droplets) follows this flow pattern AEOI can be better explained as shown in Fig. 7.5. This Figure presents three selected time-instants of the temporal evolution of the droplets and the air velocity (vectors) on the spray symmetry plane (these selected time-instants correspond with the timings marked with red asterisks in Figure 7.4). This image-sequence shows how spray grows with time as injection progresses and a vortex develops, indicating the air entrainment process into the spray. During this period, fuel flow is driven by injection. After EOI, there is a strong deceleration of the spray starting from the nozzle hole that spreads over the whole spray very fast. Later fuel movement is mainly driven by the air vortex developed during injection. This image-sequence shows fuel droplets moving toward the glow plug, causing the transient maximum in equivalence ratio (at around 1000 μs) observed in Figure 7.4.

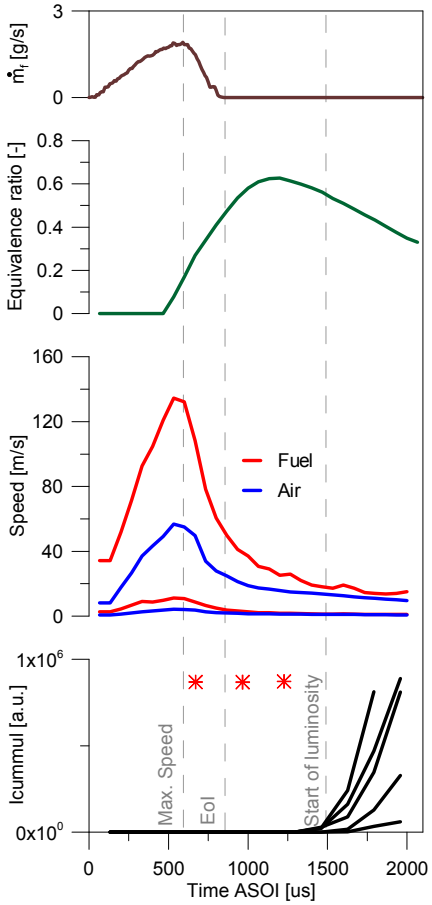

Figure 7.4. *Experimental and CFD results versus time ASOI for a* 6 *mg injection* 250 *bar. From top to bottom: mass flow rate per orifice (measured), equivalence ratio on the glow plug close vicinity, fuel and air maximum and minimum speeds in a plane that contains the cylinder axis and the axis of the closest spray to the glow plug,* I_{cummul} *for five repetitions of a visualization test. Marked with gray lines are the moment at which fuel reaches its maximum speed, EOI and the moment at which the camera detects the first luminosity spots. Red asterisks in the bottom plot signalize the time instants of each of the three pictures shown in Fig. 7.5.*

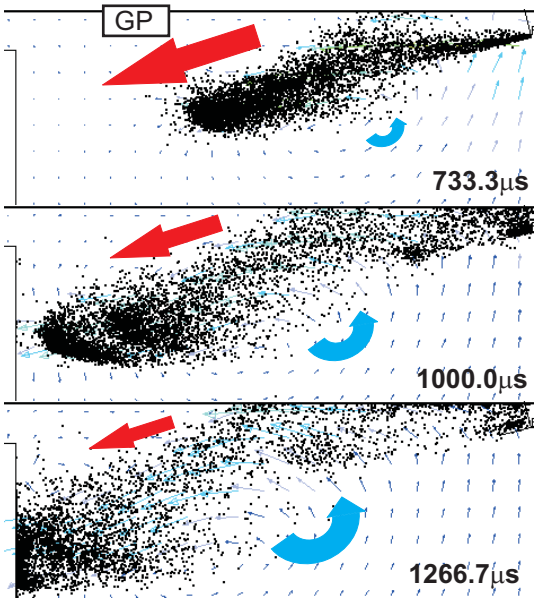

Figure 7.5. *Fuel drops and air velocity vectors in a plane that contains the cylinder axis and the axis of the spray closest to the glow plug. Three different instants have been selected as signalized with red asterisks in Fig. 7.4.*

This leaning process that increases the equivalence ratio in the glow plug area after end of injection is confirmed in Figure 7.6. Three selected time-instants of the temporal evolution of the fuel droplets and the equivalence ratio on the spray symmetry plane are presented. This Figure shows how in spite of the fact that liquid droplets have passed the glow plug area directed toward the wall, at 1000 μs ASOI equivalence ratio near the glow plug is still very low. And it is the deceleration process after EOI which drags the rich equivalence ratio zone to the glow plug area. Actually, both fuel droplets and vapor are observed to flow toward the glow plug after EOI, reaching this location finally at approximatelly 1300 μs and resulting in the maximum in equivalence ratio. After that, equivalence ratio starts decreasing. Ignition will occur on the glow plug surface at some moment after EOI and depending on the struggle between the dissipation produced by the mixing process and the development of exothermic chemical reactions. This whole sequence remarks the importance of the interaction between the spray and the surrounding air as an ignition controlling factor

This fuel leaning process and the maximum in equivalence ratio answer some of the questions that came up at the beginning of this chapter. It explains why LD values are generally grouped within a short period after EOI (between 500 and 1500μs AEOI). Since it is after EOI when the mechanisms that supply with fuel the glow plug area are activated, and it is during this period in which the maximum equivalence ratio values are reached. That is why EOI plays a major and controlling

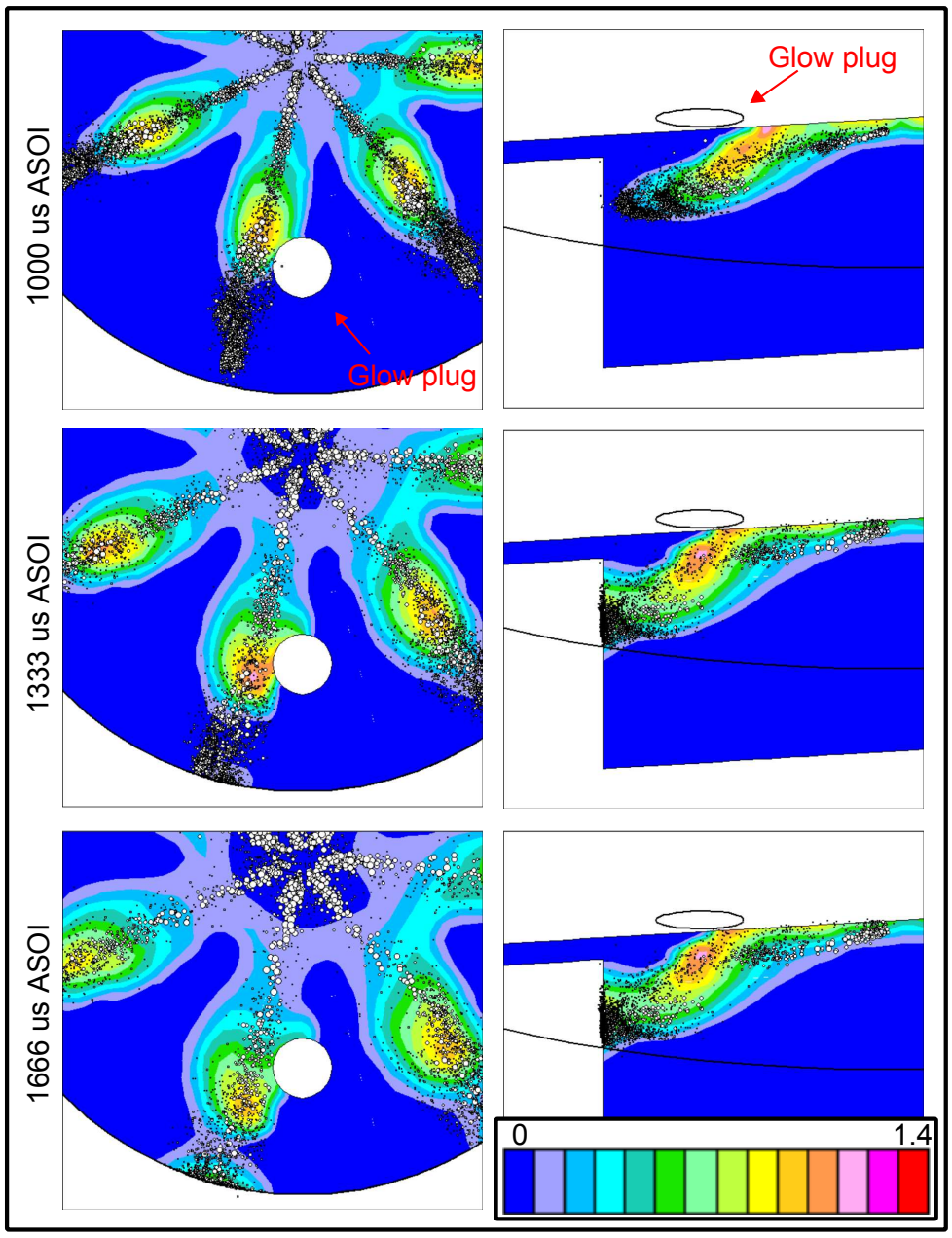

Figure 7.6. *Fuel drops and equivalence ratio in a plane that contains the cylinder axis and the axis of the spray closest to the glow plug.*

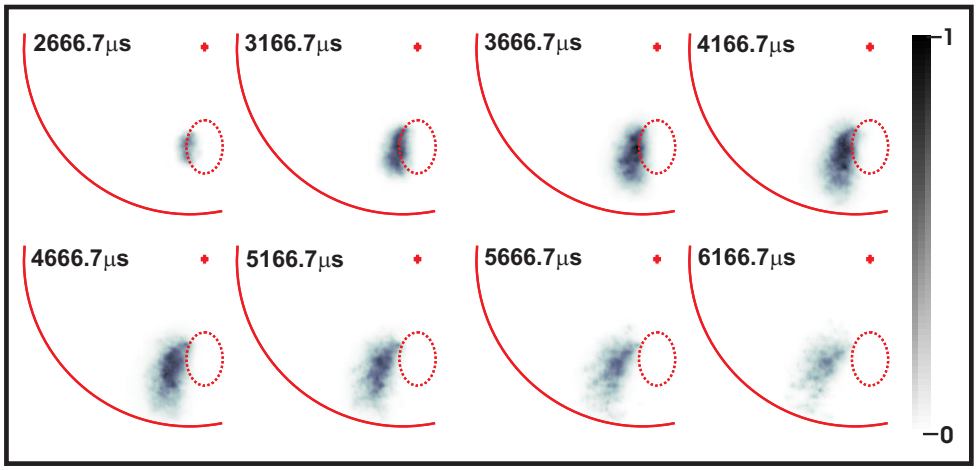

Figure 7.7. *Sequence of images showing pilot ignition and flame progress for a low rail pressure case with an orientation of* -10°*. Each image shown is an average ensemble of 20 repetitions. The acquisition time ASOI is shown in the top left corner of each picture. The average digital levels have been normalized with respect to the sequence maximum and the color scale is shown on the right side.*

role on ignition under this conditions. The fuel leaning process also explains the experimental inverse relationship found between IL and LD. For cycles where ignition occurs within a short delay (low LD), more fuel is available close to the glow plug and thus chemistry proceeds faster and a larger amount of fuel can be burnt (high IL). On the contrary, for cycles where ignition occurs late (high LD), a leaner mixture is found around the glow plug due to EOI, and thus a smaller amount of fuel is burnt (low IL).

When conditions for ignition are optimal, *i.e.* when maximum equivalence ratio occurs close to the glow plug, only small differences between fuel and air speed are observed, as shown in Fig. 7.4. This is why it is not surprising that swirl motion can modify fuel distribution on the glow plug area (as seen in Fig. 7.6) having an effect on pilot ignition. Additional evidence of the swirl motion influence on pilot flame progress is presented in Figure 7.7. An image sequence of the ignition and flame progress of a pilot injection test at low rail pressure. Each image in this figure is a 20 repetitions ensemble average image, which have been calculated in order to have a representative picture of how pilot flame progresses. The sequence shows that the first luminosity spot is detected on the glow plug surface; later, this flame starts propagating toward the piston wall but also following the swirl motion within the combustion chamber. This sequence further evidences that within this time period (2500 to 6000μs) fuel speed is not much higher than air speed (as shown in Figure 7.4) and for that reason swirl can influence fuel movement before ignition and the later flame progress. That is why orienting the closest to the glow plug spray in the

up-swirl direction has a positive effect on pilot ignition and as a consequence on start of combustion, as observed in Chapter 5.

7.3 Analysis of parametric variations

Previous section has shown that main fuel transport to the GP occurs after end of injection, when fuel velocity is low. As a conclusion, it has been observed that the different fuel speed reached by different configurations does have an effect on ignition. Three different parametric variations have allowed to make this statement: rail pressure, mass of fuel injected and nozzle geometry. The effect of rail pressure and the amount of fuel injected is explained in Sub-Section 4.3.1, as shown in Figure 4.8(a). The trend observed in that sub-section suggest that an increase in fuel speed reduces the probabilities of pilot ignition. The nozzle geometry study allowed to isolate the fuel speed effect since two different nozzles with the same number of holes and very different geometry were tested. These results allowed to confirm that pilot probability reduces if the fuel speed is increased.

Figure 7.8 shows the fuel speed effect on fuel motion by comparing two cases at different rail pressure. It shows that at higher rail pressure fuel reaches much faster the bowl wall, away from the glow plug area. This is quite evident comparing the situation for both rail pressure values at EOI (800 μs for the lower rail pressure, and 667 μs for the higher one). This means that the same amount of injected fuel mass is distributed in a wider region. Consequently, later fuel transport toward the glow plug can carry only a smaller amount of fuel, resulting in leaner maximum equivalence ratio values. If the amount of fuel mass is larger at the same rail pressure, the effect is similar. Higher velocities are reached during and at the end of injection which provokes that a larger amount of fuel misses the glow plug area compared with the shorter injection case. Even if the total injected mass is higher, most of the fuel ends up on the piston wall, and therefore ignition conditions on the glow plug are leaner. As a summary, Figure 7.9 shows the average equivalence ratio in the near glow plug vicinity as a function of time for three strategies, nominal, higher rail pressure case and higher fuel mass injected case. Compared with the nominal case the other two strategies imply a fuel speed increase, for which maximum equivalence ratio is lower. Such lower equivalence ratio (at higher speed) is less favorable from the point of view of chemical activity, and therefore ignition process is slower or it can even be suppressed. A short injection pulse at low rail pressure results in a more favorable vaporization process, which should create richer mixtures close to the glow plug and is more favorable for ignition according to chemical calculations. This trend correlates very well with the experimental results and explains why the effect of increasing fuel speed is negative.

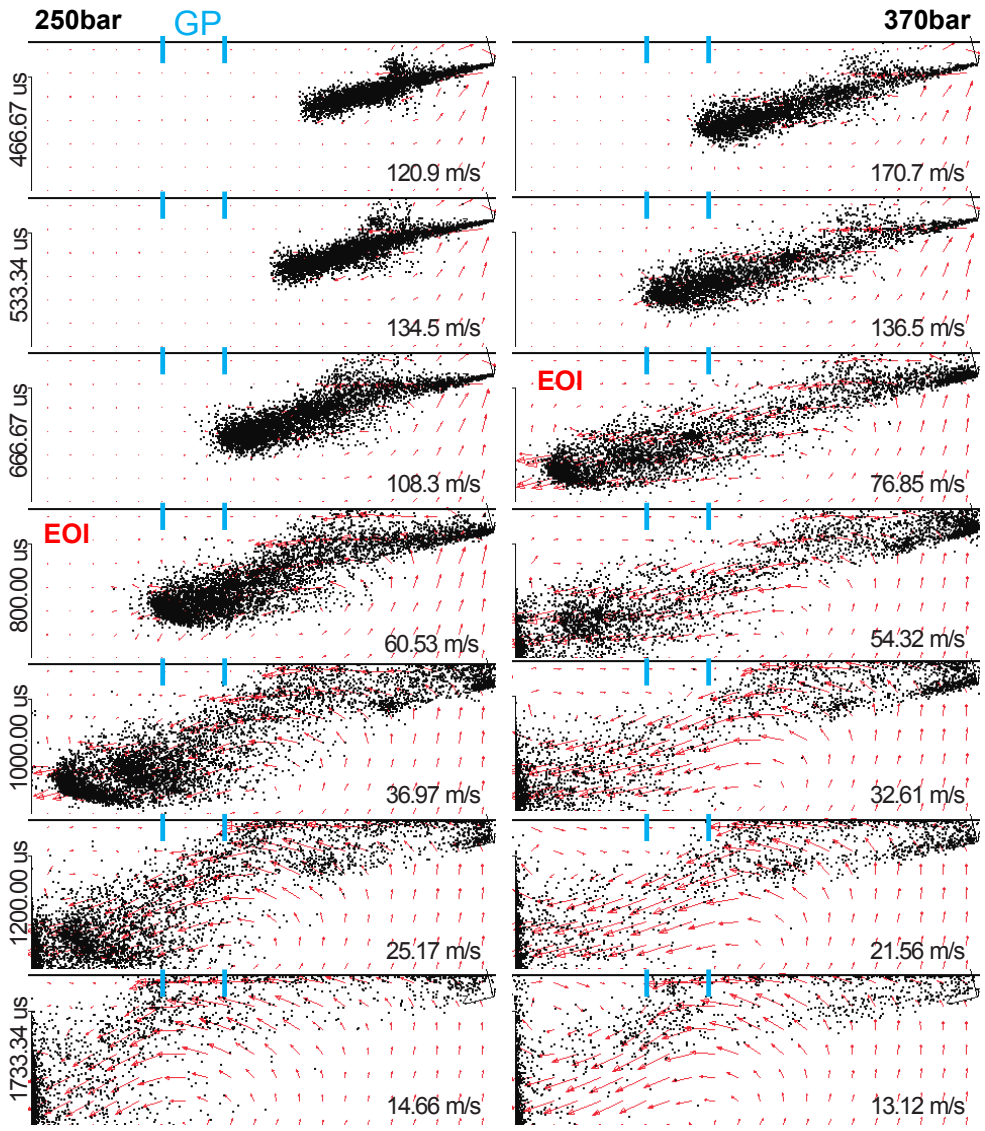

Figure 7.8. *CFD figures showing the fuel droplets and air velocity (vectors) evolution in a section which contains the cylinder and closest to glow plug spray axes. A pilot injection of* 0.86 *mg per orifice at two rail pressures,* 250 *bar (left) and* 370 *bar (right). The corresponding time ASOI of each pair of figures is shown in the left side edge. In the bottom-right corner of each image the maximum fuel velocity is also shown. The glow plug approximate location is signaled with blue lines.*

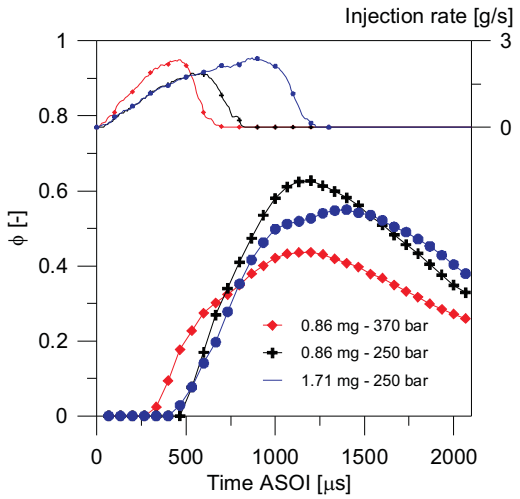

Figure 7.9. *Temporal evolution of injection rate and CFD predicted equivalence ratio for the vapor phase of the near-plug zone for three different strategies: the baseline case (*0.86 *mg per orifice,* 250 *bar), a* 1.71 *mg per orifice injection at the same rail pressure and a* 0.86 *mg per orifice injection at* 370 *bar.*

7.4 Conclusions

This Chapter has presented a full and coherent explanation of the physical and chemical processes that lead to pilot injection ignition under the conditions tested in this thesis. This has been carried out with the purpose of understanding real engine and thermodynamic parameters that control ignition and have been tested experimentally in previous chapters. Specific theoretical tools have been employed as needed in order to piece together such explanation. The analysis has been focused solely on pilot ignition for being the most determinant parameter for overall combustion initiation and development.

First, the role of the glow plug as hot spot in the combustion chamber has been presented. Indeed, the glow plug vicinity is the only possible location of the combustion chamber to reach ignition conditions for such low temperature conditions, as seen experimentally previously. But it has been shown that the role of the glow plug is mainly as accelerator of the chemical reactions that lead to ignition, and not as heat releaser to vaporization. It has also been found that chemical ignition delays can be reduced to few microseconds with the technology available nowadays and any further increase will not improve chemical kinetics. These facts lead to the conclusion that, knowing that ignition must occur on the glow plug vicinity, the controlling parameter is the mixture preparation in this area.

Regarding mixture preparation important conclusions have been reached. During injection, fuel travels rapidly from the nozzle hole to the cylinder wall passing near

the glow plug but generating a very poor fuel and air mixture in this area. For this reason, no ignition spot has been detected during the injection event. After end of injection the situation changes, fuel starts traveling toward the glow plug dragged by the air vortexes generated previously during injection. As the air vortexes are in charge of carrying fuel to the glow plug, it is necessary that injection finishes so the air velocity becomes more important that fuel velocity. And this is the reason why the first luminosity spots have been detected always after end of injection. This is also the reason why it is better for ignition to locate the closest spray in the up-swirl direction with respect to the glow plug, *i.e.* in this way swirl motion can help to drag fuel to the glow plug. The fuel and air mixture in the glow plug area becomes more fuel-rich until a maximum value is reached. From here and on, the mixture will start to become leaner with time. This is the reason why ignition is delimited within certain time period after end of injection. And it is also the reason why the later pilot ignition occurs, the lower the intensity of the pilot flame is.

Having clear a structured explanation of how ignition occurs, it is easier to understand the parametric variations presented in previous chapters. Increasing fuel speed by different ways (rail pressure, injected mass or nozzle geometry) provokes that a larger amount of fuel travels to the cylinder wall. It also results in more time to the fuel speed to reach the air speed values and a lower amount of fuel will finally reach the glow plug. This is the reason why increasing rail pressure or the amount of fuel injected, when using the same nozzle, reduces pilot ignition probability.

Bibliography

[1] Edwards C. F., Siebers D. L. and Hoskin D. H. "A study of the autoignition process of a diesel spray via high speed visualization". *SAE Paper 920108*, 1992.

[2] García Oliver José María. *El proceso de combustión turbulenta en chorros diesel de inyección directa*. Editorial Reverté, 2006.

[3] Heywood John B. *Internal Combustion Engine Fundamentals*. McGraw-Hill, Inc., 1988.

Chapter 8

Conclusions and future work

Contents

8.1 Conclusions

The present work has been developed within the general framework of improving diesel engine technology in order to reduce pollutant emissions and enhance engine performance, efficiency and fuel consumption. It has been focused on the start phase at negative (*i.e.* below 0°C) temperatures, as it is a very critical operating condition in which a large amount of pollutants are emitted to the atmosphere due to misfiring and low efficiency of the after-treatment devices. This problem affects current engine technology but it is also a big concern for the development of future designs. The general objective of this work has been to contribute to the understanding of the combustion process under such conditions in direct injection passenger diesel engines. Focus has been made on mechanisms governing ignition and combustion, as well as on the influence and importance of different geometry and operating parameters. The knowledge derived from the present study should help define the guidelines to overcome starting problems at low temperature for current and upcoming engine designs.

Different experimental and theoretical tools have been employed along this work, but the main tool is an experimental facility based on a conventional single-cylinder optical engine operated at room temperature, which is capable of reproducing in-cylinder thermodynamic conditions representative of those achieved during the first injection cycle of real passenger car engines during start at very low ambient temperatures. From the initial configuration, mainly aimed at conventional

engine studies, the facility was adapted to simulate real engine cold start. Major modifications concern:

- Compression ratio reduction and intake temperature control to reduce in-cylinder peak temperature.
- Engine speed control in the 500 *rpm* range, which is typical of real engine cold start.
- Control of all engine fluids temperature (water, oil and fuel) to the minimum value achievable to avoid moisture condensation problems on engine surfaces.
- Measurement of instantaneous intake and exhaust mass flow rate to estimate blow-by indirectly.

Under its final configuration, the facility was capable of reproducing, systematically and repeatably, low speed and low temperature conditions. Thermodynamic in-cylinder conditions were set to values achieved during the first injection cycle of the starting sequence of a real engine, where ignition probability is low, *i.e.* in the borderline between ignition and misfiring, so that the effect of the different individual geometrical and operation parameters upon ignition success can be assessed. In-cylinder pressure and high-speed visualization have been the main sources of experimental information obtained from engine tests. Other tools have been employed to give support and complement the information from the experimental combustion analysis in the optical engine, such as nozzle flow characterization and specific modeling tools.

Results and corresponding analysis presented along the different chapters of this thesis summarize conclusions from a much larger experimental database. In this sense, the most relevant investigations have been compiled into the present document, starting by a description of the main combustion characteristics for a nominal injection strategy (Chapter 4). This has provided a mental image of events compiled into a phenomenological description that can guide understanding of later parametric studies. In addition to characterizing a relatively unknown combustion event, this description has shown a detailed example of the application of the methodology developed throughout the thesis. For example, in-cylinder pressure analysis has been performed based on a single-cycle basis, since ignition conditions are on the limit between combustion and misfiring and therefore high cycle-to-cycle dispersion occurs, which prevents from using cycle-averaged pressure curves. High speed visualization was used systematically, since low intensity, local and transient phenomena strongly affect combustion development. To adequately describe combustion evolution when performing a pilot+main injection strategy, visualization studies were performed separately of both single-pilot and pilot+main injection strategies. The former studies were needed to characterize pilot flame with appropriate camera settings, without the influence of subsequent main combustion radiation.

As already commented, low temperature cold start combustion process is characterized by high cycle-to-cycle dispersion and low combustion efficiency. From

the observation of the sequence of in-cylinder events, one can divide the combustion process into two well-defined problems, namely pilot ignition and combustion progress.

Pilot ignition is probably the most critical stage in the whole combustion process since it has a direct influence on the development of an early and controlled start of main combustion. This is confirmed by the fact that, in several occasions throughout this thesis, the probability of obtaining a pilot flame is linked to that of obtaining cycle work. Therefore, a large part of the efforts in the present thesis have been devoted to the investigation of the events occurring around pilot mass injection and combustion initiation. The general description shows that ignition occurs on the glow plug vicinity and always well after end of injection. The ignition spot grows burning part of the fuel injected in the spray closest to the glow plug. Available fuel is burnt on that spray, but no propagation occurs to the adjacent ones. Eventually, heat released by pilot flame should be high enough to promote an early and controlled main combustion start but it is considerably lower than the heat released in main combustion. In fact, pilot combustion cannot be detected by means of in-cylinder pressure analysis.

Measured pilot flame parameters, namely ignition probability, ignition delay and flame intensity, have been seen to depend on injection strategy, glow plug-spray geometrical arrangement, glow plug temperature and nozzle geometry. Regarding injection strategy, increasing rail pressure and/or the amount of injected fuel have seen to negatively affect pilot ignition, *i.e.* low ignition probability, large ignition delays and low flame intensity. Both parameters provoke a fuel speed increase and, in the case of the amount fuel injected, also an increment of the mass of fuel delivered per orifice. Both effects are coupled when using a single nozzle. However, nozzle studies presented in Chapter 6 made it possible to separate both mass and velocity effects for different nozzles. The conclusions drawn indicate that for nozzles with similar maximum velocity, fuel mass increase was beneficial for the formation of a pilot flame, while for cases where injected mass is constant, an increment of fuel speed affects negatively pilot ignition. Regarding glow plug-spray geometrical arrangement, distance between the glow plug and the closest spray certainly has an effect on pilot ignition. Shortening this distance improves conditions for pilot ignition. However, locating the closest spray up-swirl of the glow plug for a fixed distance, also improves these conditions. Regarding glow plug temperature, increasing the temperature of the glow plug surface reduces ignition delay and increases the luminosity of the pilot flame. However, above a given temperature value this reduction starts to be negligible and other processes (most probably physical) start to be the controlling ones. Another interesting conclusion of the pilot flame study is that, for any of the parametric studies, ignition delay and flame intensity are related, namely if the ignition delay is large the flame intensity is low and vice-versa.

By using specific modeling tools, an explanation to some of the experimental results was given. It was confirmed that the glow plug vicinity is the only possible location of the combustion chamber to reach ignition conditions for such low temperature conditions. But it has been shown that the main effect of the glow plug is mainly as accelerator of the chemical reactions that lead to ignition, while the influence on spray vaporization is more limited. It has also been found that chemical ignition

delay can be reduced to few microseconds with current glow plug technology, and any further increase will not reduce chemical delay any further. Regarding mixture preparation important conclusions have been drawn. During injection, fuel travels rapidly from the nozzle hole to the cylinder wall passing near the glow plug but generating a very lean fuel and air mixture in this area. For this reason, no ignition spot has been detected during the injection event. After end of injection the situation changes, liquid spray velocity slows down very fast, and the resulting flow transports fuel mass toward the glow plug. This is why first luminosity spots have always been detected after end of injection, and also why locating the closest spray up-swirl of the glow plug is also better for pilot ignition, as swirl motion will also contribute to increasing local equivalence ratio close to the glow plug, which has been found to be important for chemical reaction to occur. Some time after end of injection, local equivalence ratio on the glow plug reaches a maximum, after which it becomes leaner with time. High equivalence ratio values are better for pilot ignition, so this maximum is the cause why ignition has been observed to occur only within a certain time period, with the longer the ignition delay the weaker the intensity of the flame.

Apart from pilot flame ignition, the other major issue in cold start is main combustion initiation and progress. If pilot injection ignites adequately, main combustion occurs when one of the sprays reaches the pilot flame. As injection continues, the flame progresses from the first ignition location, near the piston bowl wall, toward the rest of the chamber with an structure similar to a flame front. When injection finishes, the flame front is seen to decelerate together with the combustion rates. Besides pilot flame as ignition promoter, work in thesis has evaluated the influence on main combustion development of different parameters, with the most influencing ones being rail pressure, injection duration and nozzle geometry. Increasing rail pressure accelerates heat release rates, resulting in a shorter and more intense combustion process. Changing injected mass by modifying injection duration results in a different evolution of the flame during the combustion cycle as a result of the differences in equivalence ratios. A maximum combustion efficiency is reached with a characteristic injected mass. This results from the fact that higher injection duration (*i.e.* higher mass) may cause that some fuel is injected after the flame front has swept the combustion chamber into an atmosphere with poor oxygen conditions, and thus combustion efficiency drops. Finally, nozzle study has shown that changing either rail pressure and/or nozzle geometry acts upon cycle work by means of a single parameter, namely momentum flux. Higher momentum results in more work, as a result of a more intense fuel-air mixing process.

8.2 Future work

The work presented in this thesis has aimed at setting a basis for understanding a complex diesel combustion phase. The appropriate use of the different tools and the analysis of the information have made it possible to gain more insight into cold start combustion, as evidenced in previous conclusions. Anyway, further research, directed toward cold start combustion optimization, is still necessary. The proposal

for this future work is divided in two different but complementary paths: to improve fundamental knowledge and to validate trends in more applied studies.

One important part of the proposal for future work is to get deeper knowledge in some phenomena which could not been extensively covered in this work. First, it is important to improve experimental evidence on fuel-air ratio distribution within the chamber, and specially close to the glow plug, from end of pilot injection to start of luminosity. Due to the low vaporization rates, the presence of liquid will be certainly important. Therefore, LIF techniques should be applied in a more simple optical facility, where interference of liquid with window walls is eliminated, while keeping a geometry that resembles that of the combustion chamber. Further studies could also be directed toward defining the type of radiation present during the whole combustion. This should help define the characteristics of combustion process during initial stages as well as during the main heat release. Such measurements should also enable the separation of OH^* chemiluminescence and soot incandescence. This can be achieved performing dedicated spectroscopy studies. OH-PLIF could be used as well to confirm flame front evolution during main combustion. On the calculation side, CFD results have been presented along this thesis only in terms of inert spray evolution, since combustion models have certainly some limitations. But it would be worth to use such models to investigate and validate experimental conclusions, mainly in terms of combustion events and parametric variations.

A proposal for future work directed toward the application in current technology can be divided in two parts: validation in real engine and improvement of new designs. One path for future work can be performing tests at low temperature with the purpose of validating results presented here. Even though general trends observed in the present thesis have been confirmed with parallel projects running on multi-cylinder engines in climatic chambers, a one-to-one comparison of results has not been performed. It would be interesting to test a multi-cylinder engine with a very similar configuration to the one in the present study (displacement, injector, distance to glow plug) to check consistency of results, as well as to evaluate the relationship between in-cylinder engine processes and engine-out pollutant emissions. The other path proposed is to investigate the impact that new piston bowl designs, injector nozzles, glow plugs, etc. may have on cold startability. The optimum sequence would be to perform tests following the same methodology presented in this thesis to understand the possible more fundamental aspects of such modifications. Later, more applied tests can be performed in climatic chamber to validate trends taking into account the real engine geometry.

Bibliography

Aesoy Vilmar and Valland Harald.
Hot surface assisted compression ignition of natural gas in a direct injection diesel engine.
SAE Paper 960767, 1996. (cited on page 15)

Armas Octavio.
Diagnóstico experimental del proceso de combustión en motores diesel de inyección directa.
Tesis Doctoral, Departamento de Máquinas y Motores térmicos. Universidad Politécnica de Valencia, Valencia, 1998. (cited on page 39)

Arrègle Jean.
Análisis de la estructura y dinámica interna de chorros diesel.
Tesis Doctoral, Departamento de Máquinas y Motores térmicos. Universidad Politécnica de Valencia, 1997. (cited on page 11)

Badami M., Mallamo F., Millo F. and Rossi E.
Influence of multiple injection strategies on emissions, combustion noise and BSFC of a DI common rail diesel engine.
SAE paper 2002-01-0503, March 2002. (cited on page 21)

Badami M., Nuccio P. and Trucco G.
Influence of injection pressure on the performance of a DI diesel engine with a common rail fuel injection system.
SAE paper 1999-01-0193, March 1999. (cited on page 21)

Bielaczyc Piotr, Merkisz Jerzy and Pielecha Jacek.
Investigation of exhaust emissions from di diesel engine during cold and warm start.
SAE paper 2001-01-1260, 2001. (cited on pages 10, 56)

Bosch R.
Automotive handbook.
4th edition, 1996. (cited on page 20)

Bosch R.
Diesel engine management.
2nd edition, 1999. (cited on page 20)

Bosch W.
The fuel rate indicator: a new measuring instrument for display of the characteristics of individual injection.
SAE Paper 660749, 1966. (cited on page 44)

Bracho León Gabriela.
Experimental and theoretical study of the direct diesel injection process at low temperatures.
Tesis Doctoral, Departamento de Máquinas y Motores térmicos. Universidad Politécnica de Valencia, July 2011. (cited on pages 12, 44)

Broatch A., Ruiz S., Margot X. and Gil A.
Methodology to estimate the threshold in-cylinder temperature for self-ignition of fuel during cold start of Diesel engines.
Energy, Vol. 35, pp. 2251–2260, March 2010. (cited on pages 16, 17, 18, 33)

Broatch Alberto, Luján José M., Serrano José R. and Plá Benjamín.
A procedure to reduce pollutant gases from Diesel combustion during European MVEG-A cycle by using electrical intake air-heaters.
Fuel, Vol. 87 n^o 12, pp. 2760–2778, 2008. (cited on page 14)

CD-Adapco.
Star-CD Methodology, Version 3.26.
CD-Adapco, 2005. (cited on page 49)

Chartier Clèment, Aronsson Ulf, Andersson Öivind and Egnell Rolf.
Effect of Injection Strategy on Cold Start Performance in an Optical Light-Duty DI Diesel Engine.
SAE Paper 2009-24-0045, 2009. (cited on pages 21, 22, 23, 56)

Corcione F. E., Vaglieco B. M., Corcione G. E. and Lavorgna M.
Potential of multiple injection strategy for low emission diesel engines.
SAE paper 2002-01-1150, March 2002. (cited on page 21)

Correas David.
Estudio teórico experimental del chorro libre diesel isotermo.
Tesis Doctoral, Departamento de Máquinas y Motores térmicos. Universidad Politécnica de Valencia, 1998. (cited on page 11)

Curran H. J., Gaffuri P., Pitz W. J. and Westbrook C. K.
A comprehensive modeling study of n-Heptane oxidation.
Combustion and Flame, Vol. 114, pp. 149–177, 1998. (cited on page 48)

Desantes J. M., García-Oliver J. M., Pastor J. M. and Ramírez-Hernández J. G.
Influence of nozzle geometry on ignition and combustion for high-speed direct injection diesel engines under cold start conditions.
Fuel, Vol. 90 n^o 11, pp. 3359–3368, 2011. (cited on page 5)

Dukowicz John K.
A particle-fluid numerical model for liquid sprays.
Journal of Computational Physics, Vol. 35 n^o 2, pp. 229–253, 1980. (cited on page 49)

Edwards C. F., Siebers D. L. and Hoskin D. H.
A study of the autoignition process of a diesel spray via high speed visualization.
SAE Paper 920108, 1992. (cited on pages 10, 108)

Eller Martin (DE).
Patent: Protection tubes for sensors or glow elements, ep0945724 edition, September 1999.
(cited on page 82)

ERTRAC European Roadmap.
Electrification of road transport.
European Road Transport Research Advisory Council (ERTRAC), European Technology Platform on Smart Systems Integration (EPoSS) and European Technology Platform for the Electricity Networks of the Future (Smart Grids), November 2010. (cited on page 3)

ERTRAC Strategic Research Agenda 2010.
Towards a 50 percent more efficient road transport system by 2030 - Technical document.
European Road Transport Research Advisory Council (ERTRAC), October 2010.
(cited on pages 2, 3)

ERTRAC Working Group on Energy and Environment.
Future light-duty powertrain technologies and fuels.
European Road Transport Research Advisory Council (ERTRAC), August 2011.

García Ibáñez Javier Ángel.
Nuevo concepto de arranque en frío para motores diesel de inyección directa de alta presión.
Tesis Doctoral, Departamento de Máquinas y Motores térmicos. Universidad Politécnica de Valencia, Valencia, 2003. (cited on page 14)

García Oliver José María.
El proceso de combustión turbulenta en chorros diesel de inyección directa.
Editorial Reverté, 2006. (cited on page 109)

Giménez Plá Juan Fernando.
Diseño de un sistema de arranque en frío para motores diesel de inyección directa de pequeña cilindrada.
Tesis Doctoral, Departamento de Máquinas y Motores térmicos. Universidad Politécnica de Valencia, Valencia, 2000. (cited on page 14)

Gimeno Jaime.
Estudio de la inyección diesel mediante la medida del flujo de cantidad de movimiento del chorro.
Editorial Reverté, 2011. (cited on pages 45, 96)

Girotra M., Zhong L. R., Henein N. A. and Bryzik W.
Split injection strategy for prompt cold starting and low white smoke emissions.
In *Proceedings of the Spring Technical Conference of the ASME Internal Combustion Engine Division*, pp. 343–350, 2005. (cited on page 21)

Goetz Wendel A., Barringer Chris G. and Bozzelli Marco A.
Utilizing neat methanol and glow plug ignition in DI diesels: Laboratory testing of a single and multi-cylinder engine.
SAE Paper 941044, 1994. (cited on page 15)

Habchi Chawki, Lafossas Francois A., Beard Philippe and Broseta D.
Formulation of a One-Component Fuel Lumping Model to Assess the Effects of Fuel Thermodynamic Properties on Internal Combustion Engine Mixture Preparation and Combustion.
SAE Paper 2004-01-1996, June 2004. (cited on page 50)

Hara H., Itoh Y., Henein N. and Bryzik W.
Effect of cetane number with and without additive on cold startability and white smoke emissions in a diesel engine.
SAE paper 1999-01-1476, 1999. (cited on page 13)

Hardenberg H. O. and Hase F. W.
An empirical formula for computing the pressure rise delay of a fuel from its cetane number and from relevant parameters of direct-injection diesel engines.
SAE paper 790493, 1979. (cited on pages 12, 13)

Hatori H., Narumiya K., Tsue M. and Kadota T.
Photographical analysis of initial breakup process of diesel spray.
In *Proceedings of the Thiesel 2002 Conference on Thermo-and fluid dynamic processes in diesel engines*, pp. 33 – 43, Valencia, Spain, September 2002. CMT - Motores térmicos. Universidad Politécnica de Valencia. (cited on page 11)

Henein Naeim A., Zahdeh Akram R., Yassine Mahmoud K. and Bryzik Walter.
Diesel engine cold starting: combustion instability.
SAE Paper 920005, February 1992. (cited on page 18)

Heywood John B.
Internal Combustion Engine Fundamentals.
McGraw-Hill, Inc., 1988. (cited on pages 12, 21, 56, 109)

Huh K. Y. and Gosman A.D.
A Phenomenological Model of Diesel Spray Atomization.
In *Proceedings of the International Conference on Multiphase Flows*, September 1991. (cited on page 49)

Huynh Quynh-Nhu.
European Union economic report.
European Automobile Manufacturers Association (ACEA), March 2010. (cited on pages 2, 3)

Issa R. I.
Solution of the implicitly discretized fluid flow equations by operator-splitting.
J. Comp. Phys, Vol. 62, pp. 40–65, 1986. (cited on page 50)

Iwabuchi Y., Kawai K., Shoji T. and Yoshinaka T.
Trial of new concept diesel combustion system - premixed compression-ignited combustion.
SAE Paper 1999-01-0185, 1999. (cited on page 4)

Johnson Timothy V.
Review of CO_2 emissions and technologies in the road transportation sector.
SAE paper 2010-01-1276, 2010. (cited on pages 3, 4)

Johnson Timothy V.
Review of diesel emissions and control.
SAE paper, Vol. 2010-01-0301, 2010. (cited on page 4)

Johnson Timothy V.
Diesel Emission Control in Review.
SAE Paper 2011-01-0304, December 2011. (cited on page 3)

Karthikeyan B. and Srithar K.
Performance characteristics of a glowplug assisted low heat rejection diesel engine using ethanol.
Applied Energy, Vol. 88 n^o 1, pp. 323–329, 2011. (cited on page 15)

Kern Christoph, Dressler Wolfgang, Lindemann Gert and Rothacker Volker.
An innovative glow system for modern diesel engines.
SAE paper 1999-01-1240, March 1999. (cited on page 16)

Kimura S., Ogawa H., Matsui Y. and Enomoto Y.
An experimental analysis of low-temperature and premixed combustion for simultaneous reduction of NOx and particulate emissions in direct injection diesel engines.
International Journal of Engine Research, Vol. 3 n^o 249-259, 2002. (cited on page 4)

Körfer T, Schnorbus T, Kalenborn M, Kolbeck A, Bourgoin G, Cecur M and Raimondi E.
Integrated diesel engine concept for lowest CO2 emissions requirements.
In *Aachen Colloquium*, October 2010. (cited on page 3)

Kowalewicz A.
Combustion systems of high-speed piston internal combustion engines.
Elsevier science publishers, New York, 1984. (cited on page 15)

Kwon S. I., Arai M. and Hiroyasu H.
Ignition delay of a diesel spray injected into a residual gas mixture.
SAE paper 911841, 1991. (cited on page 13)

Lapuerta M., Armas O. and Bermúdez V.
Sensitivity of diesel engine thermodynamic cycle calculation to measurement errors and estimated parameters.
Applied Thermal Engineering, Vol. 20 n^o 9, pp. 843 – 861, 2000. (cited on page 17)

Lapuerta M., Armas O. and Hernández J.J.
Diagnosis of DI Diesel combustion from in-cylinder pressure signal by estimation of mean thermodynamic properties of the gas.
Applied Thermal Engineering, Vol. 19 n^o 15, pp. 513–529, May 1999. (cited on page 50)

Lindl Bruno and Schmitz Heinz-Georg.
Cold-start equipment for diesel direct-injection engines.
SAE Paper 1999-01-1244, 1999. (cited on pages 15, 38, 84)

Liu Z. and Karim G. A.
An examination of the role of residual gases in the combustion processes of motored engines fuelled with gaseous fuels.
SAE paper 961081, 1996. (cited on page 13)

MacMillan D., La Rocca A., Shayler P. J., Murphy M. and Pegg I. G.
The Effect of Reducing Compression Ratio on the Work Output and Heat Release Characteristics of a DI Diesel under Cold Start Conditions.
SAE Paper 2008-01-1306, April 2008. (cited on page 4)

Martín Díaz Jaime.
Aportación al Diagnóstico de la combustión en motores diesel de inyección directa.
Tesis Doctoral, Departamento de Máquinas y Motores térmicos. Universidad Politécnica de Valencia, Valencia, 2007. (cited on pages 39, 50)

Maswadeh Waleed, Tripathi Ashish, Arnold Neil S., DuBow Joel and Meuzelaar Henk L.C.
High speed, two-wavelength radiation thermometry of single micro particles during CO2 laser heating.
Journal of Analytical and Applied Pyrolysis, Vol. 28 n^o 1, pp. 55 – 70, 1994. (cited on page 82)

Meriaudeau F.
Real time multispectral high temperature measurement: Application to control in the industry.
Image and Vision Computing, Vol. 25, pp. 1124–1133, 2007. (cited on page 82)

Mueller Charles J. and Musculus Mark P.
Glow plug assisted ignition and combustion of methanol in an optical DI diesel engine.
SAE Paper 2001-01-2004, 2001. (cited on page 15)

Musculus M.
Entrainment waves in decelerating transient turbulent jets.
J. Fluid Mech., Vol. 638, pp. 117–140, 2009. (cited on page 60)

Naber Jeffrey D. and Siebers Dennis L.
Effects of gas density and vaporization on penetration and dispersion of diesel sprays.
SAE Paper 960034, 1996. (cited on page 97)

NGK-GlowPlugs.
Ceramic glow plugs.
Technical information available in http://www.ngk-dpower.com/en/technik/keramik-gluehkerzen/. (cited on page 16)

Osuka Isao, Nishimura Masataka, Tanaka Yasushi and Miyaki Masahiko.
Benefits of new fuel injection system technology on cold startability of diesel engines Improvements on cold startability and white smoke reduction by means of multi injection with common rail fuel system (ECD-U2).
SAE Paper 940586, February 1994. (cited on pages 18, 21)

Pacaud P., Perrin H. and Laget O.
Cold Start on Diesel Engine: Is Low Compression Ratio Compatible with Cold Start Requirements?
SAE Paper 2008-01-1310, April 2008. (cited on pages 4, 19, 22, 78)

Palomares Alberto.
Análisis de imágenes de chorros diesel.
Tesis Doctoral, Departamento de Máquinas y Motores térmicos. Universidad Politécnica de Valencia, Noviembre 2000. (cited on page 47)

Pastor J. V., Bermúdez V., García-Oliver J. M. and Ramírez-Hernández J. G.
Influence of spray-glow plug configuration on cold start combustion for high-speed direct injection diesel engines.
Energy, Vol. 36 n^o 9, pp. 5486–5496, 2011. (cited on page 5)

Pastor J. V., García-Oliver J. M., Pastor J. M. and Ramírez-Hernández J. G.
Experimental facility and methodology for systematic studies of cold startability in direct injection Diesel engines.
Measurement Science and Technology, Vol. 20, pp. 09519, August 2009. (cited on page 5)

Pastor J V, García-Oliver J M, Pastor J M and Ramírez-Hernández J G.
Ignition and combustion development for high speed direct injection diesel engines under low temperature cold start conditions.
Fuel, Vol. 90 n^o 4, pp. 1556 – 1566, 2011. (cited on page 5)

Payri F., Benajes J., Margot X. and Gil A.
CFD modeling of the in-cylinder flow in direct-injection Diesel engines.
Computers and Fluids, Vol. 33 n^o 8, pp. 995 – 1021, 2004. (cited on page 16)

Payri F., Broatch A., Salavert J. M. and Martín J.
Investigation of diesel combustion using multiple injection strategies for idling after cold start of passenger-car engines.
Experimental Thermal and Fluid Science, Vol. 34 n^o 7, pp. 857–865, 2010.
(cited on pages 21, 22, 56)

Payri F., Broatch A., Serrano J. R., Rodríguez L. F. and Esmorís A.
Study of the Potential of Intake Air Heating in Automotive DI Diesel Engines.
SAE Paper 2006-01-1233, April 2006. (cited on pages 14, 18)

Payri F., Pastor J. V., García J. M. and Pastor J. M.
Contribution to the aplication of two-colour imaging to diesel combustion.
Measurement Science and Technology, Vol. 18, pp. 2579–2598, 2007. (cited on page 84)

Payri R., Salvador F. J., Gimeno J. and De la Morena J.
Influence of injector technology on injection and combustion development. Part 1: Hydraulic characterization.
Applied Energy, 2010.
In press. (cited on page 96)

Peng H.-Y., Cui Y., Deng H.-Y., Shi L and Li L.-G.
Combustion and emissions of a direct-injection diesel engine during cold start under different exhaust valve closing timing conditions.
Proceedings of the Institution of Mechanical Engineers, Part D: Journal of Automobile Engineering, Vol. 222 n^o 1, pp. 119–129, 2008. (cited on page 4)

Peng Haiyong, Cui Yi, Shi Lei and Deng Kangyao.
Effects of exhaust gas recirculation (EGR) on combustion and emissions during cold start of direct injection (DI) diesel engine.
Energy, Vol. 33 n^o 3, pp. 471 – 479, 2008. (cited on pages 4, 13)

Perrin H., Dumas J. P., Laget O. and Walter B.
Analysis of Combustion Process in Cold Operation with a Low Compression Ratio Diesel Engine.
SAE Paper 2010-01-1267, April 2010. (cited on page 62)

Phatak R. and Nakamura T.
Cold startability of open-chamber direct-injection diesel engines - part I Measurement technique and effects of compression ratio.
SAE paper 831335, 1983. (cited on page 13)

Pickett Lyle M. and Siebers Dennis L.
Non-Sooting, low flame temperature mixing-controlled DI diesel combustion.
SAE Paper 2004-01-1399, 2004. (cited on page 4)

Rakopoulos C. D. and Giakoumis Evangelos G.
Diesel engine transient operation : principles of operation and simulation analysis.
Springer, 2009. (cited on page 10)

REACTION-DESIGN.
CHEMKIN-PRO, Reaction Design: San Diego, 2008. (cited on page 48)

Reitz R. D. and Diwakar R.
Structure of High-Pressure Fuel Sprays.
SAE Paper 870598, 1987. (cited on page 49)

Ryan T. and Gray A.
Homogeneous charge compression ignition (HCCI) of diesel fuel.
SAE Paper 971676, 1997. (cited on page 4)

Siebers D.
Scaling liquid-phase fuel penetration in diesel sprays based on mixing-limited vaporization.
SAE paper 1999-01-0528, 1999. (cited on page 12)

Siebers Dennis L.
Liquid-phase fuel penetration in diesel sprays.
SAE Paper 980809, 1998. (cited on page 12)

SPECIALMETALS.
http://www.specialmetals.com/products/inconelalloy600.php. (cited on page 83)

Tago Yuichiro, Akimoto Fumie, Kitagawa Kuniyuki and Arai Norio.
Measurements of surface temperature and emissivity by two-dimensional four-color thermometry with narrow bandwidth.
Energy, Vol. 30 n^o 2-4, pp. 485 – 495, 2005. (cited on page 82)

Ueda T., Zhang L. and Gabe M.
Improvement of the cold startability of common rail injection system by pilot injection in a HD diesel engine.
SAE paper 1999-08-0355, 1999. (cited on page 21)

Walter B., Perrin H., Dumas J. and Laget O.
Cold operation with optical and numerical investigations on a low compression ratio diesel engine.
SAE paper 2009-01-2714, November 2009. (cited on pages 19, 21, 78)

Weilenmann Martin, Favez Jean-Yves and Alvarez Robert.
Cold-start emissions of modern passenger cars at different low ambient temperatures and their evolution over vehicle legislation categories.
Atmospheric Environment, Vol. 43 n^o 15, pp. 2419–2429, February 2009. (cited on page 4)

Wilson Jon S.
Sensor technology handbook.
Elsevier Inc., 2005. (cited on page 83)

Yassine M. K., Tagomori M. K., Henein N. A. and Bryzik W.
White smoke emissions under cold starting of diesel engines.
SAE paper 960249, February 1996. (cited on page 4)

Zahdeh Akram R., Henein Naeim A. and Bryzik Walter.
Diesel cold starting Actual cycle analysis under border-line conditions.
SAE Paper 900441, February 1990. (cited on page 18)

Zapata Luis Daniel.
Caracterización de los procesos de inyección-combustión diesel mediante visualización y procesado digital de imágenes.
Tesis Doctoral, Departamento de Máquinas y Motores térmicos. Universidad Politécnica de Valencia, Noviembre 2010. (cited on page 47)

Zhong Lurun, Gruenewald Steve, Henein Naeim and Bryzik Walter.
Lower temperature limits for cold starting of diesel engine with common rail fuel injection system.
SAE paper 2007-01-0934, April 2007. (cited on page 21)